logged in 7/25

SANDIA REPORT SAND82—2771 • Unlimited Release • UC—70

Reprinted July 1983

Copies

Code Development in Support of Nuclear Waste Storage Investigations for a Repository in Tuff

830300

Roger R. Eaton, Mario J. Martinez,
Rodney K. Wilson, Jace W. Nunziato

Prepared by
Sandia National Laboratories
Albuquerque, New Mexico 87185 and Livermore, California 94550
for the United States Department of Energy
under Contract DE-AC04-76DP00789

HYDROLOGY DOCUMENT NUMBER 171

SF 2900-Q(6-82)

Issued by Sandia National Laboratories, operated for the United States Department of Energy by Sandia Corporation.

Printed in the United States of America
Available from
National Technical Information Service
U.S. Department of Commerce
5285 Port Royal Road
Springfield, VA 22161

NTIS price codes
Printed copy: A08
Microfiche copy: A01

Category
UC-70

SAND82-2771
Unlimited Release
March, 1983
Reprinted July, 1983

CODE DEVELOPMENT IN SUPPORT OF NUCLEAR WASTE STORAGE INVESTIGATIONS FOR A REPOSITORY IN TUFF

Roger R. Eaton
Mario J. Martinez
Rodney K. Wilson
Jace W. Nunziato
Fluid Mechanics and Heat Transfer Division 1511

Abstract

A summary of the code development provided by the Fluid and Thermal Sciences Department in support of the design and performance evaluation of a nuclear waste repository in tuff (NNWSI) is documented herein. Various aspects of equation derivation, code development, code verification and scoping calculations for flow through partially saturated media are presented.

CONTENTS

INTRODUCTION

Yucca Mountain on the Nevada Test Site has been proposed as a possible location for a nuclear waste repository.* Recent interest in investigating the hydrological flow through partially saturated regions of this mountain has prompted the development of a finite element code SAGUARO.[1] The SAGUARO code is applicable to the analysis of time dependent pore water motion and energy transport in a rigid porous media which may be saturated or partially saturated with a single fluid in liquid state (i.e., no water vapor is considered). The code is a direct derivative of the MARIAH finite element code.[2,3] The MARIAH code is applicable to completely saturated regions only. Experienced MARIAH users should have few difficulties in using SAGUARO because of their similarities. The code formats have been made nearly identical to expedite user application.

During the development of this program a series of status memorandums were written which address a broad spectrum of topics. The purpose of this report is to compile these memos under a single cover to provide a reference document covering the development, verification and scoping computations done to date. This report supersedes all previous memos.

The Appendices presented in this report were written by several different authors, therefore the nomenclature is not

*The Nevada Nuclear Waste Storage Investigations Project, managed by the Nevada Operations Office of the U.S. Department of Energy, is examining the feasibility of siting a repository for high-level nuclear wastes at Yucca Mountain on and adjacent to the Nevada Test Site. This work was funded in part by the NNWSI Project. The ultimate use of this information will be to develop appropriate criteria for design of subsurface facilities.

always consistent. In particular, the Richards equation is referred to in Appendix C, D, and E. The forms given are:

Appendix C, page 3:

$$\frac{\partial}{\partial z}\left[K(\phi)\left(\frac{\partial \psi}{\partial z}+1\right)\right]-C(\phi)\frac{\partial \psi}{\partial t}=0 \quad ,$$

Appendix D, page 3:

$$\nabla \cdot [K(\phi)\nabla \Phi] = C(\phi)\frac{\partial \Phi}{\partial t} \quad , \text{ and}$$

Appendix E, page 1:

$$\nabla \cdot \left[\frac{k(\phi)\rho g}{\mu}\nabla \Phi\right] = \frac{\partial \theta}{\partial \phi}\frac{\partial \Phi}{\partial t} \quad .$$

All of these forms can be seen to be equivalent by using the following definitions

$$K = \frac{\rho g k}{\mu} \quad ,$$

$$\Phi = \rho g(\phi + z) \quad , \text{ and}$$

$$C = \frac{\partial \theta}{\partial \phi}$$

These terms are discussed in more detail in the Appendices. One additional form of the flow equation is given in Appendix A, page 9. By neglecting the Soret effect ($D \equiv 0$) and the Boussinesq approximation ($\beta \equiv 0$) it can easily be seen that this equation is equivalent to the others. The original memorandums often referred to the finite element code MARIAH/UNSAT. This code has officially been given the name SAGUARO.

It will be observed that the one-dimensional infiltration problem has been addressed in several of the Appendices. Each solution addresses a different purpose. Some solutions are used to compare codes, others are used to evaluate various types of boundary conditions.

SUMMARY OF DEVELOPMENTAL STUDIES

Modeling Development

An outline of the derivation of the partially saturated flow equations is presented in Appendix A. This analysis draws on the continuum theory of multiphase mixtures and provides the foundation for the partial differential equations for mass flux and energy transport used in SAGUARO.

Solving for water flow through partially saturated regions poses special requirements regarding the applied boundary conditions and material property characterization. Appendix B gives a detailed outline of the SAGUARO input data requirements including those for the non-linear material curves.

Discretization and Code Verification

Appendix C presents the derivation of the finite difference and finite element methods of discretization for one-dimensional unsaturated porous media flow equations. Results obtained from these methods are presented, for comparison purposes, in Appendix D. Appendix D provides additional comparisons and summarizes the "current" status of computational capabilities for predicting energy and mass flux through partially saturated porous media. The isothermal version of the equations is of primary concern in this memo.

Results obtained from three non-related codes are presented for the classical one-dimensional infiltration problem. All results agree well with the SAGUARO code.

The material characteristic curves for permeability and moisture content are extremely nonlinear in unsaturated portion of the media. Appendix E outlines a method for obtaining material characteristic curves using experimental mercury intrusion data. The resulting nonlinear curves were used in SAGUARO to compute the time-dependent saturation in a 15 cm long core of tuff rock during an imbibition experiment. These computed saturation curves were found to be in good agreement with experimentally obtained data.

Scoping Calculations

Appendices F and G present the results of various scoping studies. The importance of using good characteristic curves is discussed in Appendix F. The curves were shifted parametrically to show how the calculated pore pressure and moisture content results for one-dimensional infiltration are a strong function of the assumed material characteristic curves and the applied boundary and initial conditions. The effect of short-term, surface water fluctuations on pore-water is discussed in Appendix G. It is concluded from these results that the short-term annual fluctuations in the applied ground surface boundary condition (rain) has no effect at repository level (depth $\simeq$ 100 m). This is an important result in that by neglecting these short-term boundary fluctuations the cost of computing typical results is appreciably reduced.

CONCLUSIONS

The studies compiled in this report give a comprehensive overview of the development history of SAGUARO. These studies give insight into the extent of the code capabilities and background into code usage. Several Appendices stress the significance of material characteristic curves. Future work will be done in the area of code application and verification. One of these areas will include the investigation of the importance of fluid vapor transport. Another is the coupling of the FEMWASTE (species transport code) to SAGUARO. It is also becoming evident that the flow through fractures may be important. Therefore the code capabilities to handle discrete fractures and statistically distributed fractures will be expanded.

REFERENCES

1. R. R. Eaton, D. K. Gartling and D. E. Larson, "SAGUARO -- A Finite Element Computer Program for Partially Saturated Porous Flow Problems," SAND82-2772, Sandia National Laboratories, Albuquerque, New Mexico, November, 1982.
2. D. K. Gartling and C. E. Hickox, "MARIAH -- A Finite Element Computer Program for Incompressible Porous Flow Problems: Theoretical Background," SAND79-1622, Sandia National Laboratories, Albuquerque, New Mexico, September, 1982.

3. D. K. Gartling and C. E. Hickox, "MARIAH -- A Finite Element Computer Program for Incompressible Porous Flow Problems," SAND79-1623, Sandia National Laboratories, Albuquerque, New Mexico, August, 1980.

Sandia National Laboratories
Albuquerque, New Mexico 87185

APPENDIX A

date: June 28, 1982

to: L. D. Tyler, 9762

from: R. K. Wilson and J. W. Nunziato, 5511

subject: Derivation of the Partially Saturated Flow Equations Utilized in the Finite Element Code SAGUARO

Introduction

As part of DOE's National Waste Terminal Storage (NWTS) Program, serious consideration is being given to the storage of commercially-generated nuclear waste in tuff at the Nevada Test Site (NTS). Current plans are to locate the repository at Yucca Mountain near the western boundary of NTS in one of four stratigraphic horizons. In order to determine whether these geological formations will provide an adequate barrier for long term, nuclear waste storage, it is important to develop an understanding of the groundwater motion through the candidate horizons and evaluate radionuclide retention in the rock as well as the travel times for nuclide transport to the biosphere. The processes involved are generally quite complex and are only further complicated by the fact that two of the horizons lie above the water table and hence represent partially saturated zones.

In this work, we will focus on the hydrological models for flow through porous media.* For the tuff horizons being

*The physics of radionuclide transport can generally be analyzed separately from the hydrology and will not be treated here.

considered, this represents modeling problems which extend far beyond classical Darcy's law. The porous medium may be either saturated or partially saturated and, due to the heat release from the decay of the waste, is subject to non-isothermal conditions. In partially saturated media, capillary forces are also expected to have a significant influence on pore water motion.

Our purpose here is to outline the derivation of the equations governing pore water motion and energy transport in saturated and partially saturated porous media, as we currently understand it.* These transport equations are the equations which are being solved in the two-dimensional, finite element code SAGUARO.

Definitions

We wish to model the flow of an incompressible fluid in a rigid porous medium, including the effects of heat transfer and the presence of air. Let n denote the (constant) connected porosity and let ϕ_a represent the volume fraction of the mobile constituent a (a = 1 for the liquid water and a = 2 for the air). Dimensionally, ϕ_a is the ratio of the volume of the mobile constituent to the total volume. The saturation s_a of constituent a is defined by

$$s_a = \frac{\phi_a}{n} \tag{1}$$

*A more complete derivation of these equations is given in reference [1].

and, clearly, all the pore volume is occupied so that

$$s_1 + s_2 = 1 \quad . \tag{2}$$

The densities of the constituents are denoted by ρ_a (a = 1,2) and ρ_s represents the (constant) rock mass grain density.

The fluid and the air are assumed to move through the porous medium with the velocities $\underset{\sim}{v}_a$. The corresponding Darcy velocity is given by*

$$\underset{\sim}{u}_a = n\, s_a\, \underset{\sim}{v}_a \quad . \tag{3}$$

Conservation Equations

We require the partially saturated rock system to satisfy the conservation equations for mass, momentum, and energy. For the mobile constituents, conservation of mass, momentum, and energy can be expressed as

$$n \frac{\partial (\rho_a S_a)}{\partial t} + \nabla \cdot (\rho_a \underset{\sim}{u}_a) = 0 \quad , \tag{4}$$

$$\nabla \cdot \underset{\sim}{\sigma}_a + n\, s_a\, \rho_a\, \underset{\sim}{b}_a + \underset{\sim}{m}_a^+ = 0 \, , \tag{5}$$

$$n\, s_a\, \rho_a \frac{\partial e_a}{\partial t} + \rho_a \underset{\sim}{u}_a \cdot \nabla e_a = - \nabla \cdot \underset{\sim}{q}_a + Q_a + e_a^+ \quad , \tag{6}$$

where ∇ is the gradient with respect to the spatial coordinates $\underset{\sim}{x}$, $\underset{\sim}{\sigma}_a$ is the symmetric partial stress tensor for each

*The underscore ~ indicates the quantity is either vector- or tensor-valued.

constituent, $\underset{\sim}{b}_a$ is the external body force vector due to gravity, $\underset{\sim}{m}_a^+$ is the momentum exchange vector between the mobile constituents and between the constituents and the solid rock mass, e_a is the internal energy (energy per unit mass), $\underset{\sim}{q}_a$ is the heat flux vector, Q_a is the external heat supply as a result of heat sources (total energy per unit time), and e_a^+ is the energy exchanged between the constituents and with the rock mass. In writing (5) and (6), we have assumed that inertial forces and the mechanical work done by the stress $\underset{\sim}{\sigma}_a$ and the momentum exchange $\underset{\sim}{m}_a^+$ are negligible. However, (6) does include convective energy transport.

For the rock mass, we have the energy equation

$$(1-n)\rho_s \frac{\partial e_s}{\partial t} = - \nabla \cdot \underset{\sim}{q}_s + Q_s - (e_1^+ + e_2^+) \quad . \tag{7}$$

In this analysis, we account for the buoyant motion of fluid resulting from temperature gradients through the usual Boussinesq approximation. Thus, the densities ρ_a are assumed to be constants ($\overset{o}{\rho}_a$) in every equation except in the momentum equations (5), where they are expressed as

$$\rho_a = \overset{o}{\rho}_a \left(1 - \beta_a \left(T - \overset{o}{T}\right)\right) . \tag{8}$$

The parameter β_a is the thermal expansion coefficient and $\overset{o}{T}$ is the reference temperature. In view of this assumption, conservation of mass and momentum, (4) and (5), can be written as

$$n \frac{\partial s_a}{\partial t} + \nabla \cdot \underset{\sim}{u}_a = 0 \tag{9}$$

$$\nabla \cdot \underset{\sim}{\sigma}_a + n\, s_a \overset{o}{\rho}_a \left(1 - \beta_a \left(T - \overset{o}{T}\right)\right) \underset{\sim}{b}_a + \underset{\sim}{m}_a^+ = 0 \tag{10}$$

Finally, we note that since we are dealing with a system in which all constituents are in thermal equilibrium, it is convenient to compute the temperature T from the total energy equation resulting from combining (6) and (7):

$$\begin{aligned} n \left(s_1 \rho_1 \frac{\partial e_1}{\partial t} + (1-s_1)\rho_2 \frac{\partial e_2}{\partial t} \right) + (1-n)\rho_s \frac{\partial e_s}{\partial t} \\ + \rho_1 \underset{\sim}{u}_1 \cdot \nabla e_1 + \rho_2 \underset{\sim}{u}_2 \cdot \nabla e_2 \\ = - \nabla \cdot (\underset{\sim}{q}_1 + \underset{\sim}{q}_2 + \underset{\sim}{q}_s) + Q \end{aligned} \tag{11}$$

where the total heat supply Q is

$$Q = Q_1 + Q_2 + Q_3 \quad .$$

Derivation of the Flow Equation

The equation for the balance of momentum of constituents can be expanded by writing constitutive equations for the partial stress $\underset{\sim}{\sigma}_a$ and the momentum exchange $\underset{\sim}{m}_a^+$. The partial stress of constituent a is assumed to be hydrostatic and we write

$$\underset{\sim}{\sigma}_a = - n\, s_a\, p_a\, \underset{\sim}{1} \tag{12}$$

where p_a is the gauge pressure of constituent a. Momentum exchange occurs through three mechanisms*: (1) momentum exchange resulting from the forces acting on the fluid due to the presence of the air, (2) momentum exchange due to thermal diffusion (Soret effect [2]) and (3) momentum exchange to a given constituent due to resistance against the solid. As a result of these three mechanisms, the constitutive equation for $\underset{\sim}{m}_a^+$ has the form

$$\underset{\sim}{m}_a^+ = p_a \nabla(n\, s_a) + n\, s_a\, \underset{\sim}{W}_a\, \frac{\nabla T}{T} - \underset{\sim}{R}_{as}\, \underset{\sim}{v}_a \quad , \tag{13}$$

where $\underset{\sim}{W}_a$ is a tensor with constant value reflecting the thermal contributions to mass flux and $\underset{\sim}{R}_{as}$ is a tensor whose components are the resistivities resulting from the drag of constituent a on the solid. These are tensor valued quantities to account for anisotropic properties of the porous rock.

It is assumed that the only body forces acting on constituent a result from gravitational effects so that we can write

$$\underset{\sim}{b}_a = - g\, \nabla z \quad , \tag{14}$$

where g is the gravitational constant and Z is the elevation measured from a reference point. Substitution of (12) - (14) into (10) thus gives

$$\underset{\sim}{R}_{1s}\, \underset{\sim}{v}_1 = - n\, s_1\, \nabla p_1 - n s_1\, \mathring{\rho}_1 [1-\beta_1 (T-\mathring{T})]\, g \nabla z + n\, s_1 \underset{\sim}{W}_1\, \frac{\Delta T}{T} \tag{15}$$

*A fourth mechanism, resistance between the fluid and air phase, is negligible.

$$\underset{\sim}{R}_{2s}\ \underset{\sim}{v}_2 = -\ n\ s_2\ \nabla p_2 - n s_2\ \overset{o}{\rho}_2[1-\beta_2(T-\overset{o}{T})]\ g\nabla z + n\ s_2 \underset{\sim}{W}_2\ \frac{\nabla T}{T} \quad . \quad (16)$$

Further assumptions are made concerning the air phase. First, gravitational effects are assumed to make negligible contributions to the motion of the air. Second, the air is assumed to escape freely so that the resistance between the air and solid is small ($\underset{\sim}{R}_{2s} \approx 0$). Third, the effects of thermal gradients on the motion of the air are negligible ($\underset{\sim}{W}_2 = 0$). As a result, (16) reduces to

$$\nabla p_2 = 0 \quad . \quad (17)$$

Since the pressure of the air at the boundary is atmospheric and since p_a is always measured as gauge pressure, it follows that $p_2 = 0$.

The momentum equation for the fluid phase (15) leads to Darcy's law with thermal effects added; that is,

$$\underset{\sim}{u}_1 = -\ \left\{ \frac{\underset{\sim}{\kappa}_1}{\mu_1} \nabla\Phi + \overset{o}{\rho}_1 g \underset{\sim}{D}_1\ \nabla T - \frac{\underset{\sim}{k}_1}{\mu_1}\ \overset{o}{\rho}_1 \beta_1 g(T-\overset{o}{T})\nabla z \right\} \quad , \quad (18)$$

where

$$\underset{\sim}{k}_1 = (ns_1)^2 \mu_1\ \underset{\sim}{R}_{1s}^{-1} \quad , \quad (19)$$

$$\underset{\sim}{D}_1 = \frac{(ns_1)^2}{\overset{o}{\rho}_1 gT}\ \underset{\sim}{W}_1\ \underset{\sim}{R}_{1s}^{-1} \quad , \quad (20)$$

are the intrinsic permeability tensor and the thermal diffusion tensor (due to the Soret effect), respectively, μ_1 is the fluid viscosity, and

$$\Phi = p_1 + \overset{o}{\rho}_1 g z \tag{21}$$

is the hydraulic head. In addition to the gauge pressure p_1 and the hydraulic head, there are two other measures of pressure. They are the pressure head, ψ, defined by

$$\psi = \frac{p_1}{\overset{o}{\rho}_1 g} \tag{22}$$

and the capillary pressure P_c which, in the absence of air pressure, is defined by

$$P_c = - p_1 = - \overset{o}{\rho}_1 g \psi \ . \tag{23}$$

Recalling the equations for balance of mass, we have

$$n \frac{\partial s_1}{\partial t} = - \nabla \cdot \underset{\sim}{u}_1 \ , \tag{24}$$

for the water phase, and (noting from (2) that $\frac{\partial s_2}{\partial t} = - \frac{\partial s_1}{\partial t}$)

$$\nabla \cdot \underset{\sim}{u}_2 = n \frac{\partial s_1}{\partial t} \ . \tag{25}$$

for the air phase. The latter equation determines the flux of air escaping the porous medium.* Substitution of (18) into (24) yields

$$n \frac{\partial s_1}{\partial t} = \nabla \cdot \left\{ \frac{\underset{\sim}{k}_1}{\mu_1} \nabla \Phi + \overset{o}{\rho}_1 g \underset{\sim}{D}_1 \nabla T - \frac{\underset{\sim}{k}_1}{\mu_1} \overset{o}{\rho}_1 \beta_1 g (T - \overset{o}{T}) \nabla z \right\} \ . \tag{26}$$

*The flux of air escaping is not a quantity computed in SAGUARO.

The capillary pressure is known to be a function of the liquid saturation [3]* so that partial differentiation of (23) with respect to time yields

$$\frac{\partial s_1}{\partial t} = - \frac{\partial s_1}{\partial P_c} \frac{\partial p_1}{\partial t} \quad , \tag{27}$$

or

$$n \frac{\partial s_1}{\partial t} = \frac{n}{\overset{o}{\rho}_1 g} \frac{ds_1}{d\psi} \frac{\partial \Phi}{\partial t} \tag{28}$$

The quantity $n(ds_1/d\phi)$ is referred to as the specific moisture capacity $C(\phi)$.

Substitution of (28) into (26) yields as a final result

$$C(\psi) \frac{\partial \Phi}{\partial t} = \nabla \cdot (\underset{\sim}{K}_1 \nabla \Phi + \underset{\sim}{D}_1 \nabla T) - \nabla \cdot (\underset{\sim}{K}_1 \overset{o}{\rho}_1 \beta_1 g (T - \overset{o}{T}) \nabla z) \tag{29}$$

where

$$\underset{\sim}{K}_1 = \frac{\overset{o}{\rho}_1 g}{\mu_1} \underset{\sim}{k}_1 \quad , \tag{30}$$

is the hydraulic conductivity. Typically, the specific moisture capacity and hydraulic conductivity are determined experimentally and put into SAGUARO in the form of the characteristic curves shown in Figure 1.

* The liquid saturation s_1 is often referred to as the moisture content θ.

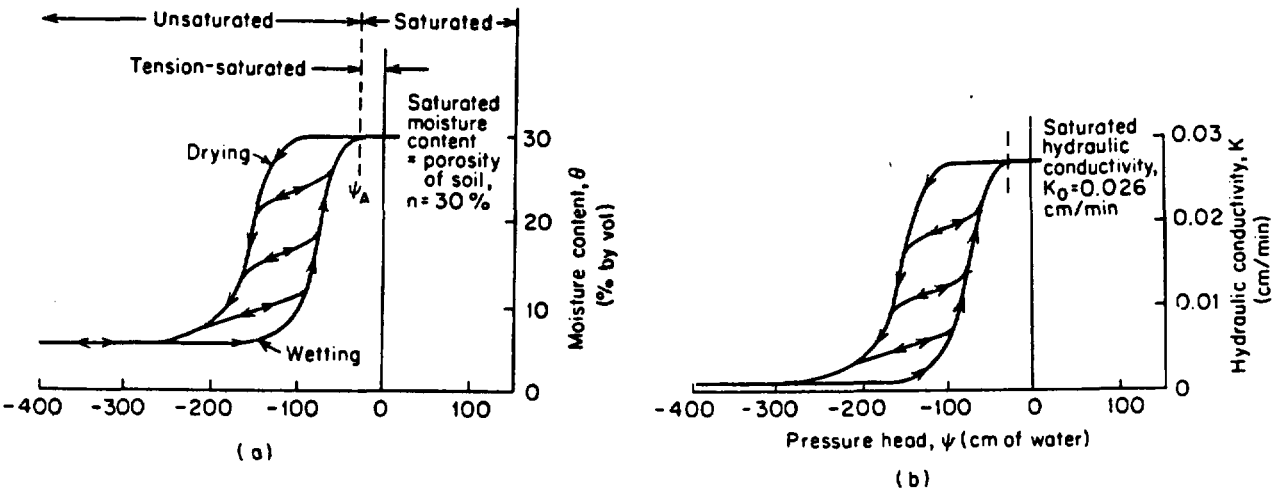

FIGURE 1. Material Characteristic Curves

Because the moisture capacitance and the hydraulic conductivity are dependent on the pressure head, equation (29) is a highly nonlinear partial differential equation. In the absence of thermal effects, this equation is identical to Richard's equation. It is important to note that in regions that are saturated, the moisture capacitance is zero so that (29) reduces from a parabolic flow equation to the usual elliptic equation that models flow through saturated media. Thus, equation (29) is applicable to both saturated and partially saturated flow problems.

The Energy Equation

The energy equation in SAGUARO is obtained from (11) by writing constitutive equations for the heat flux and the internal energy of the fluid, air, and solid constituents;

$$\underset{\sim}{q}_a = - \underset{\sim}{\lambda}_a \nabla T \; ; \; \underset{\sim}{q}_s = - \underset{\sim}{\lambda}_s \nabla T \quad , \tag{31}$$

$$e_a = \overset{o}{e}_a + C_{pa}\,(T-\overset{o}{T}) \;;\; e_s = \overset{o}{e}_s + C_{ps}\,(T-\overset{o}{T}) \;, \qquad (32)$$

where $\underset{\sim}{\lambda}_a$ and C_{pa} are the thermal conductivity tensor and constant heat capacity of constituent a, respectively. Substitution of (31) and (32) into the total energy balance equation (11) yields

$$(\rho C_p)^*_{eff}\,\frac{\partial T}{\partial t} + (\rho_1 C_{p1}\underset{\sim}{u}_1 + \rho_2 C_{p2}\underset{\sim}{u}_2)\cdot\nabla T = \nabla\cdot(\underset{\sim}{\lambda}^*_{eff}\,\nabla T) + Q \;, \qquad (33)$$

where

$$(\rho C_p)^*_{eff} = ns_1\rho_1 C_{p1} + n(1-s_1)p_2 C_{p2} + (1-n)\rho_s C_{ps} \;, \qquad (34)$$

$$\underset{\sim}{\lambda}^*_{eff} = \underset{\sim}{\lambda}_1 + \underset{\sim}{\lambda}_2 + \underset{\sim}{\lambda}_3 \;, \qquad (35)$$

are the heat capacity and thermal conductivity tensor for the mixture. To reach the final form of the energy equation,

(i) the heat content of the air is assumed to be small ($\rho_2 C_{p2} \approx 0$)

(ii) the conductivity of the air is assumed to be small ($\underset{\sim}{\lambda}_2 \approx 0$)

(iii) $\underset{\sim}{\lambda}_1$ is written as the difference between the effective thermal conductivity of the fluid and the contribution due to thermal dispersion in the fluid. If $\underset{\sim}{E}$ is the thermal dispersion tensor, $\underset{\sim}{\lambda}_1 = \underset{\sim}{\lambda}_{1_{eff}} - ns_1\,\underset{\sim}{E}$.

As a result, (33) becomes

$$(\rho C_p)_{eff} \frac{\partial T}{\partial t} + \rho_l C_{pl} \underset{\sim}{u}_l \cdot \nabla T = \nabla \cdot ([\underset{\sim}{\lambda}_{eff} - ns_l \underset{\sim}{E}] \nabla T) + Q \quad , \qquad (36)$$

where

$$(\rho C_p)_{eff} = ns_l \rho_l C_{pl} + (1-n) \rho_s C_{ps} \quad , \qquad (37)$$

$$\underset{\sim}{\lambda}_{eff} = \underset{\sim}{\lambda}_{l_{eff}} + \underset{\sim}{\lambda}_s \quad . \qquad (38)$$

This form of the energy equation (36) is sufficiently general to permit the inclusion of various models for the thermal conductivities $\underset{\sim}{\lambda}_{l_{eff}}$ and $\underset{\sim}{\lambda}_s$ which may depend on saturation s_l.

It is useful to note the nonlinear character of the energy equation and its relation to the characteristic curves. In particular, all the coefficients of (36) can be functions of the temperature. In addition, the dependence of the effective heat capacity $(\rho C_p)_{eff}$ (and possibly $\underset{\sim}{\lambda}_{eff}$) on saturation, s_l, implies a dependence on the hydraulic head Φ. Clearly, then, equations governing the pore pressure (29) and energy transport (36) are coupled. Together, (29) and (36) determine the hydraulic head Φ and the temperature T. The corresponding velocity field for the water $\underset{\sim}{u}_l$ is computed from (18). These are the equations solved in SAGUARO.

References

[1] Wilson, R. K., McTigue, D. F., and Nunziato, J. W., Flow in Partially Saturated Porous Media, Sandia National Laboratories, Report No. SAND82-2349 (1983).

[2] Bird, R. B., Stewart, W. E. and Lightfoot, E. N., Transport Phenomena, John Wiley & Sons, Inc., New York (1960).

[3] Bear, J., Dynamics of Fluids in Porous Media, American Elsevier, New York (1972).

RKW:JWN:5511:fvc

Copy to:

5500 J. K. Galt (Actg.)
5510 D. B. Hayes
5511 R. R. Eaton
5511 G. R. Hadley
5511 M. J. Martinez
5512 D. F. McVey
5513 D. W. Larson
5520 T. B. Lane
5530 W. Herrmann
5540 J. K. Galt (Actg.)
9762 P. Brannon
9762 N. Hayden
5511 J. W. Nunziato
5511 R. K. Wilson

Sandia National Laboratories

Albuquerque, New Mexico 87185

date: July 13, 1982

APPENDIX B

to: L. D. Tyler, 9762

from: R. K. Wilson, R. R. Eaton, M. J. Martinez, 5511

subject: Field and Laboratory Data Requirements for Implementing Computational Flow Field Codes

This memo summarizes the data requirements necessary for the application of existing numerical codes (thermal, hydrologic and species transport) for modeling hypothetical nuclear waste repositories at the Nevada Test Site (NTS). This required data would most likely be obtained through a combination of laboratory and field testing.

The memo is arranged in two sections:

(1) A general description of code input requirements, and

(2) A specific list of required parameters for the thermal code COYOTE [1]; the hydrological/thermal codes COYOTE/UNSAT [2], MARIAH [3,4] and SAGUARO [5]; and the species transport code FEMWASTE [6].

I. GENERAL THERMAL-HYDROLOGICAL PROBLEMS

The data needed to solve general hydrologic and thermal problems occurs as one of three types: (i) geometric, (ii) boundary and initial conditions and (iii) material properties.

(i) GEOMETRY

The solution of problems requires an accurate description of site geometry, stratigraphy and repository dimensions. Specifically,

A. The areal dimensions of the problem must be specified including the cross sections to be modeled.

B. Details of the specific stratigraphy: thickness of the layers, offset of layers due to faulting and location of perched water supplies or large void pockets.

C. The geometry of fault zones and fractures of which there are two types: (1) Large, highly permeable "zones" which are modeled discretely. These fault zones act as sources, sinks, highly transmissive paths and even barriers to fluid flow. The important geometric parameters are the location, length, thickness and dip of these zones. (2) Heterogeneous fracturing. This kind of fracture is interspersed in the material and has the effect of creating anisotropic behavior with respect to permeability and conductivity but is not significant enough to warrant discrete modeling. The spacing, orientation and aperture of these fractures is important in determining the effect on the material properties of the rock and the density and spacing of groups of these fractures is also needed for detailed modeling.

D. Location of the water table. It is essential to know the location of the water table to determine whether or not a saturated or unsaturated code is to be used. It is also important to know the time dependency of the location (changes due to rainfall and groundwater recharge).

E. Finally, accurate dimensions of access tunnels and adits, torpedo tubes or storage rooms, and other man-made changes to the site are needed to accurately predict repository behavior.

(ii) BOUNDARY AND INITIAL CONDITIONS

A. Boundary conditions: A determination should be made of the distribution of (1) fluid pressure, (2) water flux, (3) temperature, (4) heat flux and (in the case of partially saturated zones) (5) moisture content across all boundaries. It is also important to consider the time dependency of these distributions. Examples where this is important are in rainfall vs. time distributions at the surface, heat generation and/or heat flux of waste canisters and flow conditions such as changes in subsurface groundwater flow or air cooling of adits and rooms during the construction phase. It is also important to accurately determine which species are released from the waste canisters and at what concentrations or rates.

B. Initial Conditions: (1) SATURATED ZONE. It is necessary to obtain spatial distributions of PRESSURE, TEMPERATURE and SPECIES CONCENTRATION (2) UNSATURATED ZONE. It is necessary to obtain spatial distributions of MOISTURE CONTENT, TEMPERATURE and SPECIES CONCENTRATION.

(iii) MATERIAL PROPERTIES

A. ROCK

(1) Saturated Zone: (a) density
(b) porosity (both rock and fracture)

(c) principal permeabilities and the directions they make with respect to coordinate axes (in the case that the rock contains a continuous distribution of small fractures, the orientation, spacing and aperture are needed to determine the effect on anisotropy)
(d) thermal conductivity (here again the anisotropy of the material may depend on fracturing)
(e) absorption equilibrium coefficients (some of these can be concentration dependent. In addition, the fracturing may also affect the values from point to point due to surface area effects)

(2) Unsaturated Zone:
(a) density
(b) porosity (both rock and fracture)
(c) thermal conductivity (check for anisotropic due to fracturing)
(d) adsorption equilibrium coefficients (some of these can be concentration dependent. In addition, the fracturing may also affect the values from point to point due to surface area effects)
(e) moisture content vs. pressure head curves (Figure 1)
(f) hydraulic conductivity vs. pressure head curves (Figure 2)
Figures 1 and 2 are only example characteristic curves. Specific curves for all materials being used must be specified.

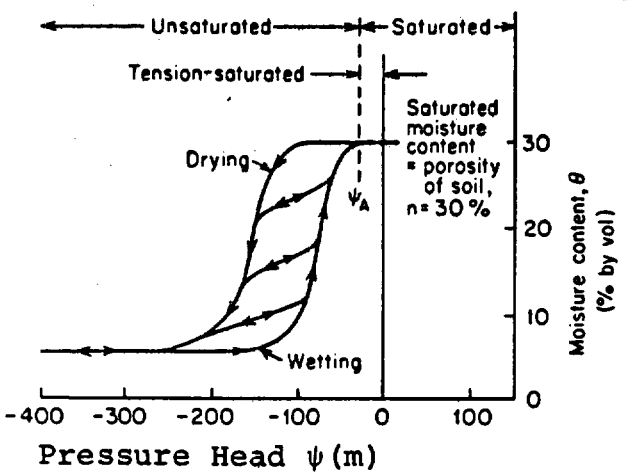

Figure 1.

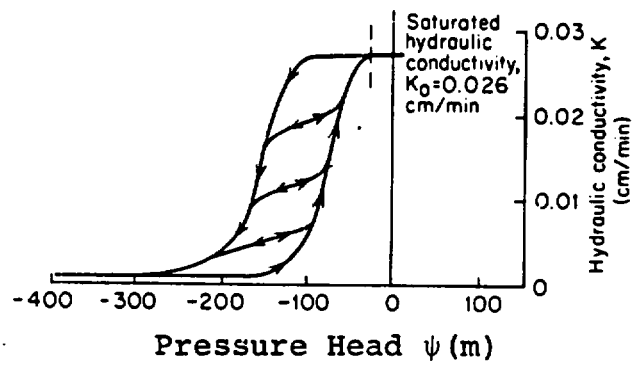

Figure 2.

(3) Fractured Zones:
- (a) permeability or hydraulic conductivity
- (b) thermal conductivity
- (c) roughness (in the case of open fractures, a detailed flow analysis might involve this quantity in determining the permeability)
- (d) does the zone act as a barrier to flow? a source? a sink? a zone of high transmissivity?
- (e) an adsorption equilibrium coefficient analogy may have to be established

NOTE! Many of the above properties may be temperature dependent. If so, the nature of the problems modeled suggest obtaining this kind of dependency.

B. WATER

Here the age of the water is a parameter which can be measured and may provide useful information. For example, if the age of the groundwater increases with depth and then suddenly decreases, this may indicate that recharge from subsurface groundwater is occuring.

II. SPECIFIC INPUT REQUIREMENTS

A. COYOTE (parabolic equation solver)

The finite element code COYOTE [1] calculates time dependent temperature fields. The following input data is required:

1. GEOMETRY (2-D): planar, axisymmetric or polar
2. BOUNDARY CONDITIONS: temperature or heat flux
3. INITIAL CONDITIONS: temperature at all spatial locations
4. MATERIAL PROPERTIES:
   - a) ρ density
   - b) c_p specific heat
   - c) K_{ij} components of thermal conductivity tensor and direction of principal axes
5. ENERGY SOURCE (for all times)

B. COYOTE/UNSAT [2]

The finite element code COYOTE can be used to calculate the isothermal head distribution in partially saturated media by providing the following input data:

1. GEOMETRY (2-D): planar, axisymmetric or polar

2. BOUNDARY CONDITIONS: pressure head [$\Phi = \rho g(\psi + z)$] or mass flux

3. INITIAL CONDITIONS: pressure head or moisture content at all spatial locations

4. MATERIAL PARAMETERS:
   a) ρ fluid density
   b) moisture content vs. pressure head (Figure 1)
   c) hydraulic conductivity vs. pressure head (Figure 2)
   d) ϕ porosity

5. SOURCE: mass source at all spatial locations and times must be specified

C. MARIAH

The finite element code MARIAH [3,4] calculates two-dimensional incompressible fluid flow through porous SATURATED media with mass and energy transfer. The following input data is required:

1. GEOMETRY (2-D): planar, axisymmetric or polar

2. BOUNDARY CONDITIONS: temperature or heat flux AND pressure or mass flux must be specified at all boundaries for all times

3. INITIAL CONDITIONS: temperatures and pressures must be specified at all spatial locations

4. MATERIAL PROPERTIES:

   (i) Rock:
   a) ρ density
   b) c_p specific heat
   c) λ_{ij} components of the thermal conductivity tensor and direction of axes (may also be specified as a function of termperature, pressure, space and time)

d) K_{ij} components of the permeability tensor and direction of axes (may also be specified as a function of temperature, pressure, space and time)

e) dispersion

f) ϕ porosity

(ii) Fluid: a) ρ density

b) μ viscosity (may be specified as a function of temperature)

c) c_p specific heat

d) λ thermal conductivity (may be specified as a function of temperature)

e) β volumetric expansion coefficient (may be specified as a function of temperature)

5. SOURCES: fluid and/or energy sources may be specified as functions of time

D. SAGUARO (previously referred informally to as MARIAH/UNSAT)

The finite element code SAGUARO [5] is a derivative of MARIAH. It is designed to calculate two-dimensional incompressible fluid flow and heat transfer in PARTIALLY SATURATED OR FULLY SATURATED porous media. SAGUARO requires all the input data for MARIAH plus the following for each material of interest:

1. Moisture content as a function of pressure head (Figure 1)

2. Permeability as a function of pressure head (Figure 2)

3. The components of the thermal mass diffusion coefficient tensor K_{ij} and directions

E. FEMWASTE

The finite element code FEMWASTE [6] models the transport of solutes through a spatially two-dimensional, saturated/unsaturated porous medium due to convection, hydrodynamic dispersion, chemical sorption and first-order radioactive decay. The input requirements for FEMWASTE are as follows on the next page:

1. GEOMETRY: planar only

2. BOUNDARY CONDITIONS: there are three types of boundary conditions accepted by FEMWASTE:

   (a) Dirichlet boundary condition: the specification of concentrations at a boundary

   $c = c_i(x,z)$ on B_1 (B_1 is a portion of B, the boundary surface)

   (b) Neumann boundary condition: the condition defined by the equation

   $-(\theta \underset{\approx}{D}\nabla c - \underset{\sim}{v}c)\cdot \underset{\sim}{n} = q_2(x,z) + (\underset{\sim}{v}\cdot\underset{\sim}{n})c$ on B_2

   (n is the outward normal to B_2)

   (c) Cauchy or mixed boundary condition combining (a) and (b):

   $-(\theta \underset{\approx}{D}\nabla c - \underset{\sim}{v}c)\cdot \underset{\sim}{n} = q_3(x,z)$ on B_3

3. INITIAL CONDITIONS: an initial concentration field must be specified for the entire domain

4. FLUID VELOCITY FIELDS: the fluid velocity field, steady-state or transient, must be computed externally to FEMWASTE and included as input data

5. PRESSURE HEAD DISTRIBUTIONS: in addition the pressure head distribution, steady-state or transient, must also be computed externally and inputed into FEMWASTE

6. MOISTURE CONTENT DISTRIBUTION: the distribution of moisture content, steady-state or transient, must be supplied as input

7. MATERIAL PROPERTIES:
   a) ρ bulk density of medium (M/L^3)
   b) ρ_f fluid density (M/L^3)
   c) α' coefficient of compressibility of the medium
   d) τ toruosity coefficient of the medium

e) ϕ porosity

f) α_L longitudinal dispersivity coefficient (L)

g) α_T transverse dispersivity coefficient (L)

h) D_m molecular diffusion coefficient (L^2/T)

i) λ_{ik} radioactive decay rate from species i to species k (T^{-1})

j) K_d equilibrium distribution coefficient (the ratio of the quantity of adsorbed material per mass of solid to the quantity of dissolved material per volume of fluid) (L^3/M)

REFERENCES

1. Gartling, D. K., COYOTE - A Finite Element Computer Program for Nonlinear Heat Conduction Problems, SAND77-1332, Sandia National Laboratories, Albuquerque, New Mexico (June 1978).

2. Eaton, R. R. and J. W. Nunziato, memo to L. D. Tyler, 4537, dated January 6, 1982, subject: Current Status of Computational Capabilities for Predicting Energy and Mass Flux Through Partially Saturated Porous Media.

3. Gartling, D. K. and C. E. Hickox, MARIAH - A Finite Element Computer Program for Incompressible Porous Flow Problems, Part I - Theoretical Background, SAND79-1622, Sandia National Laboratories, Albuquerque, New Mexico (July 1982).

4. Gartling, D. K. and C. E. Hickox, MARIAH - A Finite Element Computer Program for Incompressible Porous Flow Problems, Part II - Users Manual, SAND79-1623, Sandia National Laboratories, Albuquerque, New Mexico (August 1980)

5. Eaton, R. R., et. al., SAGUARO - Finite Element Computer Program for Partially Saturated Porous Flow Problems, SAND82- , Sandia National Laboratories, Albuquerque, New Mexico (July 1982).

6. Yeh, G. T. and D. S. Ward, FEMWASTE: A Finite Element Model of Waste Transport Through Saturated/Unsaturated Porous Media, Publication No. 1462, Environmental Sciences Division, Oak Ridge National Laboratories, Oak Ridge, Tennessee (April 1981).

Copy to:
5500 J. K. Galt (Actg.)
5510 D. B. Hayes
5511 J. W. Nunziato
5511 D. K. Gartling
5512 D. F. McVey
5513 D. W. Larson
5520 T. B. Lane
5521 R. K. Thomas
5530 W. Herrmann
5540 J. K. Galt (Actg.)
9760 R. W. Lynch
9761 L. W. Scully
9762 P. Brannon
9762 N. Hayden
9762 J. K. Johnstone
9762 R. L. Link
9763 J. R. Tillerson
9764 R. C. Lincoln
5511 R. K. Wilson
5511 R. R. Eaton
5511 M. J. Martinez

APPENDIX C

Sandia National Laboratories

Albuquerque, New Mexico 87185

date: January 13, 1982

to: Distribution

from: R. R. Eaton, 5511

subject: The highly nonlinear equations describing one-dimensional infiltration of water through unsaturated media are solved using both the Crank Nickelson finite difference scheme and the Galerkin finite element technique. It is shown that by linearizing the equations, the two techniques yield identical results.

RRE:5511:fvc

Distribution:
4530 R. W. Lynch
4537 R. M. Zimmerman
4537 D. R. Fortney
4537 R. Shaw
4537 A. R. Lappin
4537 L. D. Tyler
4537 J. K. Johnstone
5500 O. E. Jones
5510 D. B. Hayes
5511 J. W. Nunziato
5511 D. K. Gartling
5511 C. E. Hickox
5511 G. R. Hadley
5511 M. J. Martinez
5512 D. F. McVey
5512 F. G. Blottner
5513 D. W. Larson
5521 R. D. Krieg
5521 C. M. Stone
5521 R. K. Thomas
5522 R. P. Rechard
5522 R. K. Wilson
5532 B. M. Butcher
5532 W. A. Olson
5541 W. C. Luth
5511 R. R. Eaton

NOMENCLATURE

A	Coefficient for tridiagonal matrix	(1/min)
B	Coefficient for tridiagonal matrix	(1/min)
$c(\psi)$	Derivative of moisture content	(1/cm)
C	Coefficient for tridiagonal matrix	(1/min)
D	Coefficient for tridiagonal matrix	(1/min)
J	Maximum number of j mesh points	(ND)
$K(\psi)$	Hydraulic conductivity	(cm/min)
L	Length	cm
N	Coefficient for basis function	(ND)
Q	Flow-through rate at bottom boundary	(cm/min)
R	Rain rate at upper boundary	(cm/min)
t	Time	min
z	Vertical coordinate	cm
Δ	Increment in time or space	(ND)
θ	Moisture content	(ND)
ψ	Pressure head $\psi = P/\rho g$	(cm)
w	Implicit/explicit weighting factor	(ND)
z	Vertical spatial coordinate	(cm)

Subscripts:

i, j, n, s Spatial coordinate see Figure 1

Superscripts:

n	Time indicator
t	Transpose
-	Current time step minus one

INTRODUCTION

To date, the majority of the analysis done in support of the design of a nuclear waste repository in tuff have been made assuming the rock is fully saturated. The focus of the computational effort is now being shifted from saturated to unsaturated media because of the possibility of locating the waste repository above the water table.

In an initial attempt to understand the characteristics of unsaturated flow, the current study was made in which the time-dependent equations describing isothermal, one-dimensional flow of water through a non-, partially- or fully-saturated media have been solved using two basically different computational methods. The first method uses a weighted implicit/explicit finite difference scheme. The spatial derivatives are centered in space and a forward difference in time is used. The resulting tri-diagonal matrix is solved using Taylor's method which gives a time dependent pressure head and moisture content for all spatial coordinates. These same equations are solved using Galerkin's weighted residual finite element method. The solutions obtained from both methods are compared with published results.

Finite Difference Method

The basic equation for the isothermal flow of water through a partially saturated media ($0 \leq$ saturation ≤ 1) as given by Freeze and Cherry[1] is:

$$\frac{\partial}{\partial z}\left[K(\psi)\left(\frac{\partial \psi}{\partial z}+1\right)\right]-c(\psi)\frac{\partial \psi}{\partial t}=0 . \qquad (1)$$

Equation 1 is commonly referred to as the Richards equation. It simulates the Darcy type flow of a fluid through a porous media which is not necessarily fully saturated. The coefficient K and c are strong functions of the pressure head ψ. The presence of air in the formation is neglected. This essentially says that any trapped air can always escape a partially saturated zone without influencing the flow of the fluid.

Using Darcy's law[1], the boundary mass flux conditions can be expressed as

$$\frac{\partial \psi}{\partial z}=\frac{R}{K(\psi)}-1 \qquad \text{at } z=Z_{max} \qquad (2)$$

and

$$\frac{\partial \psi}{\partial z}=\frac{Q}{K(\psi)}+1 \qquad \text{at } z=Z_{min}. \qquad (3)$$

These boundary conditions allow the user to specify the liquid influx at the top and bottom boundaries. Using the grid given in Figure 1, the equivalent finite difference expression can be written as

$$\frac{1}{\Delta z}\left\{K_n\left(1+\frac{1}{\Delta z}\left[w(\psi_{j+1}^{n}-\psi_j^{n})+(1-w)(\psi_{j+1}^{n-1}-\psi_j^{n-1})\right]\right)\right.$$
$$\left.-K_s\left(1+\frac{1}{\Delta z}\left[w(\psi_j^{n}-\psi_{j-1}^{n})+(1-w)(\psi_j^{n-1}-\psi_{j-1}^{n-1})\right]\right)\right\}$$
$$-\frac{c_j^{n+\frac{1}{2}}}{\Delta t}(\psi_j^{n}-\psi_{j-1}^{n-1})=0 \qquad (4)$$

This general equation

$$-A_j\psi^n_{j-1} + B_j\psi^n_j - C_j\psi^n_{j+1} = D_j \qquad (5)$$

can be represented by the following matrix equation:

$$
\begin{vmatrix}
B_2 & -C_2 & & & & \\
-A_3 & B_3 & -C_3 & & & \\
 & & & & & \\
 & & -A_j & B_j & -C_j & \\
 & & & & & \\
 & & & & -A_{J-1} & B_{J-1}
\end{vmatrix}
\begin{vmatrix}
\psi_2 \\ \psi_3 \\ \cdot \\ \cdot \\ \cdot \\ \psi_j \\ \cdot \\ \cdot \\ \cdot \\ \cdot \\ \psi_{J-1}
\end{vmatrix}
=
\begin{vmatrix}
D_2 + A_2 \\ D_3 \\ \cdot \\ \cdot \\ \cdot \\ D_j \\ \cdot \\ \cdot \\ \cdot \\ \cdot \\ D_{J-1} + C_{J-1}
\end{vmatrix}
$$

where the coefficients for $2 < j < J-1$ are given by

$$A_j = - K_s w/\Delta z \quad , \tag{6}$$

$$B_j = - (K_n + K_s)w/\Delta z - \Delta z c_j^{n-1}/\Delta t \quad , \tag{7}$$

$$C_j = - K_n w/\Delta z \quad , \tag{8}$$

$$D_j = - K_n[1 + (1-w)(\psi_{j+1}^{n-1} - \psi_j^{n-1})]/\Delta Z$$

$$+ K_s[1 + (1-w)(\psi_j^{n-1} - \psi_{j-1}^{n-1})]\Delta Z$$

$$- \Delta z c_j^{n+1/2} \phi_j^{n-1}/\Delta t \quad , \tag{9}$$

$$\text{and } K_n = (K_{j+1} + K_j)/2.0 \quad , \tag{10}$$

$$K_s = (K_j + K_{j-1})/2.0 \tag{11}$$

At the boundaries $\phi_1 + \phi_j$ are obtained from the boundary conditions (2) and (3).

$$\psi_1 = (\frac{Q}{K_s} - 1)\Delta Z \tag{12}$$

$$\psi_j = (\frac{R}{K_n} + 1)\Delta Z \tag{13}$$

Finite Element Method

Equation 4 is also solved using Galerkin's orthogonalization method of weighted residuals which can be expressed for the infiltration problem as

$$\int_0^{Zmax} [N]^t \left(\frac{\partial}{\partial z} \left[K(\psi) \left(\frac{\partial \psi}{\partial z} + 1 \right) \right] - c(\psi) \frac{\partial \psi}{\partial t} \right) dz = 0 \qquad (14)$$

where $[N]^t$ is a column vector composed of the coefficients of the basis or weighting function. The details of this weighted residual solution methods is given by Segerlind[2].

The interpolating function ϕ, used to approximate ψ, K and c is defined over a single element and therefore Equation 14 may be written in terms of a summation over all elements.

$$\sum_{e=1}^{R} \int_{\Delta z} \left[N^e \right]^t \left(\frac{\partial}{\partial z} \left[K(\psi) \left(\frac{\partial \psi}{\partial z} + 1 \right) \right]^e - c(\psi) \frac{\partial \psi^e}{\partial t} \right) dz = 0 \quad . \qquad (15)$$

It is assumed that ψ, K and c can be approximated by expansions. The basis function or shape function for this problem will be assumed to be linear and of the general form

$$\phi = N_i \phi_i + N_j \phi_j = \left[\left(1 - \frac{z}{L} \right), \frac{z}{L} \right] \begin{Bmatrix} \phi_i \\ \phi_j \end{Bmatrix} = [N^e] \{ \phi \} \qquad (16)$$

where $\phi = \psi$, c, or K and $\Delta Z = Z_j - Z_i$.

The order of Equation 15 is reduced to first order by performing an integration by parts (Green's theorem) on the first term.

$$\int [N]^t \frac{\partial}{\partial z} \left[K(\psi) \frac{\partial \psi}{\partial z} + 1 \right] dz$$

$$= [N]^t K(\psi) \left(\frac{\partial \psi}{\partial z} + 1 \right) \Big|_i^j - \int \frac{\partial [N]^t}{\partial z} K(\psi) \left(\frac{\partial \psi}{\partial z} + 1 \right) dz \qquad (17)$$

Insert Equation 16 and 17 into Equation 15 and evaluate across each element to obtain:

$$[N]^t K(\psi)\left(\frac{\partial \psi}{\partial z} + 1\right)\Big|_i^j - \int_0^{\Delta z} \frac{\partial [N]^T}{\partial z}[N]\begin{Bmatrix} K_i \\ K_j \end{Bmatrix} \frac{\partial [N]}{\partial z} \begin{Bmatrix} \psi_i \\ \psi_j \end{Bmatrix} dz$$

$$- \int_0^{\Delta z} \frac{\partial [N]^t}{\partial z}[N]\begin{Bmatrix} K_i \\ K_j \end{Bmatrix} dz$$

$$- \int_0^{\Delta z} [N]^t [N]\begin{Bmatrix} C_i \\ C_j \end{Bmatrix}[N] \frac{\partial \begin{Bmatrix} \psi_i \\ \psi_j \end{Bmatrix}}{\partial t} dz = 0 \qquad (18)$$

Evaluating the integrals in Equation 18 using the basis functions (eq. 16) and the time derivative,

$$\overset{\circ}{\underset{\sim}{\psi}} = \frac{\partial \psi}{\partial t} = \frac{\psi - \psi^-}{\Delta t} \qquad (19)$$

gives the general ordinary differential equation

$$\underset{\sim}{C}\,\overset{\circ}{\underset{\sim}{\psi}} + \underset{\sim}{A}\,\underset{\sim}{\psi} + \underset{\sim}{B} = \underset{\sim}{D}(t) \quad . \qquad (20)$$

Where

$$\frac{1}{\Delta t}\underset{\sim}{C} = \frac{\Delta z}{12(\Delta t)}\begin{bmatrix} 3c_i + c_j & c_i + c_j \\ c_i + c_j & c_i + 3c_j \end{bmatrix} = \begin{bmatrix} \gamma_1 & \gamma_2 \\ \gamma_3 & \gamma_4 \end{bmatrix} \tag{21}$$

$$\underset{\sim}{A} = \frac{1}{2\Delta z}\begin{bmatrix} (K_i + K_j) & -(K_i + K_j) \\ -(K_i + K_j) & +(K_i + K_j) \end{bmatrix} = \begin{bmatrix} a_1 & a_2 \\ a_3 & a_4 \end{bmatrix} \tag{22}$$

$$\underset{\sim}{C} + \underset{\sim}{A} = \begin{bmatrix} \gamma_1 + a_1 & \gamma_2 + a_2 \\ \gamma_3 + a_3 & \gamma_4 + a_4 \end{bmatrix} = \begin{bmatrix} \alpha_1 & \alpha_2 \\ \alpha_3 & \alpha_4 \end{bmatrix} \tag{23}$$

$$\underset{\sim}{B} = \frac{1}{2}\left(K_i + K_j\right)\begin{bmatrix} -1 \\ 1 \end{bmatrix} = \begin{bmatrix} \beta_1 \\ \beta_2 \end{bmatrix} \tag{24}$$

$$\underset{\sim}{D}(t) = \begin{bmatrix} \text{Flow Through at Bottom.} \\ \text{Flow through at top.} \end{bmatrix} = \begin{bmatrix} -Q_i \\ \\ R_j \end{bmatrix}. \tag{25}$$

The general equation for a single element now becomes

$$\begin{bmatrix} \alpha_1 & \alpha_2 \\ \alpha_3 & \alpha_4 \end{bmatrix}\begin{Bmatrix} \psi_i \\ \psi_j \end{Bmatrix} - \begin{bmatrix} \gamma_1 & \gamma_2 \\ \gamma_3 & \gamma_4 \end{bmatrix}\begin{Bmatrix} \bar{\psi_i} \\ \bar{\psi_j} \end{Bmatrix} + \begin{bmatrix} \beta_1 \\ \beta_2 \end{bmatrix} = \begin{bmatrix} -Q_i \\ \\ R_j \end{bmatrix}. \tag{26}$$

The expansion of this matrix equation for all elements j = 1 through j = J gives:

$$
\begin{aligned}
j = 1 \quad & \alpha_1(1)\cdot\delta_1 + \alpha_2(1)\cdot\delta_2 - \gamma_1(1)\cdot\bar{\delta}_1 - \gamma_2(1)\cdot\bar{\delta}_2 + \varepsilon_1(1) = Q_1 \\
j = 2 \quad & \alpha_3(1)\cdot\delta_1 + \alpha_4(1)\cdot\delta_2 - \gamma_3(1)\cdot\bar{\delta}_1 - \gamma_4(1)\cdot\bar{\delta}_2 + \varepsilon_2(1) = R_1 \\
& \alpha_1(2)\cdot\delta_2 + \alpha_2(2)\cdot\delta_3 - \gamma_1(2)\cdot\bar{\delta}_2 - \gamma_2(2)\cdot\bar{\delta}_3 + \varepsilon_1(2) = Q_2 \\
j = 3 \quad & \alpha_3(2)\cdot\delta_2 + \alpha_4(2)\cdot\delta_3 - \gamma_3(2)\cdot\bar{\delta}_2 - \gamma_4(2)\cdot\bar{\delta}_3 + \varepsilon_2(2) = R_2 \\
& \alpha_1(3)\cdot\delta_3 + \alpha_2(3)\cdot\delta_4 - \gamma_1(3)\cdot\bar{\delta}_3 - \gamma_2(3)\cdot\bar{\delta}_4 + \varepsilon_1(3) = Q_3 \\
& \alpha_3(3)\cdot\delta_3 + \alpha_4(3)\cdot\delta_4 - \gamma_3(3)\cdot\bar{\delta}_3 - \gamma_4(3)\cdot\bar{\delta}_4 + \varepsilon_2(3) = R_3 \\
& \qquad\qquad\qquad\qquad \vdots \\
j = J-1 \quad & \alpha_3(J-2)\cdot\delta_{J-2} + \alpha_4(J-2)\cdot\delta_{J-1} - \gamma_3(J-2)\cdot\bar{\delta}_{J-2} - \gamma_4(J-2)\cdot\bar{\delta}_{J-1} + \varepsilon_2(J-2) = R_{J-1} \\
& \alpha_1(J-1)\cdot\delta_{J-1} + \alpha_2(J-1)\cdot\delta_J - \gamma_1(J-1)\cdot\bar{\delta}_{J-1} - \gamma_2(J-1)\cdot\bar{\delta}_J + \varepsilon_1(J-1) = Q_J \\
j = J \quad & \alpha_3(J-1)\cdot\delta_{J-1} + \alpha_4(J-1)\cdot\delta_J - \gamma_3(J-1)\cdot\bar{\delta}_{J-1} - \gamma_4(J-1)\cdot\bar{\delta}_J + \varepsilon_2(J-1) = R_J \,.
\end{aligned}
$$

Since $R_j = -Q_{j+1}$, all intermediate values of R and Q can be eliminated from the problem by adding sets of two equations each as shown by the j = 1 to j = J brackets. This process is commonly referred to as assembly.

The assembled equations result in a tridiagonal matrix with the general form:

$$\bar{B}_1\psi_1 \quad - \bar{C}_1\psi_2 \quad = \bar{D}_1$$

$$-\bar{A}_2\psi_1 \quad + \bar{B}_2\psi_2 \quad - \bar{C}_2\psi_3 \quad = \bar{D}_2$$

$$-\bar{A}_3\psi_2 \quad + \bar{B}_3\psi_3 \quad - \bar{C}_3\psi_4 \quad = \bar{D}_4$$

$$\vdots$$

$$-\bar{A}_{J-1}\psi_{J-2} + \bar{B}_{J-1}\psi_{J-1} - \bar{C}_{J-1}\psi_J = \bar{D}_{J-1}$$

$$-\bar{A}_J \ \psi_J \quad + \bar{B}_j \ \psi_J \qquad\qquad = \bar{D}_J$$

where for $2 \leq j \leq J - 1$

$$\bar{A}_j = - \alpha_3 \ (j-1) \tag{27}$$

$$\bar{B}_j = \left(\alpha_4(j-1) + \alpha_1(j)\right) \tag{28}$$

$$\bar{C}_j = - \alpha_2 \ (j) \tag{29}$$

$$\bar{D}_j = \gamma_3(j-1) \ \bar{\psi_{j-1}} + (\gamma_4(j-1) + \gamma_1 \ (j))\bar{\psi_j}$$

$$+ \gamma_2(j) \ \bar{\psi_{j+1}} - (\beta_2(j-1) + \beta_1(j)) \tag{30}$$

The coefficients at j = 1 and j = J differ depending on the boundary conditions applied. For applied R and Q (flow through) quantities

$$B_1 = \alpha_1(1)$$

$$C_1 = -\alpha_2(1)$$

$$D_1 = -Q + \gamma_1(1) \ \bar{\psi_1} + \gamma_2(1) \ \bar{\psi_2} - \beta_1(1)$$

$$A_J = -\alpha_3(J-1)$$

$$B_J = \alpha_4(J-1)$$

$$D_J = R + \gamma_3(J-1)\ \bar{\phi}_{J-1} + \gamma_4(J-1)\ \bar{\phi}_J - \beta_2(J-1)$$

For some problems, it is sometimes desirable to specify the ϕ value instead of R (rain). For this condition

$$B_J = 1 \times 10^{20} \quad \text{and}$$

$$D_J = \phi_J \times 10^{20} \quad .$$

Prior to solving the resulting matrix, it is necessary to define $K = K(\phi)$, $\theta = \theta(\phi)$ and $c = c(\phi)$. These expressions are specific functions of the material (soil) being considered. For the examples considered in this paper, a curve fit for the wetting portion of Figures 2 and 3 taken from Freeze[1] are used. The curves for K, θ, $\frac{\partial\theta}{\partial\psi}$ are given by Figures 4, 5, and 6 respectively.

Sample Problem

The boundary-value problem defined by the finite difference and finite element methods given above are solved for the first 100 cm of soil below the ground surface with the initial distribution of moisture content, pressure head and hydraulic head shown in Figures 7, 8, and 9. The transient behavior occurs in

response to a constant-intensity rainfall that feeds the soil surface at the rate R = .13 cm/min. This rate is 5 times the saturated hydraulic conductivity of the soil, K_o = .026 cm/min. The boundary conditions applied allow for a maximum ponding rate of 10 cm. The results obtained using the finite difference solution method, described herein, for θ, ϕ, and h are given on Figures 7, 8, and 9 for times of 0, 12, 24, 36, 48 and 60 minutes after the rain started. One hundred and one mesh points are used. Figure 8 shows that the surface becomes saturated after 12 min. The moisture content increases down the profile with time until the entire region is saturated at 60 minutes. Figure 8 shows the pressure-head changes. The pressure head does not reach the ϕ = 0 point for 30 minutes which implies that the upper few centimeters of surface saturation indicated by the moisture-content profile are in "tension-saturated" state. At t = 36 minutes the pressure head has reached 10 cm indicating that 10 cm of water are ponded above the ground surface at this time. The initial water table which is at -95 cm. remains constant for the first 36 min. of rainfall after which time it begins to rise in response to the infiltrating moisture from above. The hydraulic head, h, curve (Figure 9) is a direct response to the ϕ curve ($h = \phi + z$). The results of these calculations agree well with those given by Freeze and Cherry[1]. The differences are attributed to the simplified fits to the charateristic curves given by Freeze and Cherry relating K and θ to ϕ.

Comparison of Results

Table 1 gives a comparison of results given by the finite element and finite difference solution methods. The first column gives the results of the finite element method as developed herein. Column two gives the results of the finite element method using boundary conditions identical to those used in the finite difference formulation. Column three gives the results of the finite difference solution described herein. It can be seen that all three procedures, although not identical, give results which are very similar. The difference is caused by the different weighting of the nonlinear coefficients in the two methods and by the method in which the boundary conditions are applied.

Finite Difference-Finite Element Solutions for the Linear Problem

Because of the difference in weighting of the equation coefficients $K(\phi)$ and $c(\phi)$, and the method of representing the time derivative of ϕ, it is not possible to obtain an exact one to one correspondence between the two solution methods for the nonlinear problem. However, if these coefficients are considered to be constant (linearized) and the time derivative is approximated by

$$\frac{\partial \psi}{\partial t} = \frac{\psi_* - \bar{\psi}_*}{\Delta t}$$

where $\psi_* \equiv \dfrac{\psi_{j+1} + 4\psi_j + \psi_{j-1}}{6}$

TABLE 1

Comparison of Finite Element with Finite Difference Computational Results (t = 36 min.)

Distance Below Ground Surface (cm)	Pressure head, P/ρg (cm)		
	Finite Element	F. E. with F. D. Boundary Conditions	Finite Difference
0	10.0	10	10
10	-19.2	-18.2	-16.2
20	-45.6	-44.2	-41.6
30	-49.7	-49.4	-49.5
40	-42.5	-42.4	-43.7
50	-32.8	-32.7	-34.3
60	-22.7	-22.7	-24.4
70	-12.7	-12.7	-14.4
80	- 2.7	- 2.7	- 4.4
90	7.3	7.3	5.6
100	17.3	17.3	15.6

the two solutions methods yield identical stiffness matrixes. The stiffness matrix coefficients for this case are

$$A = \frac{K}{\Delta z} - \frac{c\Delta z}{6\Delta t} \quad ,$$

$$B = 2\left(\frac{K}{\Delta z} + \frac{c\Delta z}{6\Delta t}\right) \quad ,$$

$$C = \left(\frac{k}{\Delta z} - \frac{c\Delta z}{6\Delta t}\right) \quad \text{and}$$

$$D = \frac{c\Delta z}{6\Delta t}\left(\bar{\psi}_{j+1} + 4\bar{\psi}_j + \bar{\psi}_{j-1}\right) \quad .$$

When identical boundary conditions are applied, then the results from the two methods are obviously identical.

Conclusions

This exercise was undertaken as an initial attempt to understand some of the characterictics of unsaturated flow and the procedures by which solutions can be calculated. It was shown that the results for this isothermal problem could be obtained equally well using finite difference methods or finite element methods. The results obtained are in good agreement with existing published results. It is also shown that the two methods can be made identical for the (linear) constant coefficient cases.

REFERENCES

1. Freeze, R. A. and J. A. Cherry, Groundwater, Prentice-Hall, Inc., Englewood Cliffs, New Jersey, 1979.

2. Segerlind, L. J., Applied Finite Element Analysis, John Wiley and Sons, Inc., New York, 1976.

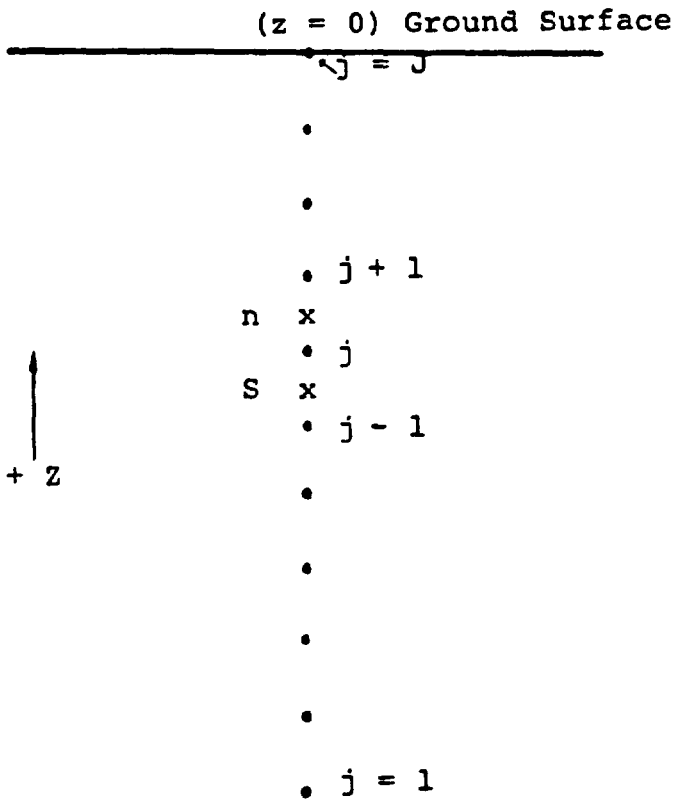

FIGURE 1. Geometry Notation.

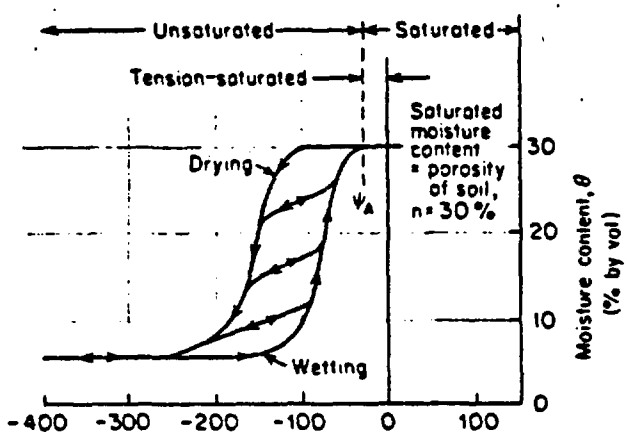

Pressure Head, ψ (cm of water)

Figure 2. Typical characteristic curve Relating Moisture Content to Pressure Head.

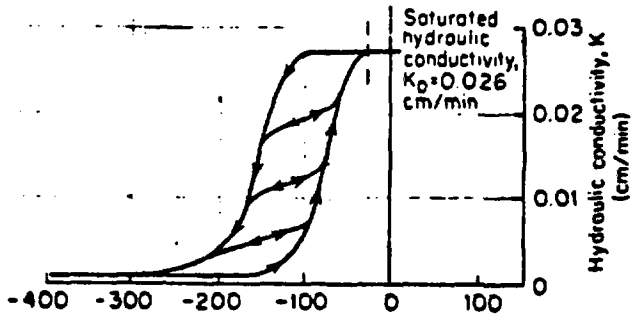

Pressure Head, ψ (cm of water)

Figure 3. Typical Characteristic Curve Relating Hydraulic Conductivity to Pressure Head.

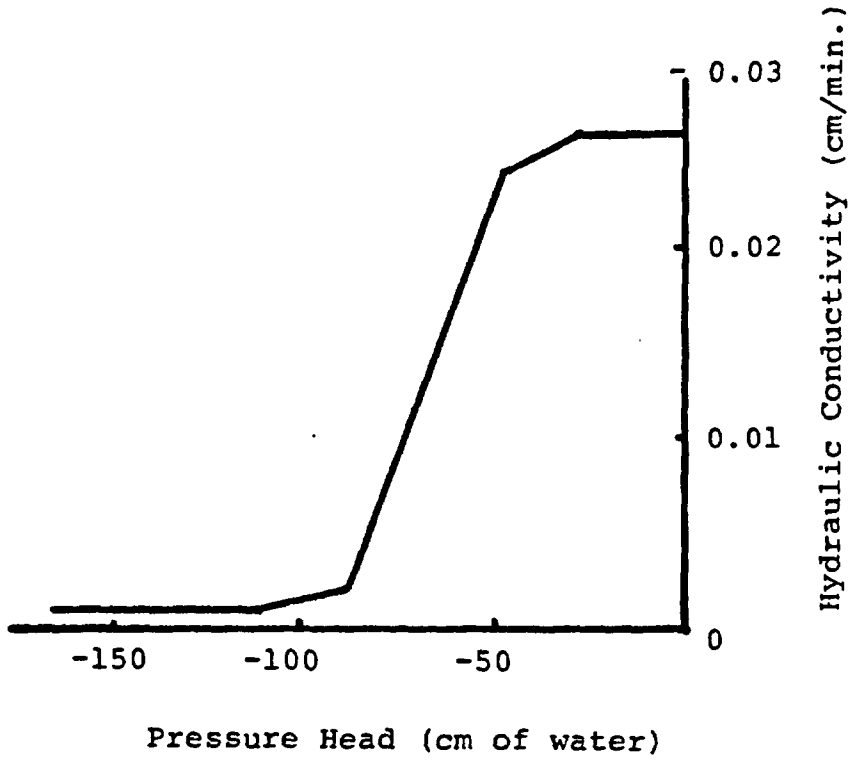

FIGURE 4. Hydraulic Conductivity of Soil.

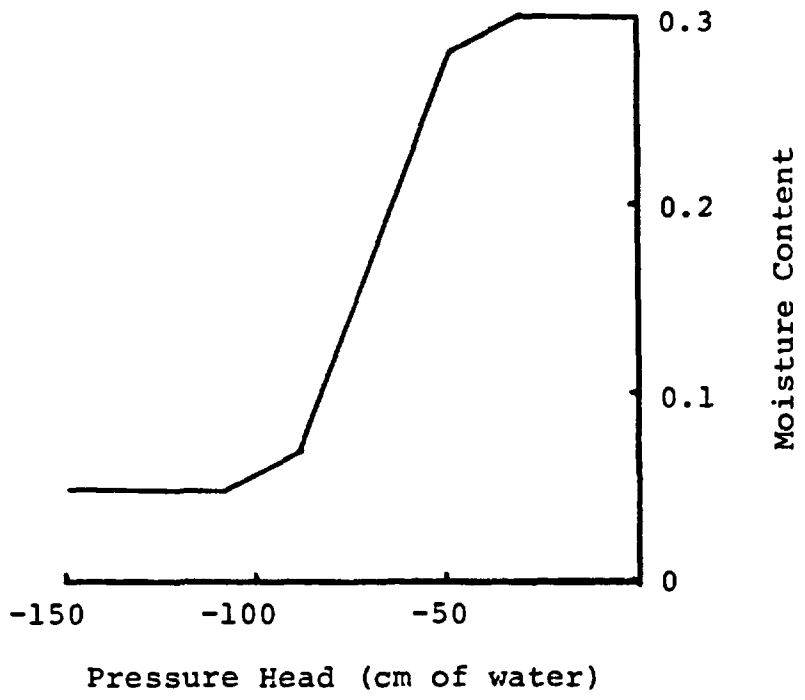

FIGURE 5. Moisture Content.

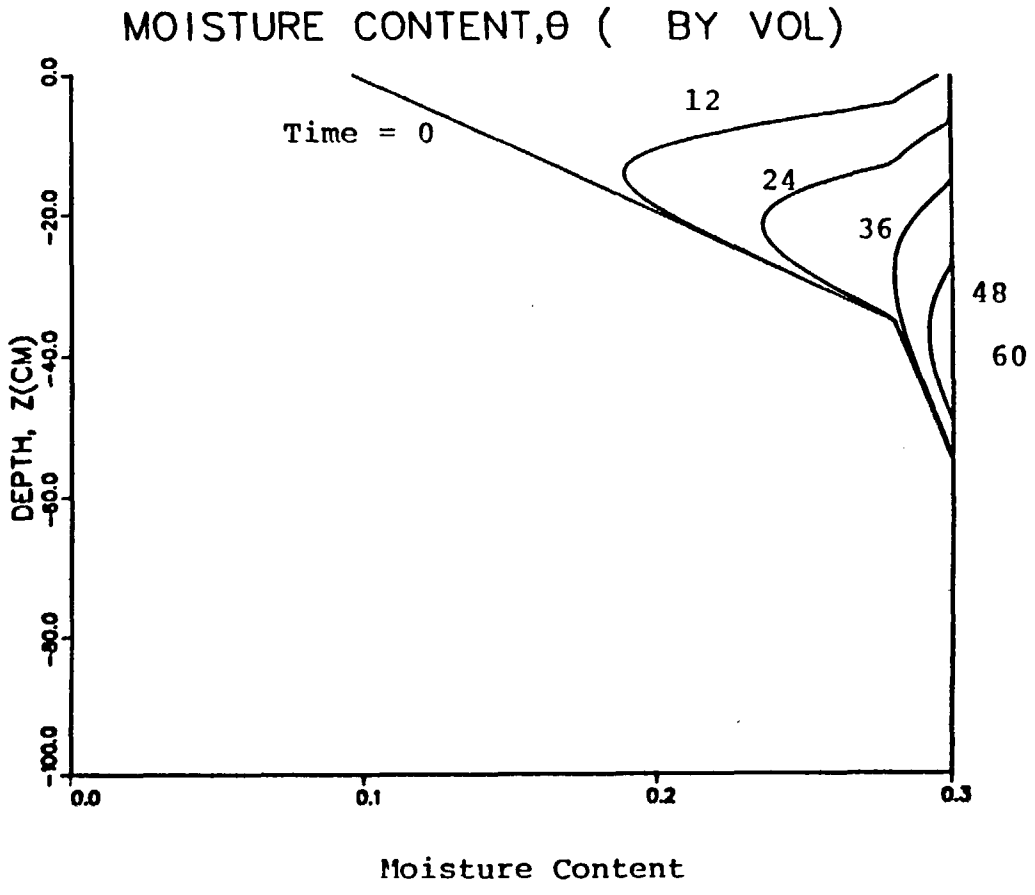

FIGURE 7. Moisture Content for Times = 0, 12, 24, 36, 48 and 60 min.

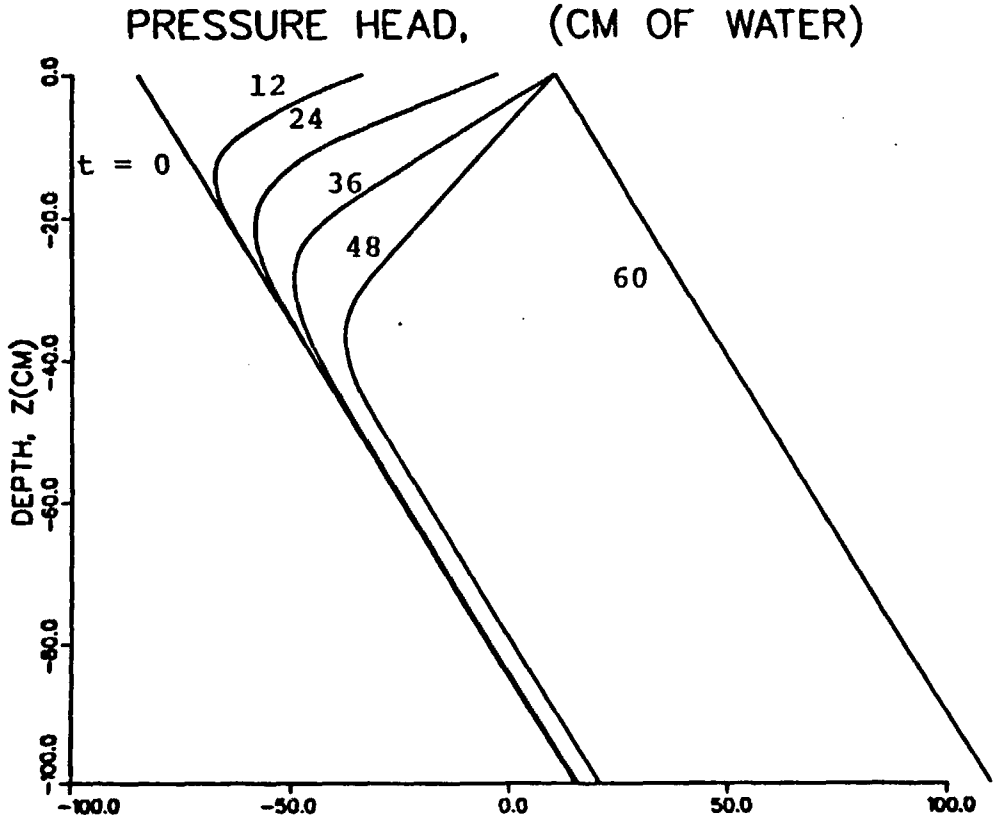

FIGURE 8. Pressure head for Time = 0, 12, 24, 36, 48 and 60 min.

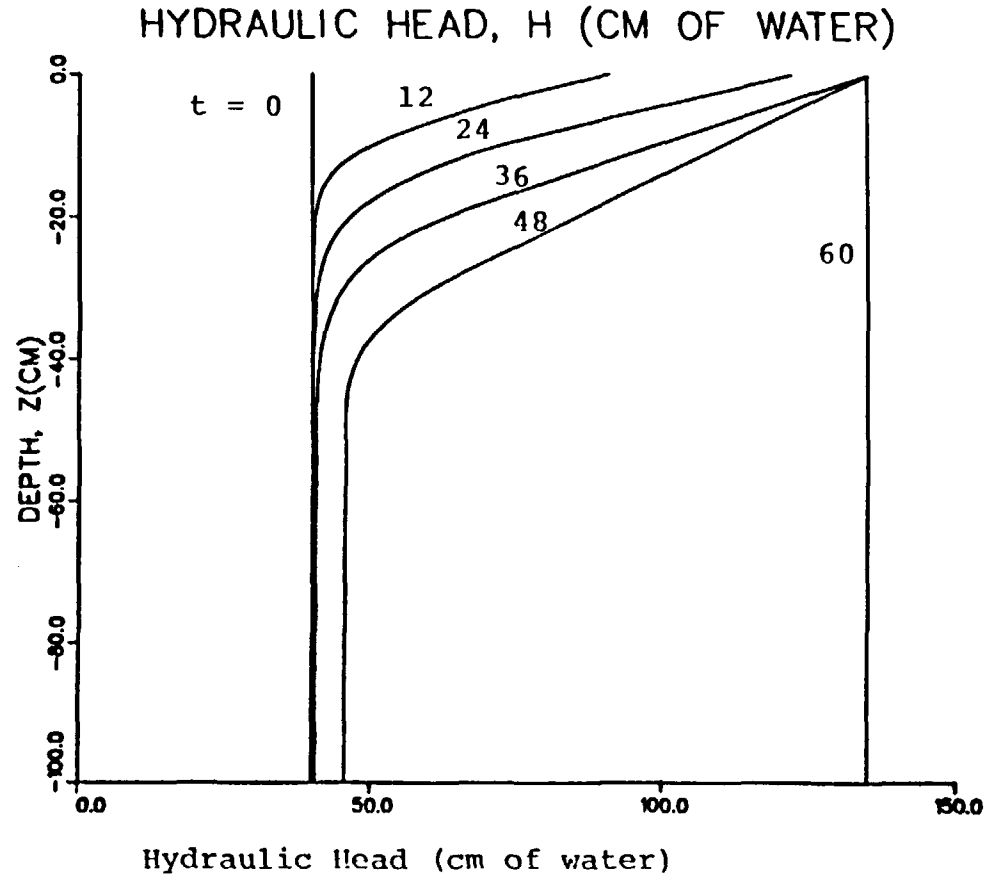

FIGURE 9. Hydraulic head for Time = 0, 12, 24, 36, 48 and 60 min.

APPENDIX D

Sandia National Laboratories

Albuquerque, New Mexico 87185

date: January 6, 1982

to: L. D. Tyler, 4537

from: R. R. Eaton and J. W. Nunziato, 5511

subject: Current Status of Computational Capabilities for Predicting Energy and Mass Flux Through Partially Saturated Porous Media

In response to your request to develop computational tools for predicting flows through porous media containing regions which are not necessarily fully saturated*, modifications have been made to the existing COYOTE[1] and MARIAH[2] codes. This memo discusses the action which has been taken to:

1. Modify the time-dependent, finite element, heat conduction code COYOTE to make it applicable for calculating isothermal flow of water through partially saturated porous media. This code will be referred to as COYOTE/UNSAT.

2. Extend the finite element code MARIAH, which was originally written to calculate the mass and thermal transport through saturated porous rock, to a code which is applicable for analyzing heat and mass transport through porous material with regions which are partially saturated. This code will be referred to as SAGUARO.

Both of these revisions of the codes are based on the Richards flow equation[3] and have two-dimensional capabilities (axisymmetric or planar). Motivation for developing the computational capabilities within Sandia are two-fold: 1) Assure compatibility between our partially saturated computational studies and associated thermal and stress calculations done within Organization 5500, and 2) In-house development will make it possible to combine the statistical fracture work currently being done by D. Gartling, 5511, and B. Thomas, 5521 with the partially saturated flow model.

*In this memo, unless otherwise specified, regions which are not necessarily fully saturated are referred to as partially saturated.

The number of codes existing with similar capabilities is very limited. One such code is the one-dimensional finite-element code developed by Baca and King[4]. The equations solved in both the Baca code and SAGUARO are similar. However, the Baca code uses a log transformation for the pressure which results in the code not being applicable to completely saturated regions. This restriction is seldom significant for doing near surface calculations in arid site vadose zones; the region for which the Baca code was written. This restriction could be limiting for analyzing regions in tuff where both fully saturated and unsaturated rock are found.

RRE:JWN:5511:fvc

Copy to:

4511 G. E. Barr
4530 R. W. Lynch
4531 L. W. Scully
4537 D. R. Fortney
4537 A. R. Lappin
4537 B. S. Langkopf
4538 R. C. Lincoln
5500 O. E. Jones
5510 D. B. Hayes
5511 D. K. Gartling
5511 G. R. Hadley
5511 C. E. Hickox
5511 M. J. Martinez
5511 D. F. McTigue
5511 D. C. Reda
5512 D. F. McVey
5512 R. H. Nilson
5521 R. D. Krieg
5521 R. K. Thomas
5522 R. K. Wilson
5532 B. M. Butcher
5511 R. R. Eaton
5511 J. W. Nunziato

NOMENCLATURE

$c(\psi)$	Derivative of moisture content $(\frac{\partial \theta}{\partial \psi})$	(1/m)
C_p	Specific heat	(J/kg°c)
D_{ij}	Thermal diffusivity	(m^2/°c·s)
E_{ij}	Thermal dispersion tensor	(J/s·m°c)
g	Gravitational constant	(m/s^2)
k	Permeability	(m^2)
$K(\psi)$	Hydraulic conductivity	(m/s)
Q	Heat source	($J/s \cdot m^3$)
v_i	Fluid velocity	(m)
α	Porosity	
θ	Moisture content	(ND)
ρ	Water density	(kg/m^3)
ϕ	Pressure head potential $\phi = \rho g(\psi+z)$	(N/m^2)
ψ	Pressure head $\psi = p/\rho g$	(m)
λ_{ij}	Thermal conductivity tensor	(J/s·m°c)

Subscripts:

eff	Effective
f	Fluid

Conversion of COYOTE to COYOTE/UNSAT

The conversion of the thermal code COYOTE to a partially saturated flow code was possible because of the similarities between the thermal conduction equation

$$\nabla\cdot[\lambda(T)\nabla T] = \rho C_p(T)\,\frac{\partial T}{\partial t} \qquad (1)$$

and the mass transport equation

$$\nabla\cdot[K(\phi)\nabla\phi] = c(\phi)\,\frac{\partial \phi}{\partial t} \quad , \qquad (2)$$

(See nomenclature list for definitions of terms.)
Equation 2 is commonly referred to as the Richards equation. It simulates the Darcy-type flow of an incompressible fluid through a porous media which is not necessarily fully saturated. The coefficients K and c are strong functions of the pressure head ϕ. The presence of air in the formation is neglected. This essentially says that any trapped air can always escape a partially saturated zone without influencing the flow of the fluid.

Converting the COYOTE code was a straight forward procedure because: 1) the original code was designed to solve equation 1 in which the coefficients (K and ρC_p) can be highly nonlinear, and 2) the basic structure exists within the code which allowed for construction of "user subroutines" in which these coefficients can be specified as complicated functions of the dependable variable. For partially saturated flows, the coefficients $K(\phi)$

and $c(\phi)$ are functions of ϕ as shown in the typical curves shown in Figure 1. The curves show the significance of the hystersis effects on the (K, ϕ) and (θ, ϕ) relationship. It is through these curves that the influence of capillary action is accounted for.

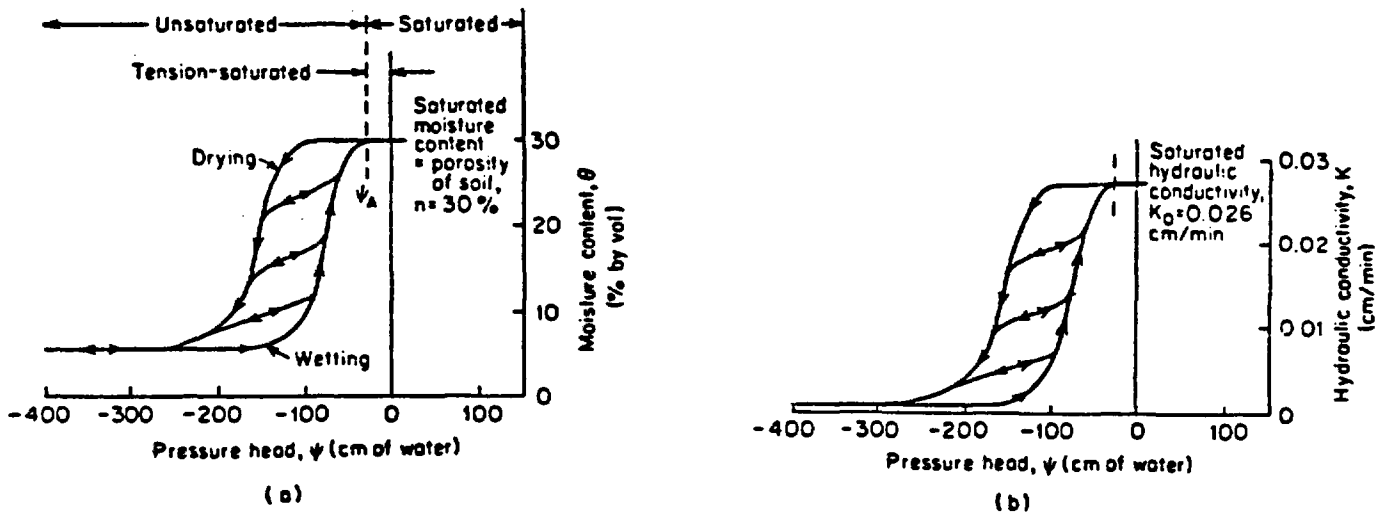

Figure 1: Characteristic curves relating hydraulic conductivity and moisture content to pressure head for sand/soil, see reference 3.

Details concerning the application of COYOTE/UNSAT to a specific problem is given below in the Sample Calculation section.

Conversion of MARIAH to SAGUARO

The original MARIAH code is a finite element computer program designed for the solution of two-dimensional, incompressible flows in porous media, including the effects of heat transfer. The continuity/momentum equation is

$$\frac{\partial}{\partial X_i}\left(\frac{-k}{\mu}\frac{\partial \phi}{\partial X_i}\right) = \frac{\partial}{\partial X_i}\left(\frac{-k}{\mu}\rho_o g\beta\Delta T\frac{\partial Z}{\partial X_i}\right) \quad , \tag{3}$$

and the energy equation is

$$(\rho C_p)_{eff}\frac{\partial T}{\partial t} + \rho_{fo} C_f \langle v_i\rangle \frac{\partial T}{\partial X_i} - \frac{\partial}{\partial X_i}\left[(\lambda_{eff} - \alpha E_{ij})\frac{\partial T}{\partial X_j}\right] - Q = 0. \tag{4}$$

The original mass transport equation (eq. 3) applies to quasi-steady flows and includes the Boussinesq approximation to account for buoyant effects. The time-dependent energy equation accounts for energy transport by convection and conduction.

The MARIAH code (good for saturated regions only) has been converted to extend it range of applicability to the partially saturated and unsaturated regions as follows. The form of the energy equation remains unchanged. The momentum/continuity equation has been replaced by

$$\nabla\cdot[K(\phi)\nabla\phi] + \nabla\cdot[D(\phi,T)\nabla T] = c(\phi)\,\frac{\partial\phi}{\partial t} \quad .$$

$D(\phi,T)$ is the coefficient of thermal diffusion, the process by which mass is transported as a result of temperature gradients. This diffusion term originates as a refinement to the Darcy equation for velocity. The relationship K and c as functions of ϕ are the same as those discussed above in the COYOTE/UNSAT section. The diffusion coefficient ($D(\phi,T)$) must also be defined for non-isothermal problems.

Sample Calculations

In order to demonstrate the capability of the modified codes to calculate the head potential in mixed regions, sample calculations were computed for one-dimensional, time-dependent infiltration of rain into a partially saturated soil (Figure 2).

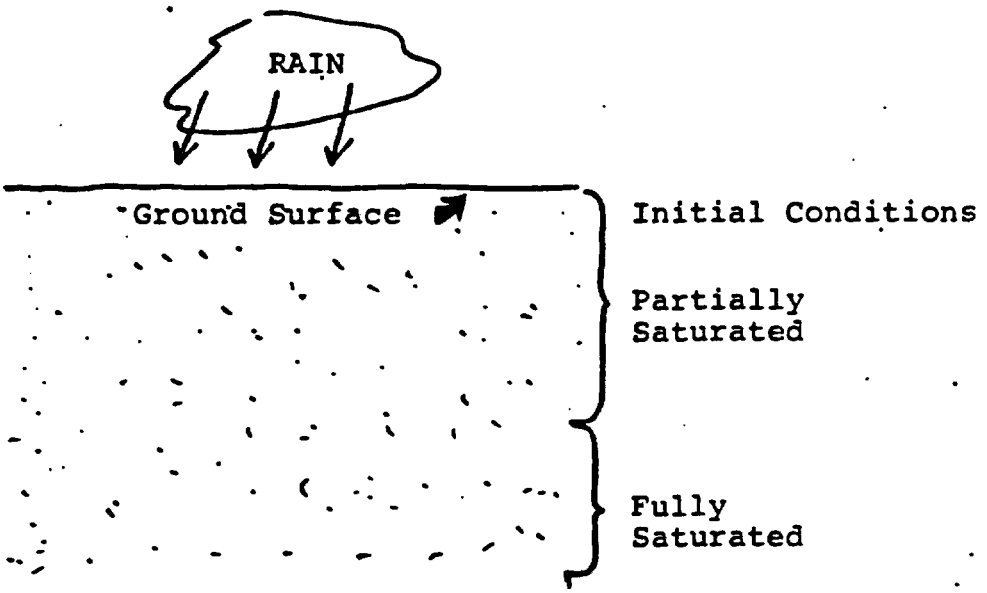

FIGURE 2. Geometry Used in Sample Infiltration Problem

In order to keep the sample calculations as simple as possible, the wetting portion of the curves shown in Figure 1 were reduced to those shown in Figure 3. Although computed results are sensitive to the exact shape of these curves, it was felt that the validity of the procedure could be adequately shown with these less complicated curves. Of course, similar calculations can be done using the drying portion of the curves and thus we would have bounds on the correct solution.

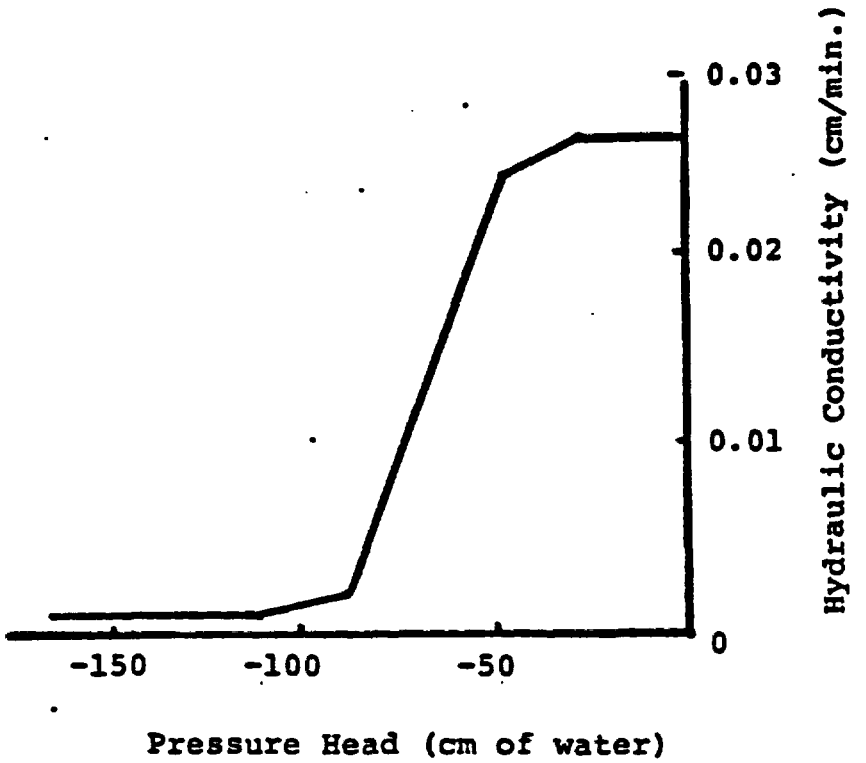

FIGURE 3a. Hydraulic Conductivity of Soil.

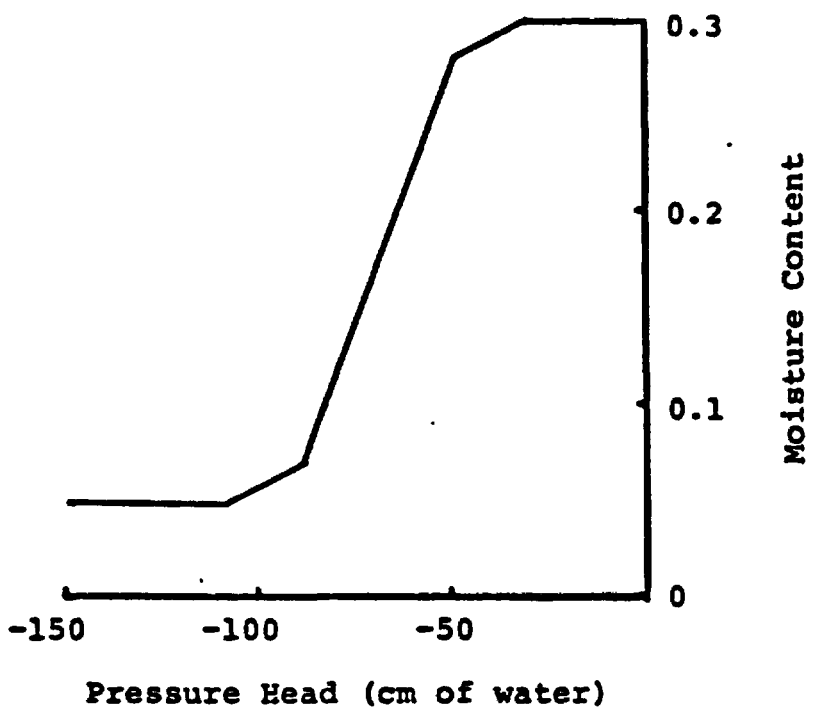

Figure 3b. Moisture Content

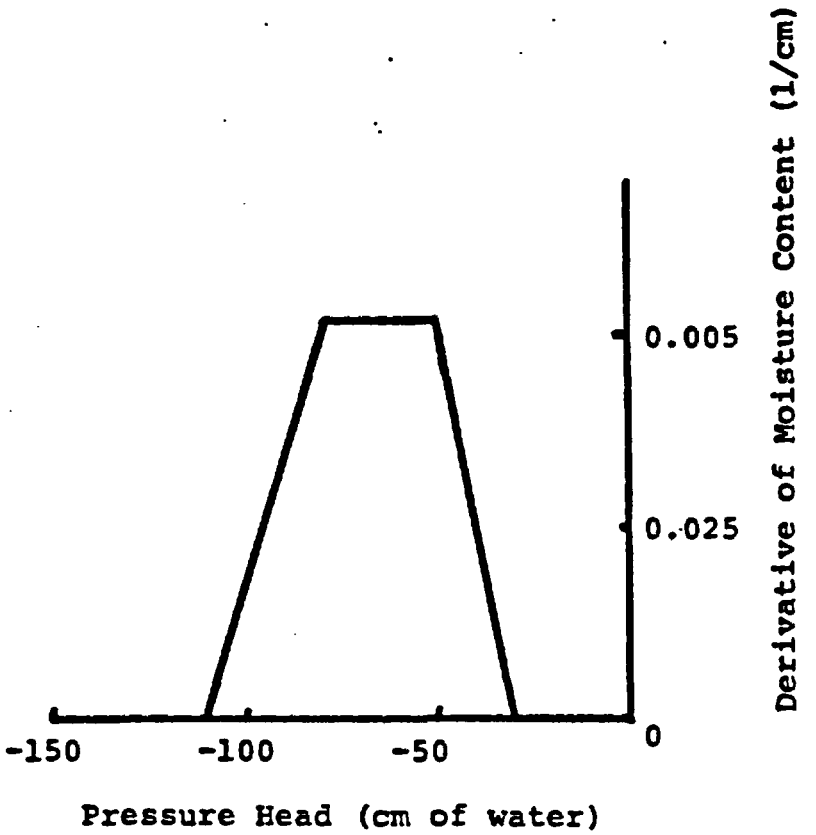

FIGURE 3c. Derivative of Moisture Content with Respect to Pressure Head.

The boundary conditions for the test case are:

1. Rain is such that it feeds the soil at a rate of .13 cm/min until the maximum allowable ponding height of 10 cm is reached. Surface pressure is then held at 10 cm.
2. The initial pressure head (ϕ) is given by Figure 4 which says at t = 0 the fluid velocity is zero everywhere.

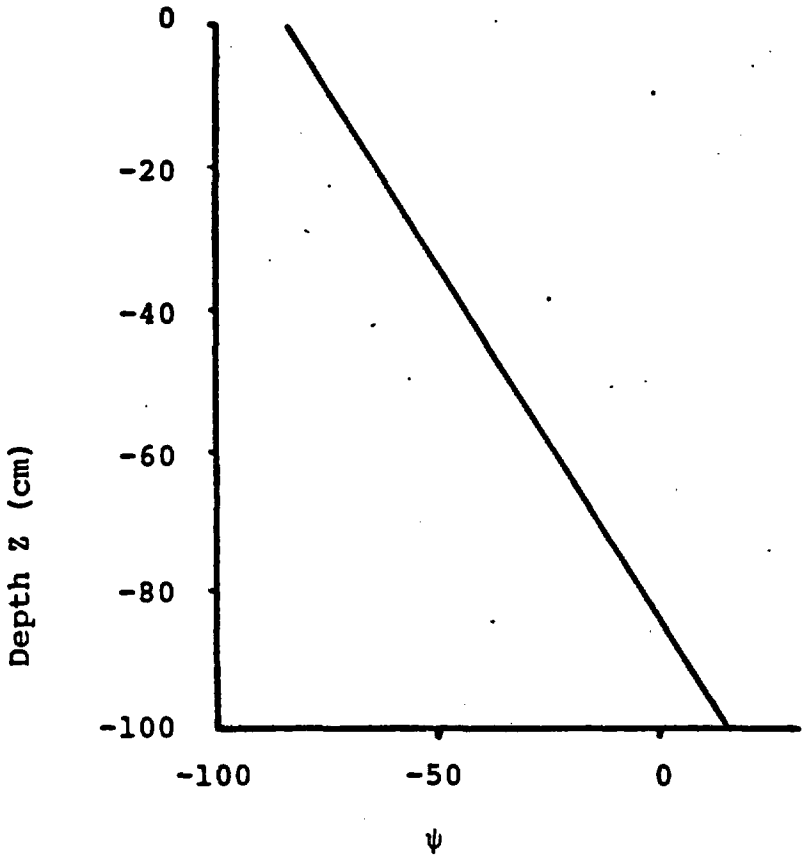

FIGURE 4. Initial Pressure Head

The computational results of this calculation is given in Figure 5. They compare well with the results obtained using the one-dimensional finite difference and finite element solution described in reference 5. The computed results from COYOTE/UNSAT and SAGUARO agree to 3 significant figures.

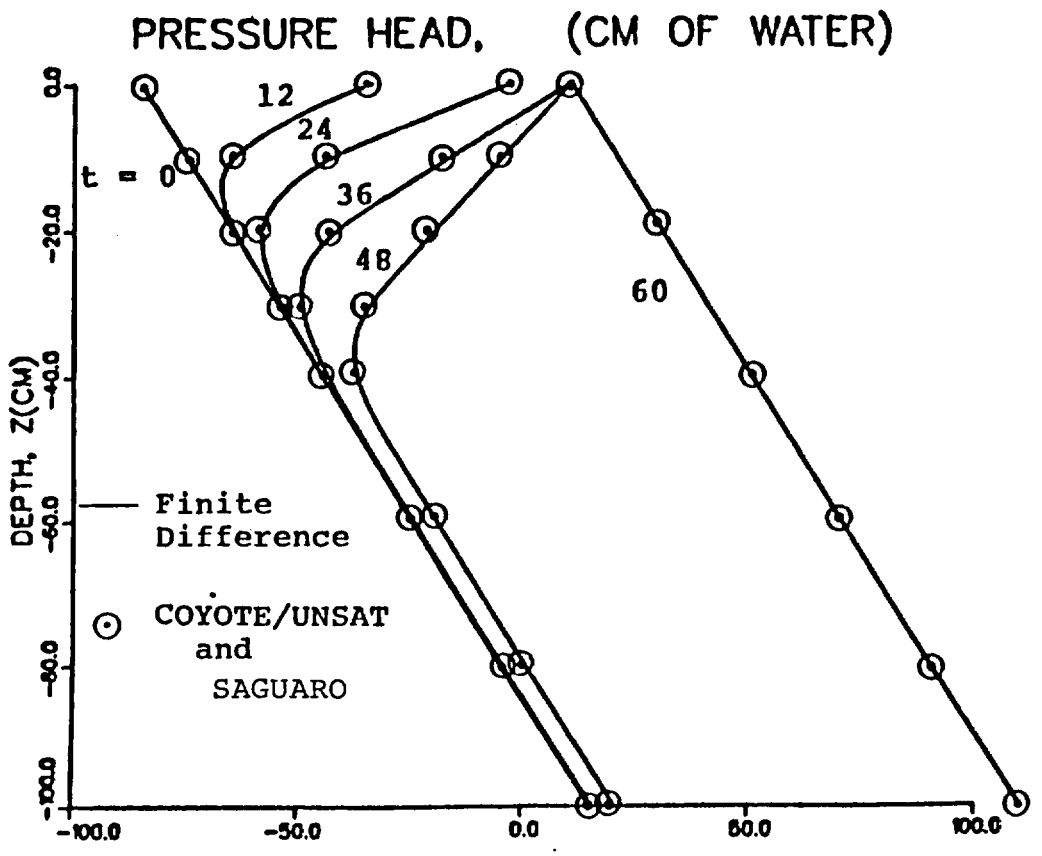

FIGURE 5. Pressure head for Time = 0, 12, 24, 36, 48 and 60 min.

Conclusions and Future Work

Two computer codes are now available for limited application to problems having regions which are fully-, partially-, and/or unsaturated. The COYOTE/UNSAT code is limited to isothermal problems. The SAGUARO code includes the effect of mass transport and energy transport and therefore is not limited to nonisothermal problems. To access these codes, contact R. Eaton, 5511.

Future work will include the following:

1. Benching marking of SAGUARO for cases in which thermal gradients are significant.
2. Develop characteristic curves for $K(\phi)$, $\theta(\phi)$, and $D(\phi,T)$ for tuff-like materials.
3. Investigate the importance of including water vapor transport. The equations discussed in this memo do not account for change of phase of water or energy transport resulting from water vapor motion.
4. Investigate bouyancy effects and how to account for them.
5. Data will be collected in order to make possible repository draw down calculations on a global scale.

REFERENCES

1. Gartling, D. K., "COYOTE - A Finite Element Computer Program for Nonlinear Heat Conduction Problems," SAND77-1332, Sandia Laboratories, Albuquerque, New Mexico, June, 1978.

2. Gartling, D. K. and C. E. Hickox, "MARIAH - A Finite Element Computer Program for Incompressible Porous Flow Problems", SAND79-1623, Sandia Laboratories, Albuquerque, New Mexico, August, 1980.

3. Freeze, R. A., and J. A. Cherry, Groundwater, Prentice-Hall, Inc., 1979.

4. Baca, R. G. and I. P. King, "Finite Element Models for Simultaneous Heat and Moisture Transport in Unsaturated Soils", RHO SA-31, Rockwell Hanford Operations, Richland, Wa., March, 1978.

5. Eaton, R. R., Memo to Distribution dated 12/22/81, Subject: "The Highly Nonlinear Equations Describing One-dimensional Infiltration of Water Through Unsaturated Media".

APPENDIX E

Sandia National Laboratories

Albuquerque, New Mexico 87185

date: March 31, 1982

to: L. D. Tyler, 4762

from: R. R. Eaton, 5511

subject: Comparison of Numerical Calculation with Experimentally Obtained Results from Imbibition Experiments on Partially Saturated Welded Tuff

Recent interest in investigating the hydrology in the partially saturated region of Yucca Mountain has prompted the development of a numerical code SAGUARO. The code is applicable to hard-rock applications in which the moisture content may vary from zero (unsaturated) to one (fully saturated). The code solves for mass and energy transport, as outlined in References 1 and 2. For the isothermal case considered in this report, the mass transport equation in the code reduces to the Richards equation in which the mass flux is obtained using Darcy's law. The derivation of this equation assumes that the air in the partially saturated zones offer no resistance to the movement of water. The resulting momentum-continuity equation is

$$\nabla \cdot \left[\frac{k(\psi)\rho g}{\mu} \nabla \Phi \right] = \frac{\partial \theta}{\partial \psi} \frac{\partial \Phi}{\partial t} \quad .$$

where

g	- gravitational constant	m/s^2
$k(\psi)$	- intrinsic permeability	m^2
t	- time	s
p	- water density	kg/m^3
μ	- water viscosity	$kg/m \cdot s$
θ	- moisture content	
ϕ	- porosity	
Φ	- hydraulic head = $pg\left(\psi + Z\left(\frac{\partial X_i}{\partial Z}\right)\right)$	m

In order to use this equation to predict the movement of water through partially saturated media, the intrinsic permeability, $k(\psi)$, and the derivative of the moisture content, $\frac{\partial \theta}{\partial \psi}$, must be obtained as a function of pressure-head (ψ) for the specific materials to be considered.

The code has previously been benchmarked for soils using the characteristic k and $\frac{\partial \theta}{\partial \psi}$ curves given in Freeze & Cherry[3]. This report discusses the procedure for obtaining these characteristic curves for tuff using mercury intrusion porosimetry measurements. As an additional step in benchmarking the code, these curves were then used in SAGUARO to simulate the imbibition test performed by Hadley[4] on a sample of tuff material.

Formulation of Characteristic Curves

The experimental mercury intrusion data was obtained by True Technology of Dallas, Texas[5]. This pressure vs.

mercury fill rate data is given in Table I. The procedure for obtaining this data and converting from mercury/air to water/air is discussed in Reference 6. An outline of that procedure is discussed here for completeness. A simple capillary model is assumed to describe the phenomena. In this model, the rock is assumed to be comprised of a group of capillary tubes of various sizes. As mercury is forced into the pores, it is assumed that all the large diameter pores fill first. As the pressure on mercury is increased, smaller and smaller tubes fill until finally the entire sample of rock is saturated with mercury. Obtaining a water pressure versus moisture content curve is accomplished by determining expressions for the water/pressure and mercury/pressure to fill a capillary tube of radius r. These force balance equations for mercury and water respectively are (see Figure 1).

$$P_{Hg} = P_a + \frac{\sigma\ 2\pi r\ \cos\theta_{Hg}}{2\pi r^2} \qquad (1)$$

$$= P_a + \frac{2\sigma}{r}\cos\theta_{Hg} \quad \text{and}$$

$$P_w = P_a - \frac{2\sigma\ \cos\theta_{H_2O}}{r} \quad . \qquad (2)$$

Eliminating r from equation 1 and 2 results in

$$P_w = P_a - \left(P_{Hg} - P_a\right) \Big/ \left(\frac{\sigma_{Hg} \cos\alpha_{Hg}}{\sigma_{H_2O} \cos\alpha_{H_2O}} \right) , \qquad (4)$$

or

$$\psi_w = \frac{P_w}{\rho g} = \frac{1}{\rho g} \left[P_a - \left(P_{Hg} - P_a\right) \Big/ \left(\frac{\sigma_{Hg} \cos\alpha_{Hg}}{\sigma_{H_2O} \cos\alpha_{H_2O}} \right) \right] \qquad (5)$$

Typical values for the constants are

σ_{Hg} = 480 dynes/cm. , σ_{H_2O} = 70 dynes/cm

$\cos\alpha_{Hg}$ = 140° $\cos\alpha_{H_2O}$ = 0°

Using this equation and the relation $\theta_{H_2O} = (1 - \theta_{Hg})$, to account for the non-wetting nature of water on rock, the mercury intrusion data in Table 1 can be converted to water pressure vs. moisture content. The resulting data is plotted in Figure 2.

The code requires the derivative of this moisture content curve $(\frac{\partial\theta}{\partial\psi})$. The original curve has an extremely steep slope near θ_{H_2O} = 1.0. The area under the original $(\partial\theta/\partial\psi)$ curve is too concentrated in a small $\Delta\psi$ range to be compatible with the time-dependent finite element code. Therefore, the θ_{H_2O} vs. ψ curve is smoothed while forcing full saturation (θ = 1.0) to occur at the same ψ, Figure 2, curve A. The derivative of this approximate curve is given in Figure 3. The area under this curve is a

measure of the material capacitance or the ability of the porous material to store additional amounts of water. The final step in obtaining a capacitance curve ($\frac{\partial\theta}{\partial\psi}$ vs. ψ), which is compatible with the structure of the code, is to smooth the derivative curve maintaining the same $\Delta\psi$ interval and enclosed curve area. This is shown with a dashed curve in Figure 3. The permeability curve is assumed to have the same general shape as the θ curve, Figure 4, as is implied in the infiltration example presented in Reference 3, pg. 42.

Computational Results

The code SAGUARO[1] was run using the characteristic curves given on Figures 3 and 4. The experimental geometry simulated is shown in Figure 5. The initially dry sample of tuff was submerged in a water bath at time zero. The rate of water migration into the sample through the exposed lower face was monitored using a gamma beam densitometer[7]. The resulting experimental results shown in Figure 6 were taken from Hadley's report[4]. Numerically, the experiment was duplicated, Figure 7, using one-hundred finite elements as shown in Figure 8. All surfaces were considered no flow boundaries except for the bottom face through which the water enter the sample at constant pressure. Figure 9 shows the numerical results superimposed on the experimental data. Using a

$K_{saturated} = 3 \times 10^{-18}$ m^2 gives the best correlation with experiment regarding early arrival time of some water at the upper end of the block, and of the smeared out moisture front through the region. It appears from Figure 9 that the entrapped air in the unsaturated pores resists the influx of water near the top end ($x > 10$ cm) at late times ($t > 2$ days).

Conclusions and Discussion

It is concluded that the isothermal Richard's equation can be used under certain conditions to give reasonable water infiltration rates into a dry sample of tuff rock. This implies that the capillary model used to convert the mercury pore symmetry data to water intrusion data is applicable.

Additional consideration will be given to this problem. The question remains as to how this procedure involving a small (14 cm) sample extends to the repository scale problem which may include large-scale inhomogenities including fractures and faults. The extremely big negative pore pressures restrict the applicable types of experimental procedures. The large negative pressures, "tension head" or "suction head" as referred to in Freeze and Cherry, are the results of small pore radius within the tuff blocks and large water surface tension effects.

Typical pore diameters are often smaller than one micron. At these diameters bubble formation (cavitation) within the matrix is restricted from reaching its critical minimum size required for stability. This phenomena is discussed in Reference 8. A better understanding of this phenomena and how it pertains to flow through unsaturated porous media is required. Additional effort will be concentrated on:

1. Obtaining a better understanding of the limitations of Richard's equation with respect to materials with small pore diameters where the capillary forces are large.
2. Investigate additional experimental procedures which might be applicable to tight rock, such as the long column, high pressure, experimental procedure used by Glenden Gee at Pacific Northwest Laboratory.

References

1. Eaton, R. R., Memo to L. D. Tyler, 4537, dated January 6, 1982, Subject: Current Status of Computational Capabilities for Predicting Energy and Mass Flux Through Partially Saturated Porous Media.

2. Gartling, D. K., and C. E. Hickox, "MARIAH - A Finite Element Computer Program for Incompressible Porous Flow Problems", SAND79-1623, Sandia Laboratories, Albuquerque, NM, August, 1980.

3. Freeze, R. A. and J. A. Cherry, Groundwater. Prentice-Hall, Inc., 1979.

4. Hadley, G. R., Memo to Distribution dated January 27, 1982, Subject: Drying Experiments on Welded Tuff.

5. Letter from Pat McCann of Micromeritics Instruments Corporation to Kevin Murphy dated September 29, 1981, containing Auto Pore data for Tuff.

6. Auto Pore 9200 Pamphlet, A Description of Mercury Intrusion Porosimetry Techniques, Micromeritics Instruments Corporation, 5680 Goshen Springs Road, Norcross, Georgia, 30093.

7. Reda, D. C., Hadley, G. R., and Turner, J. R., "Application of the Gamma-Beam Attenuation Technique to the Measurement of Liquid Saturation for Two-Phase Flows in Porous Media", Proceedings of the 27th International Instrumentation Symposium, Instrument Society of America, Indianapolis, Indiana, April 27-30, 1981.

8. Purcell, W. R., "Capillary Pressures- Their Measurement Using Mercury and the Calculation of Permeability Therefrom T. P. 2544 Petroleum Transactions, AIME, February, 1949.

Distribution:

4760 R. W. Lynch
4761 L. W. Scully
4763 J. R. Tillerson
4763 D. R. Fortney
4764 R. C. Lincoln
5500 O. E. Jones
5510 D. B. Hayes
5511 J. W. Nunziato
5511 D. K. Gartling
5511 G. R. Hadley
5511 C. E. Hickox
5511 M. J. Martinez
5511 D. F. McTigue
5511 R. K. Wilson
5512 D. F. McVey
5512 A. J. Russo
5513 D. W. Larson
5520 T. B. Lane
5522 R. P. Rechard
5530 W. Herrmann
5541 W. C. Luth
5511 R. R. Eaton

TABLE 1

Air/Mercury		Air/Water	
P_{psia}	θ_{Hg}	ψ(cm)	θ_{H_2O}
1.4	0	1.01×10^3	1.0
8.9	.038	$.90 \times 10^3$	.962
16.9	.111	$.79 \times 10^3$	.889
28.6	.114	$.63 \times 10^3$	.886
53.6	.149	$.28 \times 10^3$	.851
73.6	.173	$-.01 \times 10^3$	.827
113.4	.206	$-.57 \times 10^3$	.794
357.5	.299	-4.00×10^3	.701
1,114.0	.397	-14.64×10^3	.603
2,611.0	.625	-35.71×10^3	.375
5,377.0	.799	-76.64×10^3	.201
12,556.0	.921	-175.63×10^3	.078
22,153.8	.960	-310.66×10^3	.040
29,406.0	.973	-412.71×10^3	.027
33,831.0	.980	-474.97×10^3	.020
39,047.0	.987	-548.36×10^3	.013
51,882.0	.997	-728.95×10^3	.003
59,706.0	1.000	-839.00×10^3	0.000

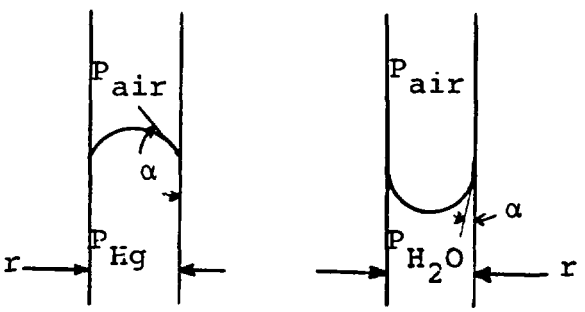

FIGURE 1: Capillaries of radius r for mercury/air and water/air.

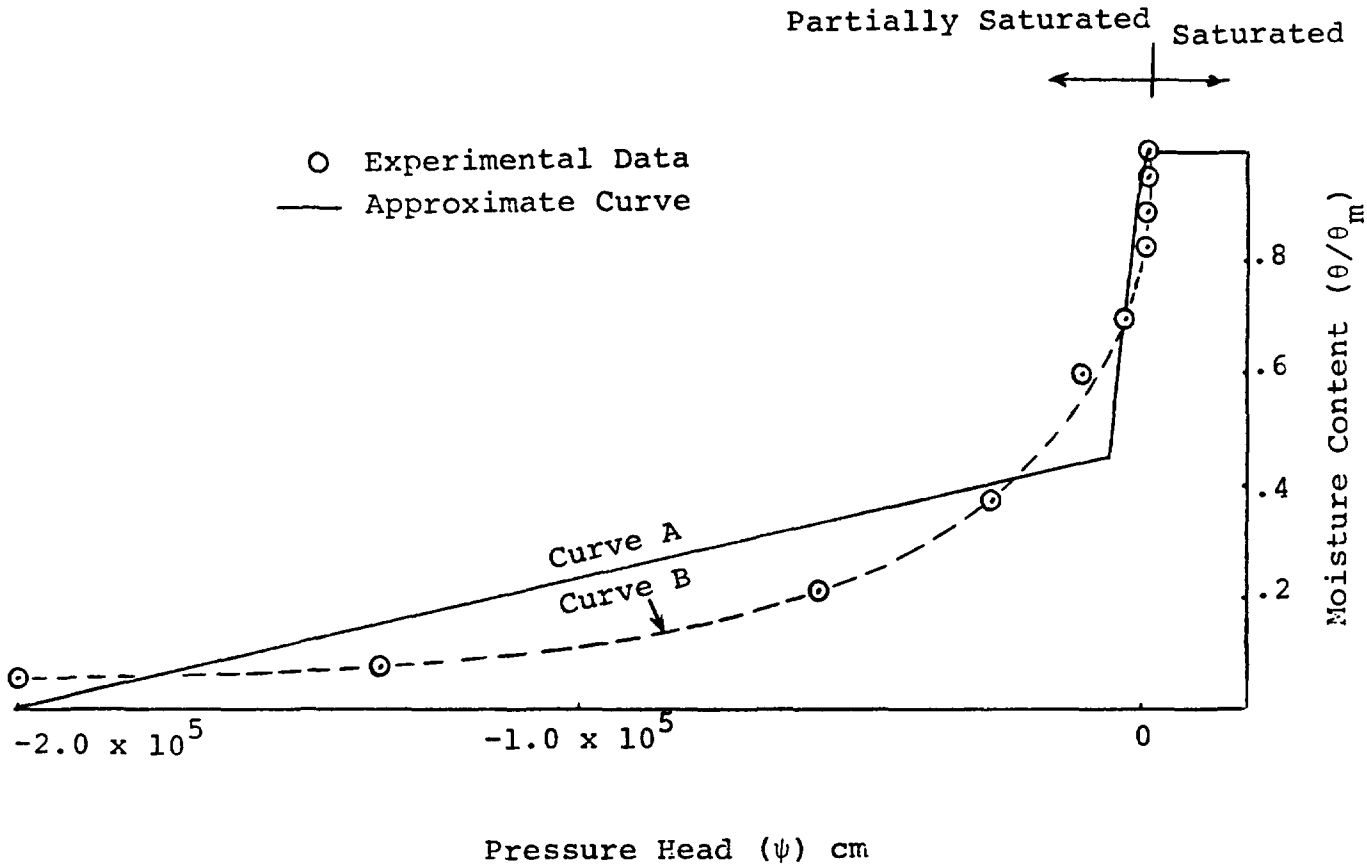

FIGURE 2: Characteristic curve for moisture content as a function of pressure head. Solid curve reduces large slope near saturation.

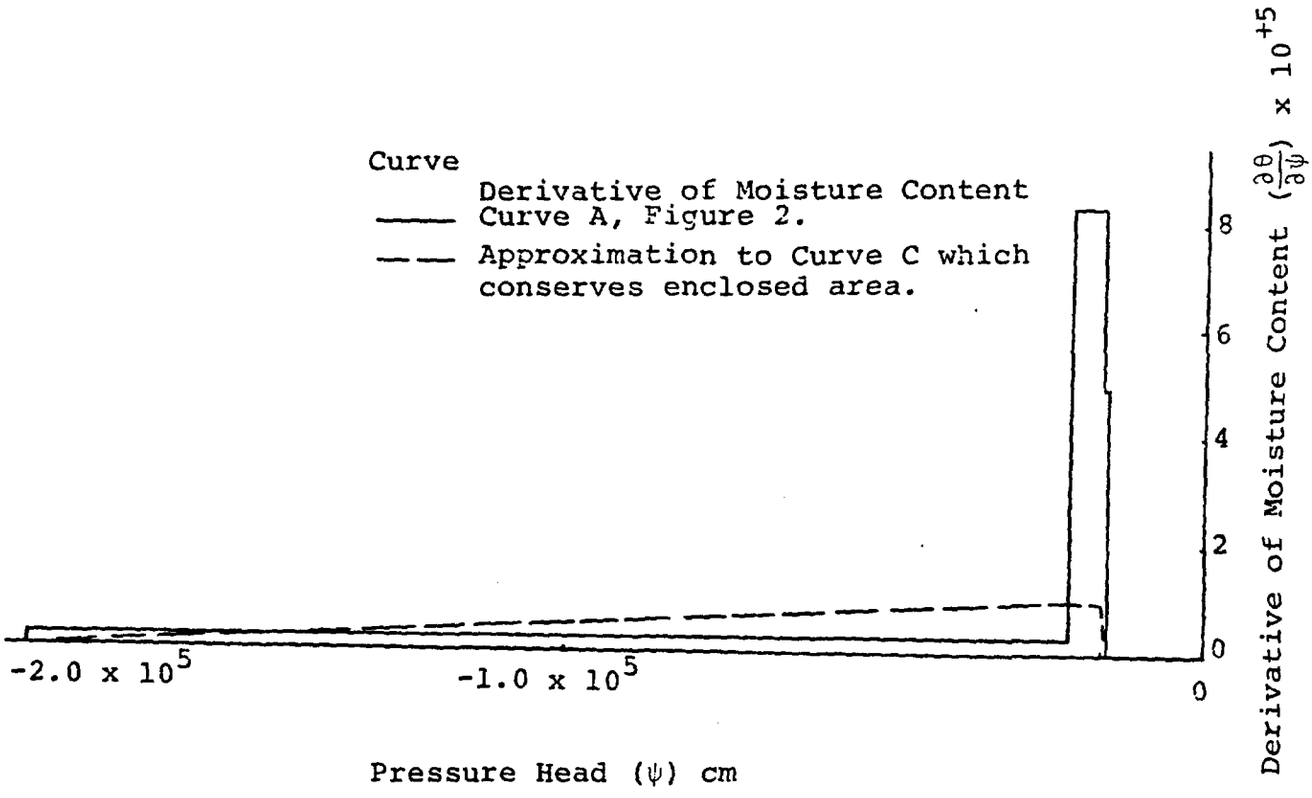

FIGURE 3: Characteristic curve for derivative of moisture content as a function of pressure head. Dashed curve eliminates first order discontinuities in curve while maintaining same area under curve.

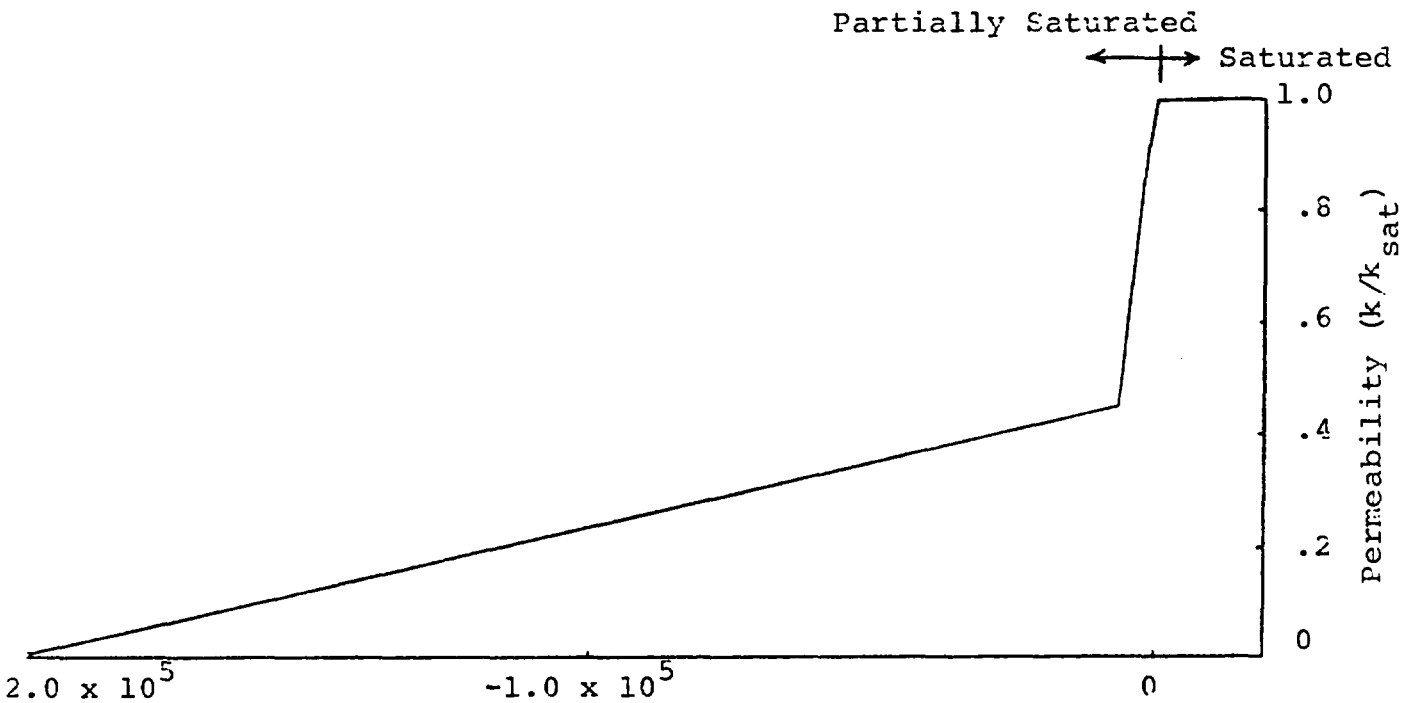

FIGURE 4: Characteristic curve for permeability as a function of pressure head $k|_{\psi < 2 \times 10^5} = k_{sat}/20.$

FIGURE 5: SCHEMATIC OF APPARATUS TO MEASURE WATER SATURATION PROFILES IN ROCKS

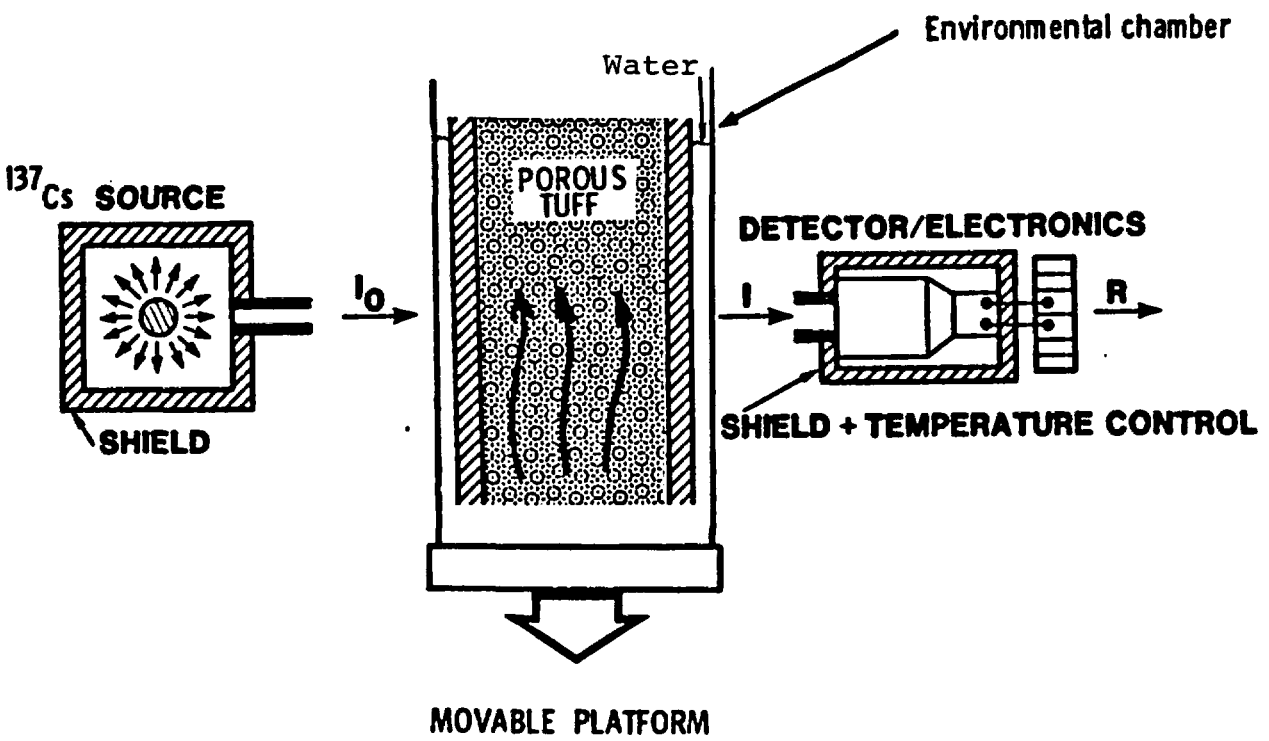

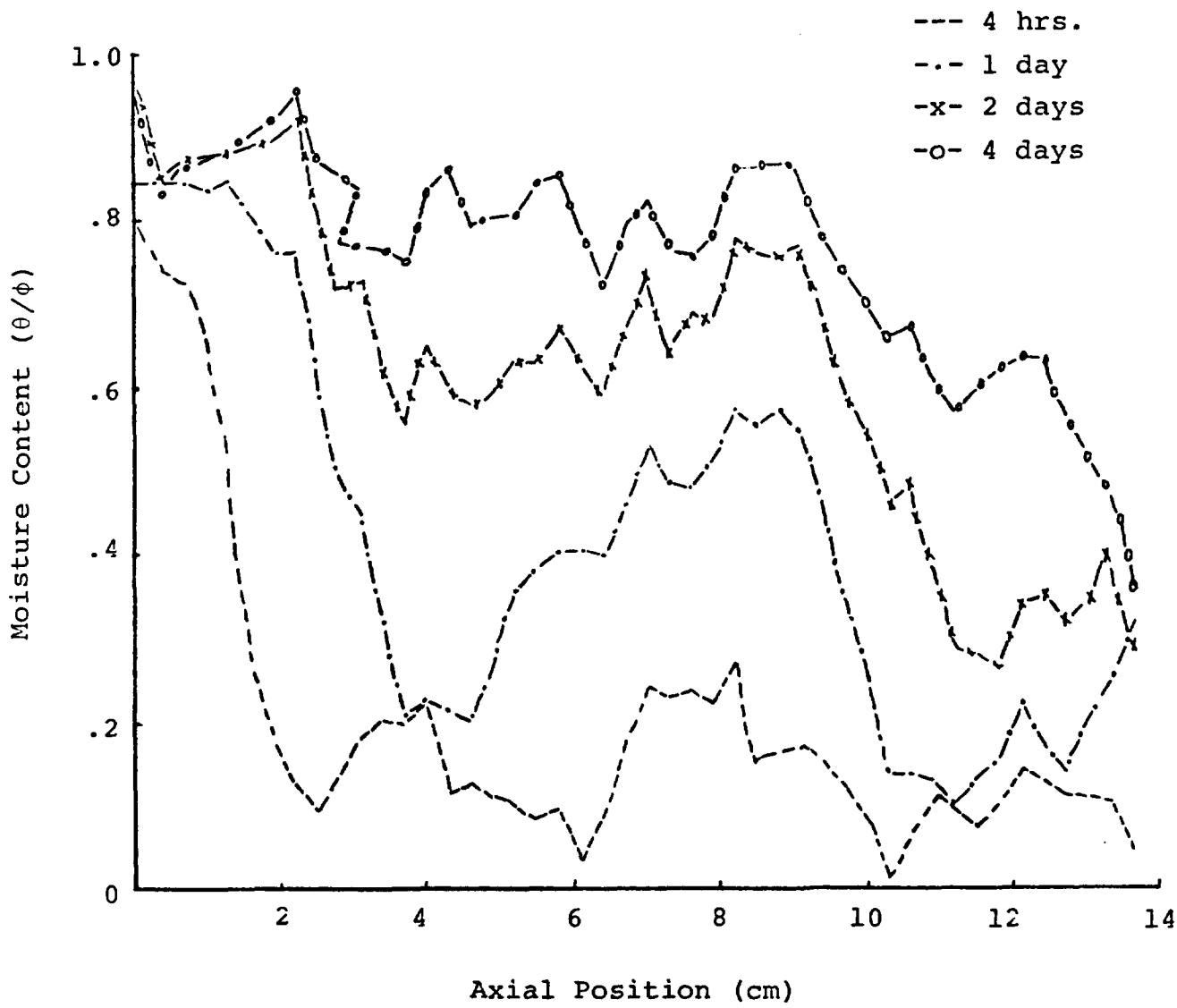

FIGURE 6: Experimental results showing water intrusion in tuff (Reference 4).

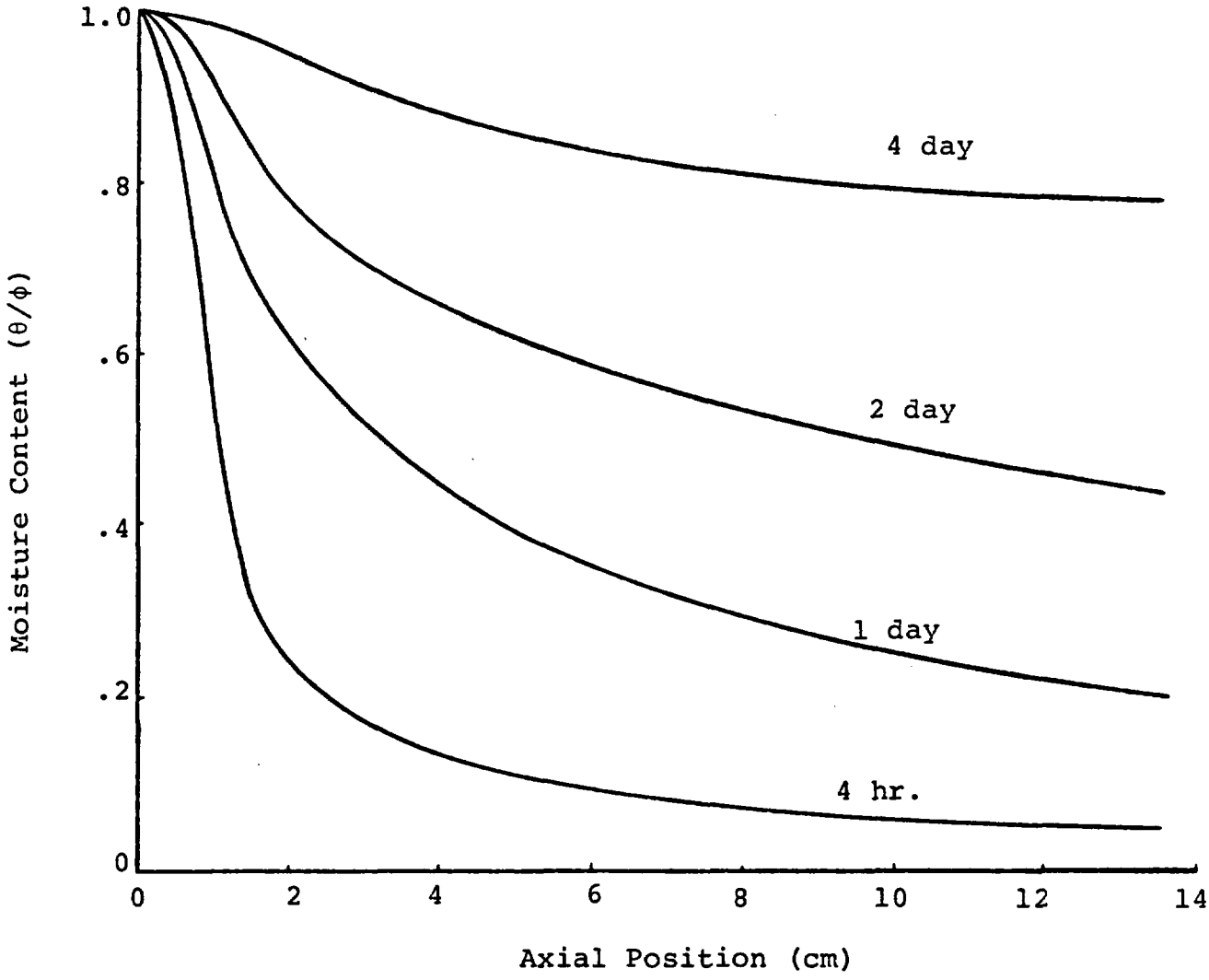

FIGURE 7: Calculation of water intrusion into tuff.

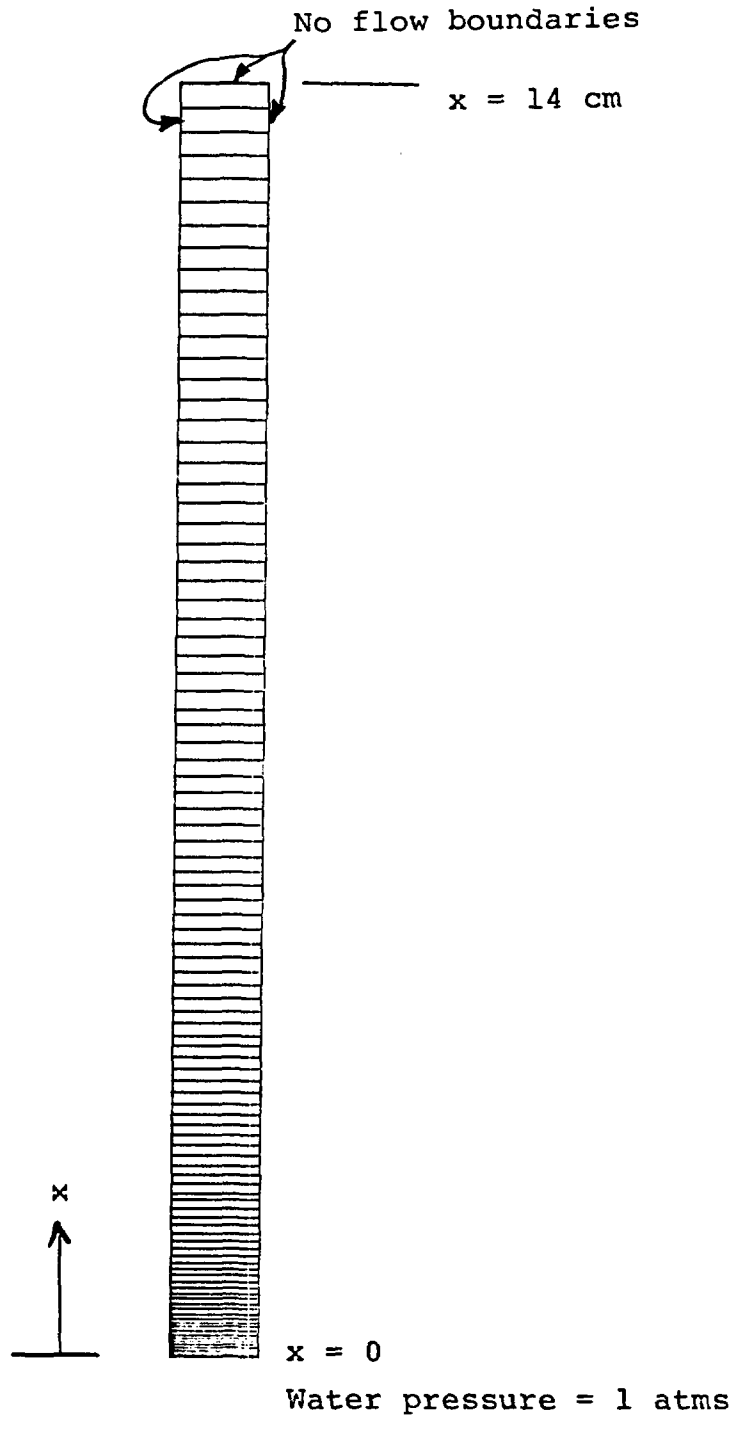

FIGURE 8: Computational finite element mesh, 100 elements.

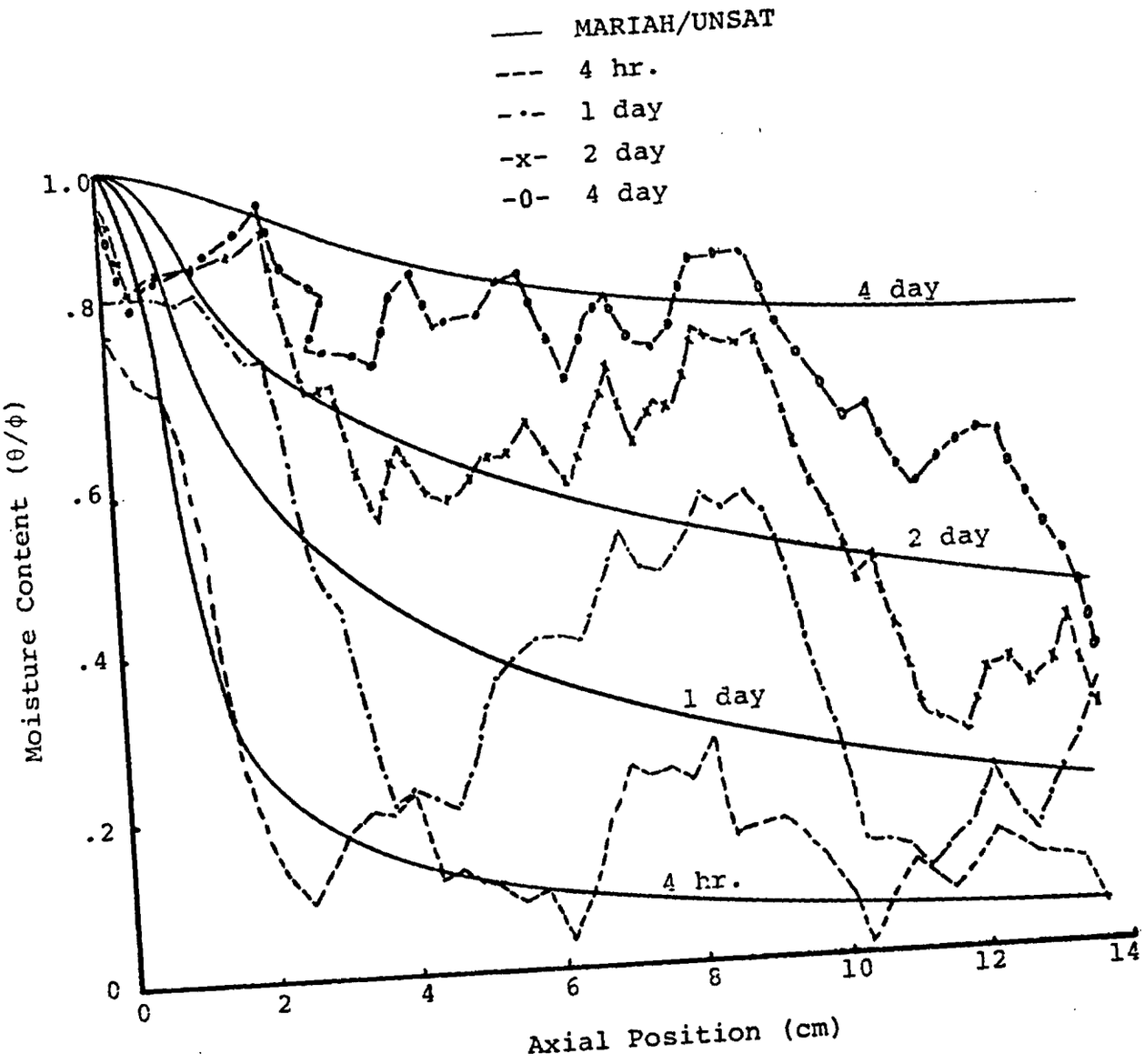

FIGURE 9: Comparison of experimental and computational results.
($k = 3 \times 10^{-18}$ m^2)

APPENDIX F

Sandia National Laboratories
Albuquerque, New Mexico 87185

date: July 14, 1982

to: Distribution

from: R. R. Eaton, 5511

subject: The Importance of Accurate Material Characteristic Curves and Boundary Conditions for Performing Computations in Unsaturated Media.

Introduction

Computing Darcy type flow of a fluid through a porous medium which is not completely saturated requires knowledge of the relation between the fluid pressure within the material pores and (1) hydraulic conductivity and (2) moisture content. These two functional relations, which are not required for saturated calculations, are not readily available for all materials of interest. Consequently, it is sometimes necessary to make calculations using sketchy or sparce experimental data to define these relationships. The purpose of this paper is to determine the sensitivity of resulting calculations to parametrically varying the characteristic curves which define the hydraulic conductivity and moisture content as a function of pressure. The computational tool used for this study was a one-dimensional finite difference code[1] which runs interactively on the NOS or VAX.

Problem Definition

The classical problem chosen for this study involves the one-dimensional infiltration of rain into solid which is partially saturated (see Figure 1). The boundary conditions for the test case are:

1. Rain is such that it feeds the soil at a rate of .13 cm/min until the maximum allowable ponding height of 10 cm is reached. Surface pressure is then held at 10 cm.

2. The initial pressure head (ϕ) given by Figure 1 is linear, which says at t = 0 the fluid velocity is zero everywhere.

The computational mesh for this problem consisted of one hundred mesh points, each having a ΔZ value of 1.0 cm. The units chosen for this problem are gm, cm, and seconds.

Results for this base problem was reported on in Reference 1. In that study, a series of straight lines were used to represent the material characteristic curves. The code has been revised such that these curves are now constructed internally in the code using sets of data points for pressure versus moisture content and pressure versus hydraulic conductivity.

Table 1 lists a set of points taken from the characteristic curves given in Reference 2.

Table 1. Data Points Taken From Published Characteristic Curves (Freeze, Reference 2)

Pressure Head (ψ) cm of Water	Hydraulic Conductivity K (cm/min)	Moisture Content θ(% by Volume)
-180	.001	.057
-160	.001	.059
-140	.0014	.065
-120	.0028	.075
-100	.0057	.095
-80	.0136	.165
-60	.0227	.261
-40	.0258	.291
-20	.026	.299
-00	.026	.300

The code fits these points using a spline curve fit subroutine. The spline subroutine also provides the derivative of the moisture content, $(\partial\theta/\partial\psi)$. This quantity is required for the coefficient of the time derivative term, $(\partial\psi/\partial t)$. These three curves are shown in Figure 2. They provide the data for what is referred to as the "base case" for this study. It can be seen from this figure that the ten sets of data points (Table 1) result in reasonably smooth curves, Figures 2a and 2b. The derivative of curve b, Figure 2c, is not as smooth. However, the code and, consequently, the results are not particularly sensitive to the irregular shaped tails as long as area under the curve is correct. Physically, this area is related to the material's ability to absorb water. It was found in this study that this procedure for defining the curves was easy to use and compatible with the computer code.

Parametric Study

The base case discussed above was varied in four ways to provide a realistic set of conditions for a parametric study. The data points defining the hydraulic conductivity curve and the moisture

content curve were shifted both to the right and left by 20 cm of water to provide a total of five cases as outlined in Table 2. The resulting curves are given in Figure 3.

Table 2. Input Characteristic Data for Parametric Study

CASE	Hydraulic Conductivity	Curve Figure 3	Moisture Content	Curve Figure 3
1. (base)	zero shifted	b	zero shifted	b
2.	right shifted	c	zero shifted	b
3.	left shifted	a	zero shifted	b
4.	zero shifted	b	right shifted	c
5.	zero shifted	b	left shifted	a

These cases were computed interactively on the NOS using a one-dimensional time dependent code[1] which solves Richard's equation

$$\frac{\partial}{\partial z}\left(K(\psi)\left(\frac{\partial \psi}{\partial z} + 1\right)\right) = c(\psi)\,\frac{\partial \psi}{\partial t} \quad . \tag{1}$$

where

$c = \frac{\partial \theta}{\partial \psi}$

K = hydraulic conductivity (cm/min)

t = time (min)

z = vertical distance (cm)

ψ = pressure head (cm)

θ = content

Results

The resulting moisture content, pressure head, and hydraulic head for these five cases are given in Figures 4 through 9, for the initial pressure head distribution given in Figure 1. Figures 4 through 6 demonstrate the effect of fixing the moisture content curve while varying the hydraulic conductivity curve. The time required for 100% saturation for the three cases varies only from 52 to 58 minutes, as can be seen from the curves. However, it must not be concluded that flow through unsaturated media is insensitive to the hydraulic conductivity characteristic curve because, as it turns out for this test problem, the time to

saturation is stongly coupled to the applied boundary condition at the ground surface. The applied boundary condition (see b.c. 1 above) stipulates that the surface influx (rain) is .13 cm/min until a ponding height of 10 cm is reached. At this computational time, the b.c. is changed such that the ponding height (surface pressure) is held constant and the influx is automatically adjusted by the code. Consequently, during the early part of the run (P surface < 10 cm) the influx rate for all cases is the same regardless of K value. Only at late times, when P surface = 10 cm, is the influx rate for case 3 increased because of the increased (left shifted) conductivity curve, and the influx rate for case 2 decreased. At early times, the shape of the moisture content curves reflect the differences in conductivity. The smaller the conductivity, the faster the regions near the surface approach saturation. The fluid enters through the surface but does not get transported to lower depths.

Figures 7 through 9 show the effect on saturation from shifting the moisture content characteristic curve, Figure 3b, while holding the hydraulic conductivity characteristic curve fixed. These curves show that the saturation rate differs significantly. Times to full saturation of 24 minutes for left shifted moisture curve, Figure 3b (curve a) to 109 minutes for the right shifted curve (curve c) were computed. The first impression from these results could lead one to conclude that saturation rates are a strong function of the characteristic curve. As before, however, one must consider not only the characteristic curves but also the initial and applied boundary conditions. For these problems, the initial pressure distribution was assumed constant. Therefore, the water table (depth at which full saturation first occurs) location actually varies by ± 20 cm as the moisture content curve is shifted. This results in initial moisture content which varies drastically, see Figure 7a versus Figure 7c. Simply, case 4 starts at time zero with about 4 times the void space used in case 5. It is reasonable then that it would take longer to fill (saturate) with water.

Conclusions and Future Work

It is concluded from this study that the time required to fully saturate a region by one-dimensional infiltration is a result of

1. Hydraulic conductivity characteristic curve
2. Moisture content characteristic curve
3. Initial conditions
4. Applied boundary conditions

All of these factors work in a coupled fashion to determine the end result. The most sensitive combination of parameters is the initial pressure profile and moisture content characteristic curve. Varied combinations of these two curves can effect the time required to saturate by a factor of four for the cases investigated.

A similar type of study will be made along a one-dimensional line through section c-c of Yucca Mountain using the best available data for the characteristic curves, material properties, and geometry. The object of this study will be to study the sensitivity of solutions to applied conditions, including characteristic curve shapes and hystersis, and to study the time required for typical surface influx to reach proposed repository elevations.

RRE:5511:ms

Distribution:
5500 J. K. Galt (Actg)
5510 D. B. Hayes
5511 J. W. Nunziato
5511 R. R. Eaton
5511 D. K. Gartling
5511 G. R. Hadley
5511 C. E. Hickox
5511 M. J. Martinez
5511 D. F. McTigue
5511 D. C. Reda
5511 R. K. Wilson
5512 D. F. McVey
5512 A. J. Russo
5513 D. W. Larson
5520 T. B. Lane
5522 R. P. Rechard
5530 W. Herrmann
5541 W. C. Luth
9760 R. W. Lynch
9761 L. W. Scully
9761 J. A. Fernandez
9762 L. D. Tyler
9762 J. K. Johnstone
9763 J. R. Tillerson
9763 D. R. Fortney
9764 R. C. Lincoln

REFERENCES

1. Eaton, R. R., Memo to Distribution dated January 13, 1982, Subject: The Highly Nonlinear Equation Describing One-Dimensional Infiltration of Water Through Unsaturated Media Are Solved Using Both Crank-Nicholson Finite Difference Scheme and the Galerkin Finite Element Technique.

2. Freeze, R. A. and Cherry, V. A., Ground Water, Prentice-Hall, Inc., Englewood Cliffs, New Jersey, 1979.

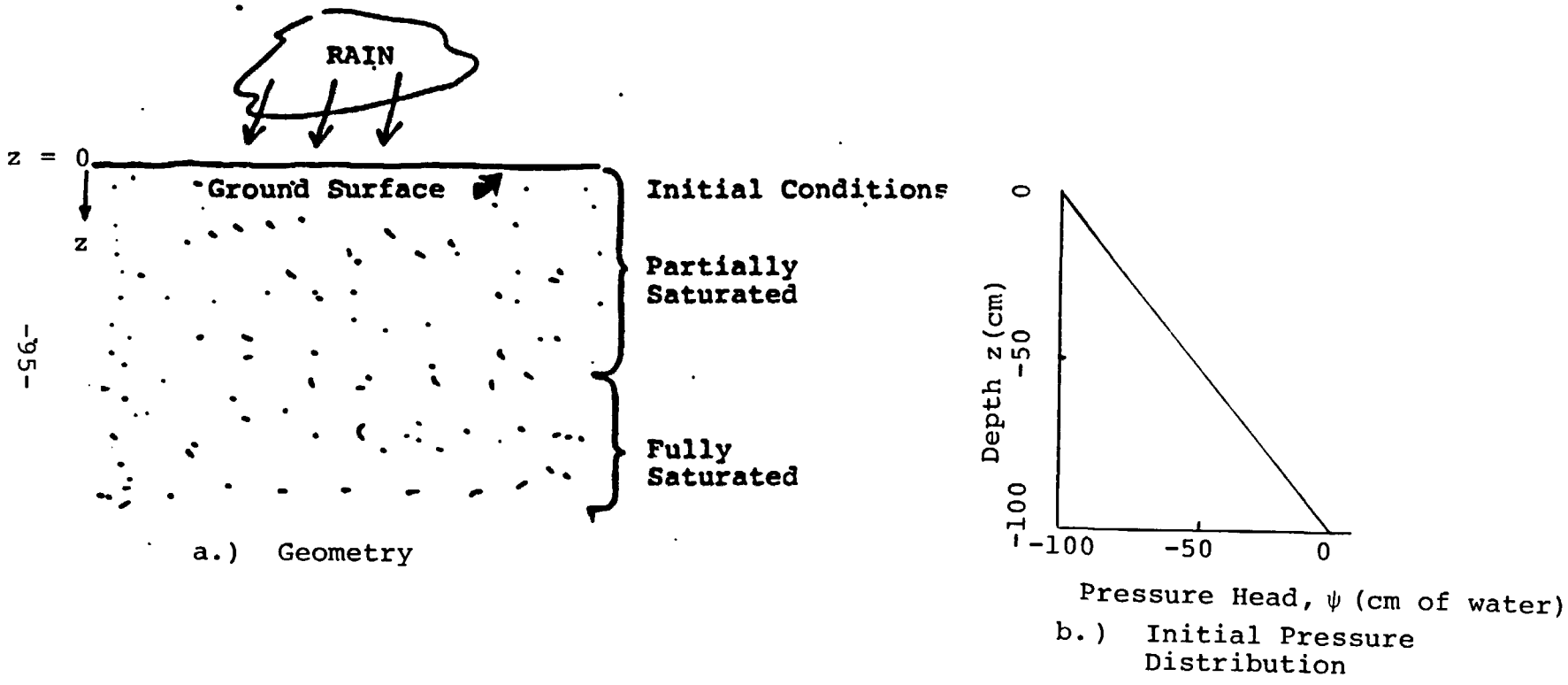

Figure 1. Sample Problem Definition.

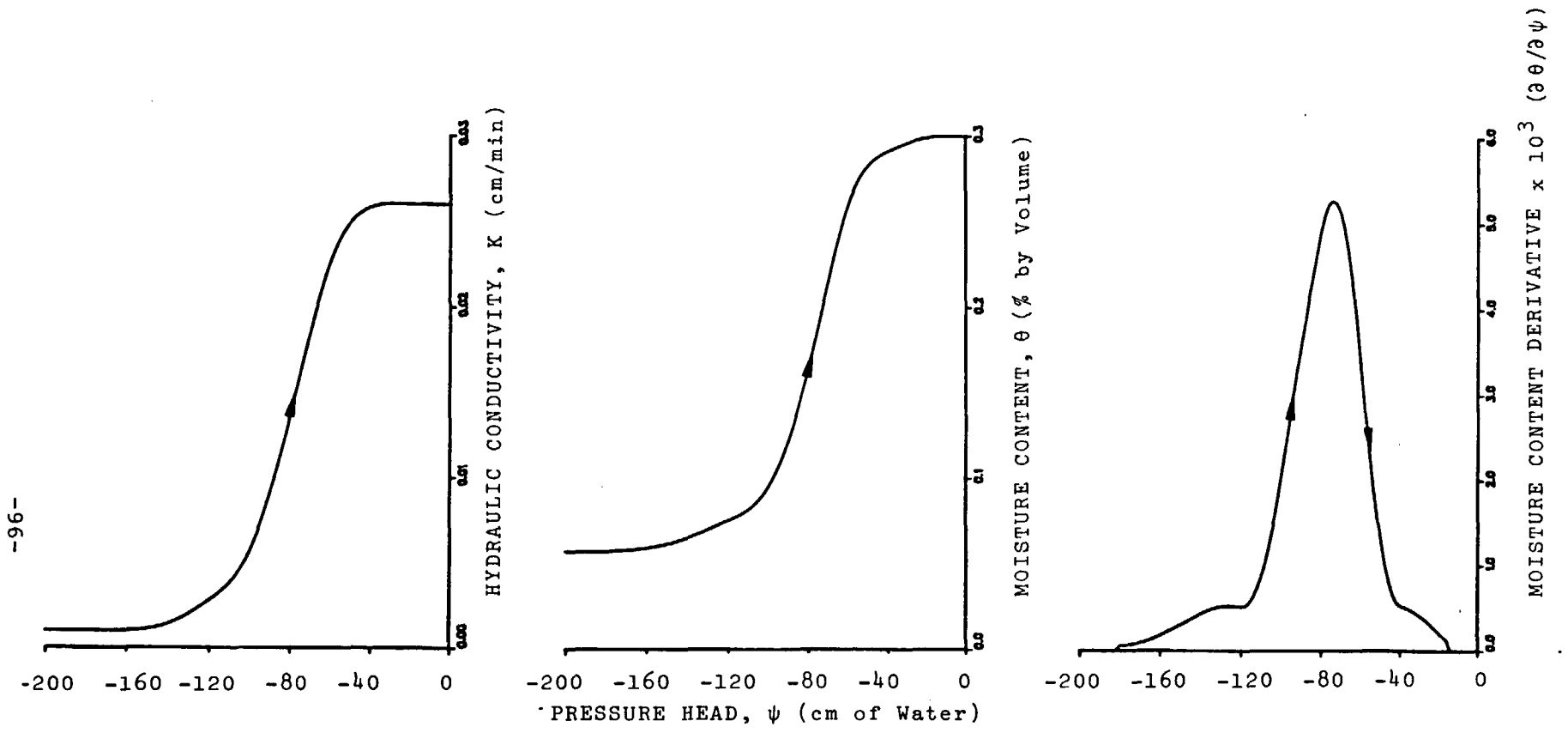

a.) Hydraulic Conductivity b.) Moisture Content c.) Derivative of Moisture Content

Figure 2. Characteristic Wetting Curves Relating Hydraulic Conductivity, Moisture Content, and Derivative of Moisture Content to Pressure Head for a Naturally Occuring Sand Soil.

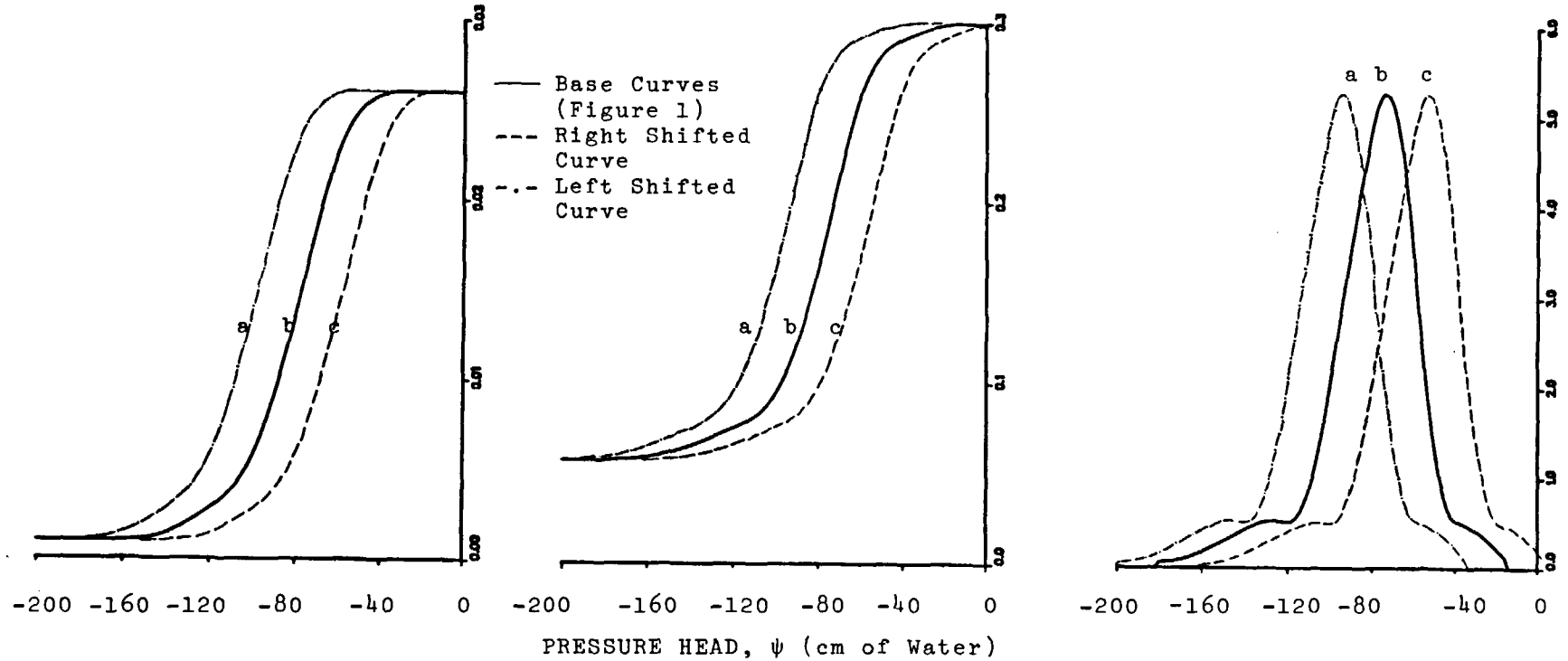

a.) Hydraulic Conductivity b.) Moisture Content c.) Derivative of Moisture Content

Figure 3. Parametric Set of Characteristic Curves Which Have Been Shifted Horizontally by ± 20 cm of Water.

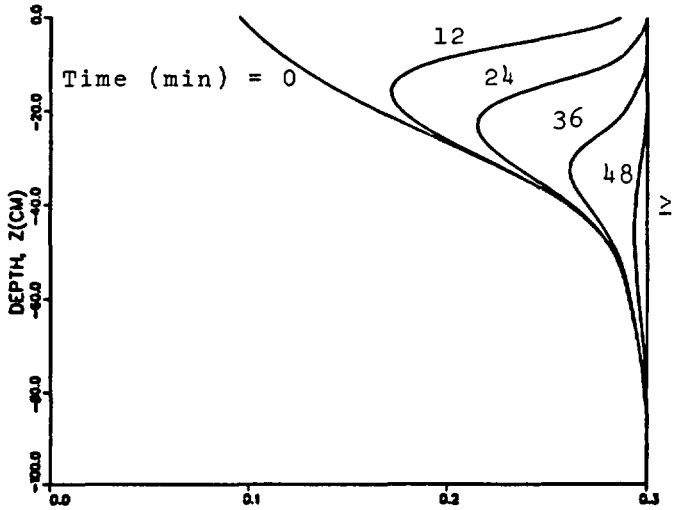

Figure 4. Moisture Content as a Function of Depth for the Base Moisture Content Characteristic Curve (curve b) and Three Different Hydrauli Conductivity Curves.

a.) Left Shifted Hydraulic Conductivity, Curve (a), Case 3.

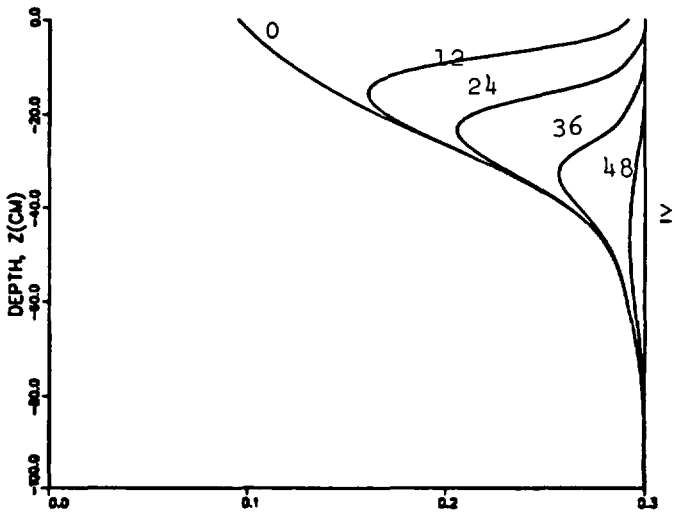

b.) Base Hydraulic Conductivity, Curve (b), Case 1.

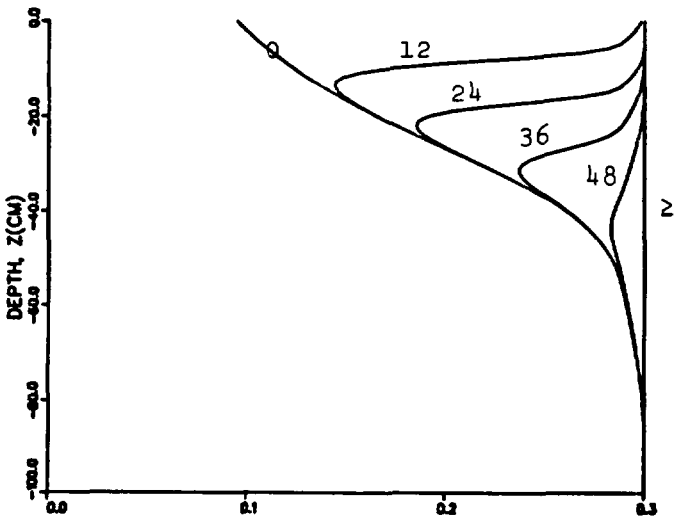

c.) Right Shifted Hydraulic Conductivity, Curve (c), Case 2.

MOISTURE CONTENT, θ (% BY VOL)

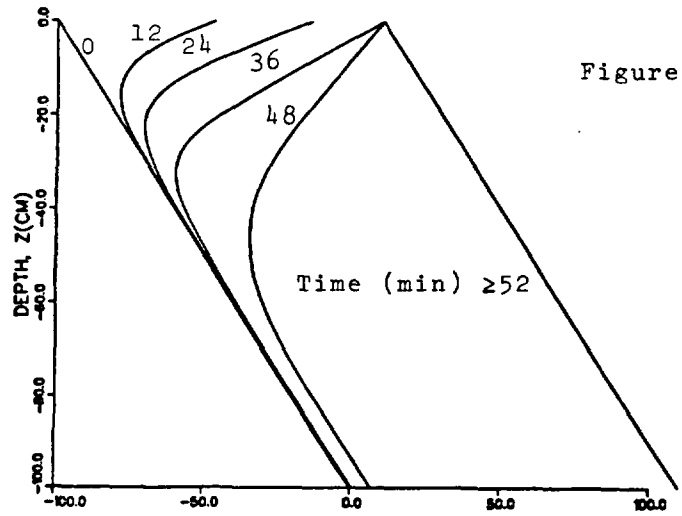

Figure 5. Pressure Head as a Function of Depth for the Base Moisture Content Characteristic Curve (curve b) and Three Different Hydraulic Conductivity Curves.

a.) Left Shifted Hydraulic Curve (a), Case 3.

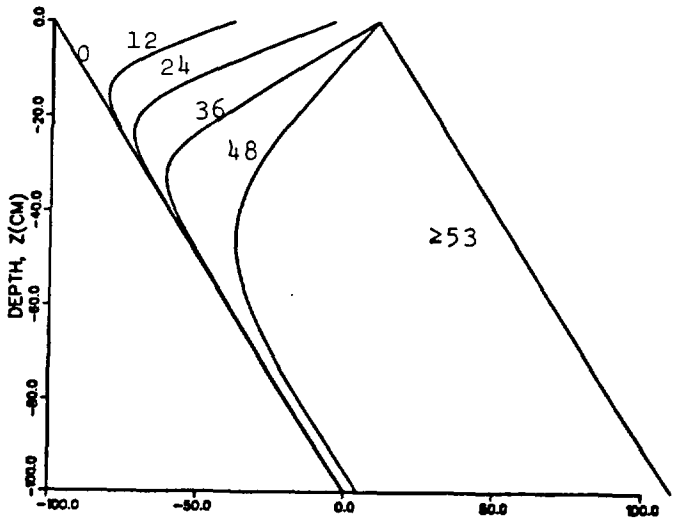

b.) Base Hydraulic Conductivity, Curve (b), Case 1.

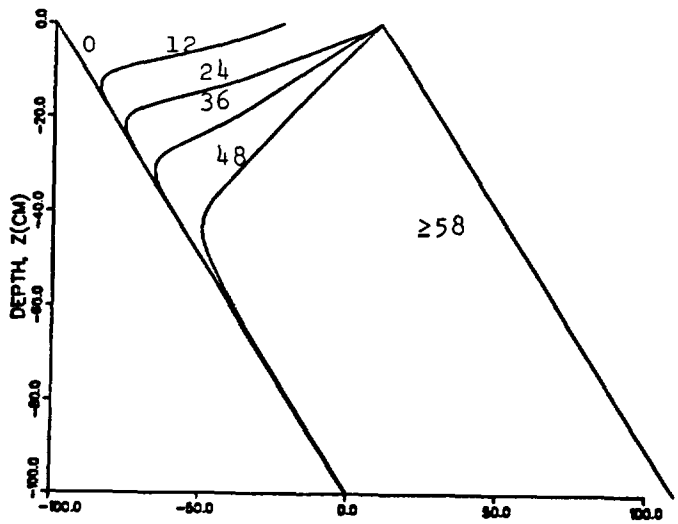

c.) Right Shifted Hydraulic Conductivity, Curve (c), Case 2.

PRESSURE HEAD, ψ (CM OF WATER)

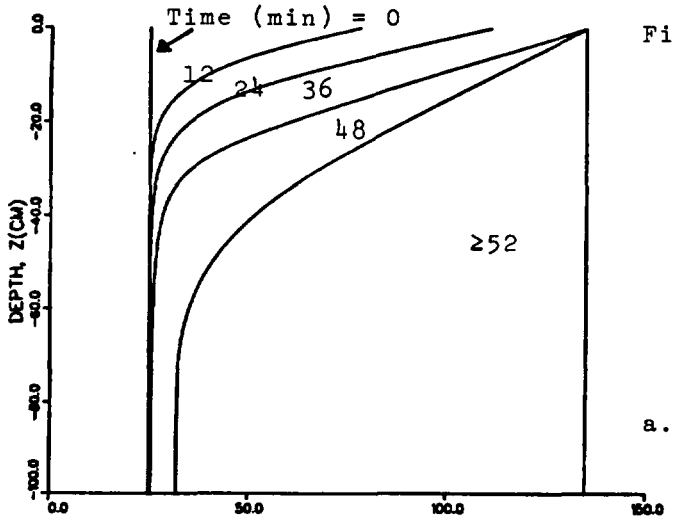

Figure 6. Hydraulic Head as a Function of Depth for the Base Moisture Content Characteristic Curve (curve b) and Three Different Hydraulic Conductivity Curves.

a.) Left Shifted Hydraulic Conductivity Curve (a), Case 3.

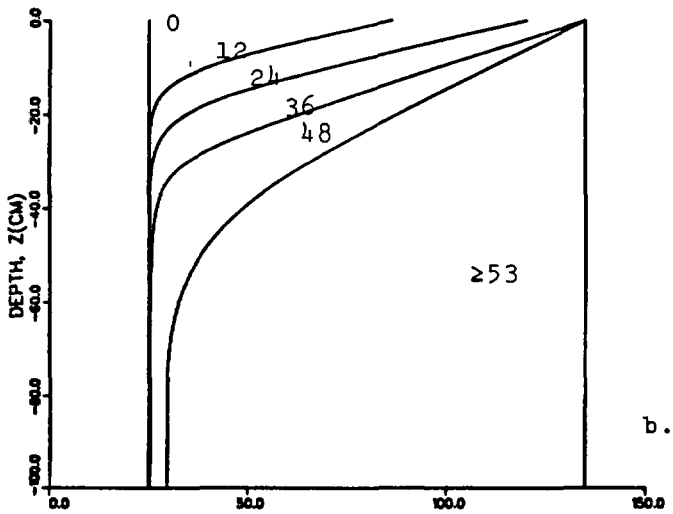

b.) Base Hydraulic Conductivity, Curve (b), Case 1.

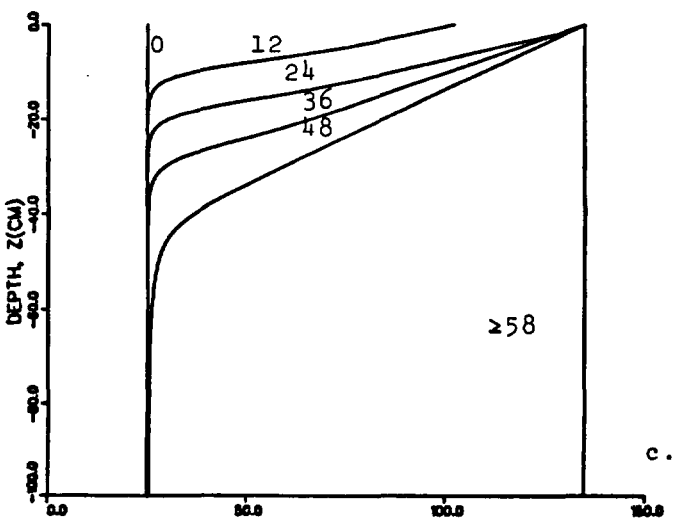

c.) Right Shifted Hydraulic Conductivity, Curve (c), Case 2.

HYDRAULIC HEAD, H (CM OF WATER)

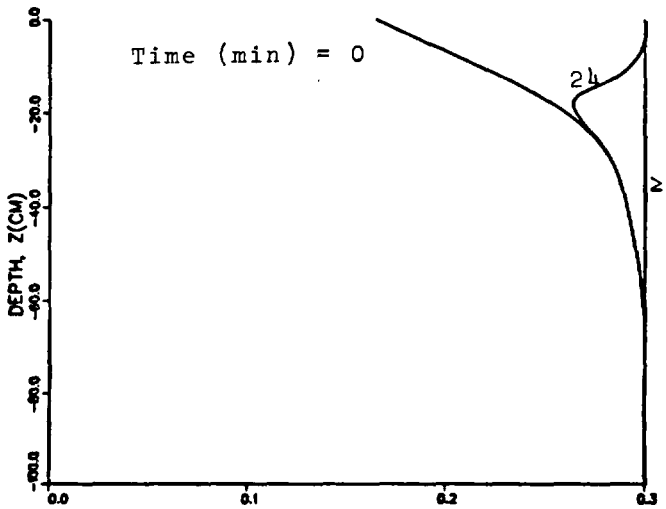

Figure 7. Moisture Content as a Function of Depth for the Base Hydraulic Conductivity Curve (curve b) and Three Different Moisture Content Curves.

a.) Left Shifted Moisture Content Curve (curve a), Case 5.

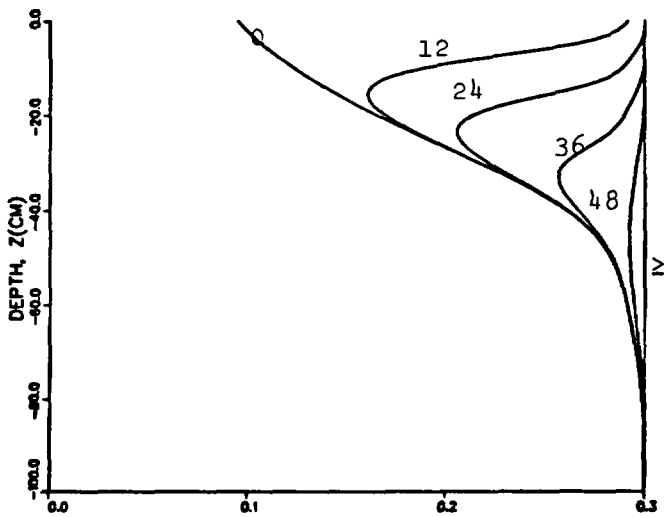

b.) Base Moisture Content Curve (curve b), Case 1.

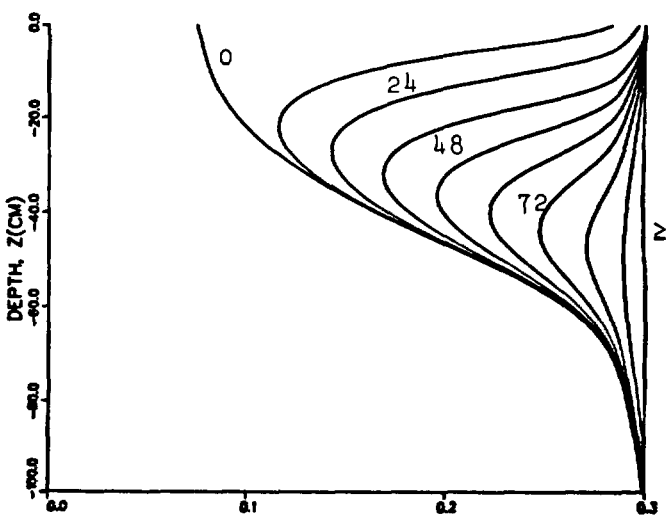

c.) Right Shifted Moisture Content Curve (curve c), Case 4.

MOISTURE CONTENT, θ (% BY VOL)

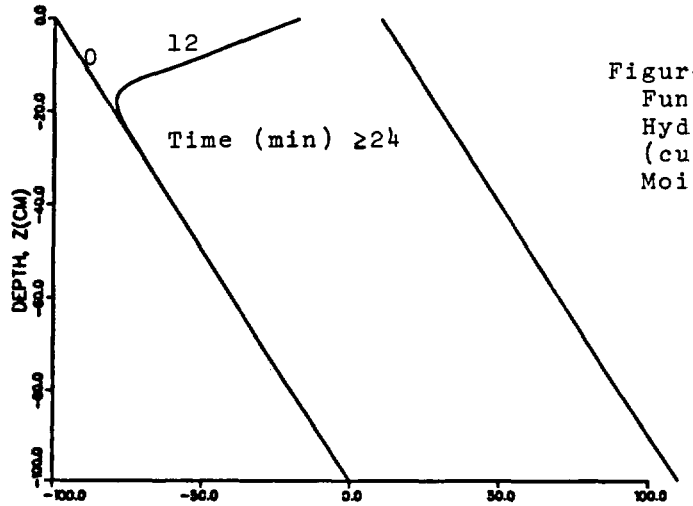

Figure 8. Pressure Head as a Function of Depth for the Base Hydraulic Conductivity Curve (curve b) and Three Different Moisture Content Curves.

a.) Left Shifted Moisture Content Curve (curve a), Case 5.

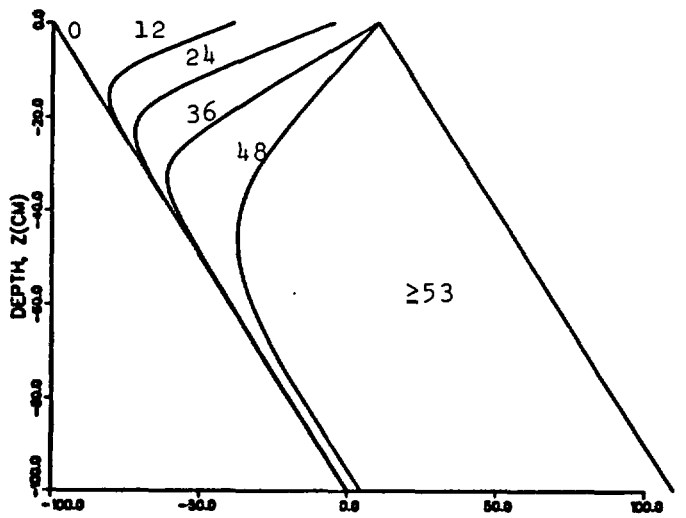

b.) Base Moisture Content Curve (curve b), Case 1.

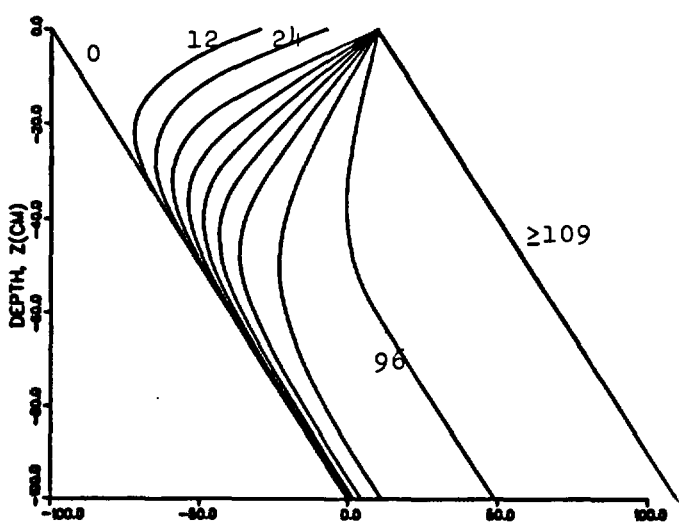

c.) Right Shifted Moisture Content Curve (curve c), Case 4.

PRESSURE HEAD, (CM OF WATER)

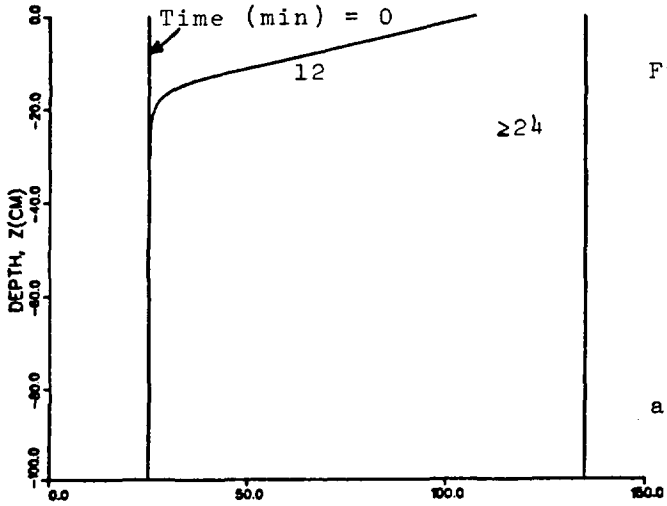

Figure 9. Hydraulic Head as a Function of Depth for the Base Hydraulic Conductivity Curve (curve b) and Three Different Moisture Content Curves.

a.) Left Shifted Moisture Content Curve (curve a), Case 5.

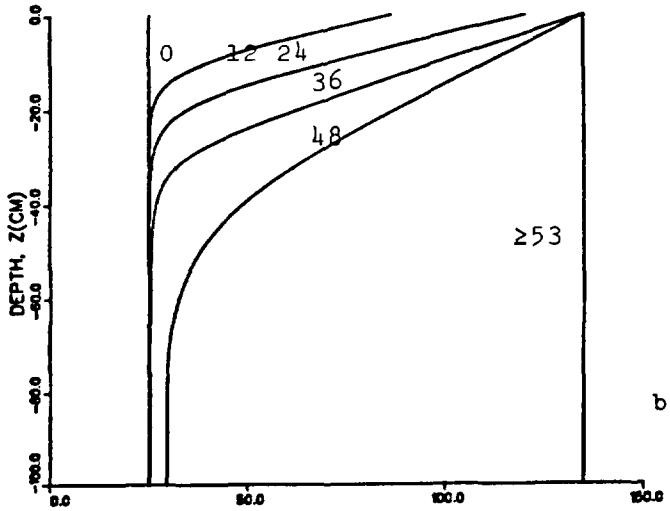

b.) Base Moisture Content Curve (curve b), Case 1.

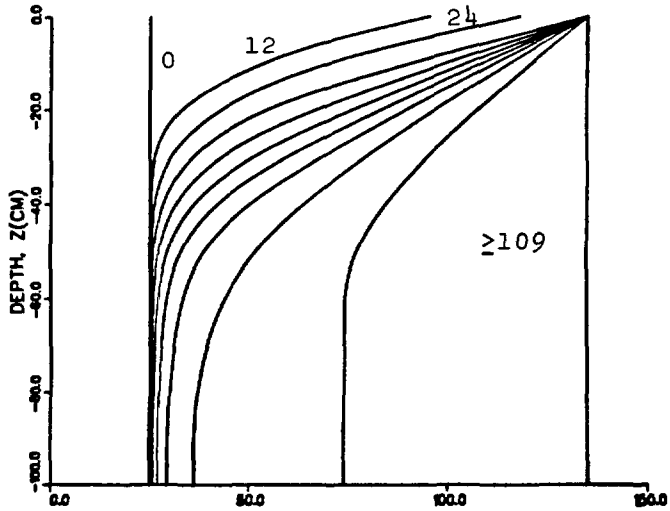

c.) Right Shifted Moisture Content Curve (curve c), Case 4.

HYDRAULIC HEAD, H (CM OF WATER)

APPENDIX G

Sandia Laboratories

Albuquerque, New Mexico
Livermore, California

date: October 15, 1982

to: Distribution

from: R. R. Eaton 1511

subject: The Effect of Short-Term, Surface Water Fluctuations on Pore-Water Motion at Repository Horizons

INTRODUCTION

A series of computations have been made using the finite element code SAGUARO to determine the importance of short-term seasonal variations in rain on pore-water motion in the vicinity of a hypothetical nuclear waste repository. If these fluctuations can be determined to be small or of no signficance, then the cost of long-time calculations can be significantly reduced.

PROBLEM DEFINITION

The problem of one-dimensional infiltration through a multi-layered rock mass was considered (Figure 1). The properties of the various rock layers are given in Table 1. The non-dimensional curves for the permeability, moisture content and derivative of moisture content curves for all rock are given in Figures 2 thru 4. The dimensional values for each strata were obtained by use of the saturated values of permeability (K_{sat}) and porosity(ϕ) given in Table 1. The region was subdivided into 47 finite elements. All surfaces except the top were considered impermeable. Three cases were run. The source boundary condition at the ground surface for the first case is given in Figure 5. In this case, the influx (rain) was varied from +7.7 in/yr to -6.3 in/yr with an average influx of 0.7 in/yr. In the second case, the influx was held constant at 0.7 in/yr, Figure 6. The maximum time computed was 10 years. The third case also used the influx given in Figure 5 with a maximum time = 100 years. In the first two cases, the computational time step was set at 1/6 year. The time step in case 3 varied from 1/6 year to 10 years.

RESULTS AND CONCLUSIONS

Figures 7 and 8 show the head ($p + \rho gz$) and pore water velocity at seven depths as a function of time. Figures 9 and 10 give the head and velocity as a function of depth for six times. Figures 11 and 12 give moisture content as a function of time and distance respectively.

It can be seen from Figure 7a and 8a that the large variations in the applied boundary mass flux (curve 6) are essentially "damped" out at z = 1318 m (a depth of 49 m). At a depth of 100 m, no oscillatory motion can be seen on the figures. A comparison of these values of head and velocity with those given in Figures 7b and 8b (steady boundary flux) show the pore water velocity to be approximately the same at the 100 m depth. The same effect can be seen using Figure 9a and 9b for pressure and Figures 10a and 10b for velocities. Near the surface (z > 1300 m), the applied fluctuations boundary condition has an effect on the pore water pressure and velocity. At greater depths, the annual fluctuations are essentially damped out. Figures 7c, 8c, 9c, 10c show the results of using the non-fluctuating boundary condition for t_{max} = 100 yrs.

Figures 11 and 12 give the moisture content as a function of time and distance for a boundary flux = 0.7 in/yr. These figures show that the region would require a time much greater than 100 years to saturate.

It is concluded from these results that the short-term annual fluctuations in the applied ground surface boundary condition (rain) has no effect at repository level (depth ≈ 100 m). This result is important from a modeling view point. The allowable computational time can be of the order of 60 times less if the detail of near-surface oscillations is neglected. Therefore, the cost of the computations can be greatly reduced.

TABLE 1

Material Properties

	Material	Density Kg/m^3	Saturated Permeability (m^2)	Porosity
Rock	7 (top)	1700	8.0 E - 16	.32
	6	2300	8.0 E - 15	.10
	5	1960	1.6 E - 14	.23
	4	1880	8.0 E - 15	.24
	3	2140	6.4 E - 14	.20
	2 (bottom)	1840	1.6 E - 16	.24
	1 (water)	994	---	---

RRE:1511:fvc

Distribution
1500 W. Herrmann
1510 D. B. Hayes
1511 J. W. Nunziato
1511 R. R. Eaton
1511 N. E. Bixler
1511 M. J. Martinez
1511 D. C. Reda
1511 R. K. Wilson
1512 D. F. McVey
1513 D. W. Larson
1520 T. B. Lane
1522 R. P. Rechard
1541 H. C. Hardee
9760 R. W. Lynch
9761 L. W. Scully
9761 J. A. Fernandez
9762 L. D. Tyler
9762 N. K. Hayden
9762 J. P. Brannen
9762 Y. T. Lin
9762 J. K. Johnstone
9763 J. R. Tillerson

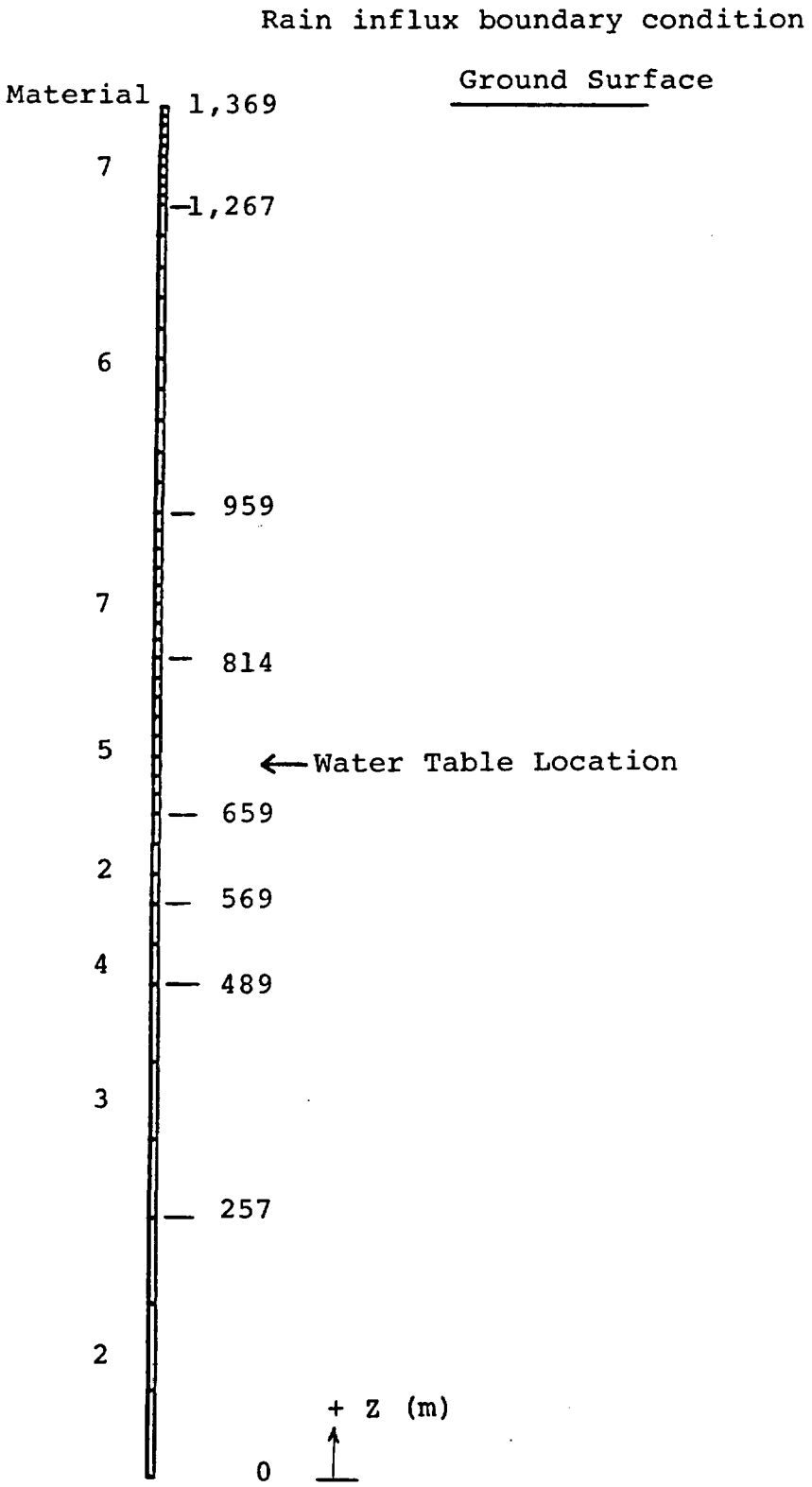

FIGURE 1. Geometry, 47 Finite Elements

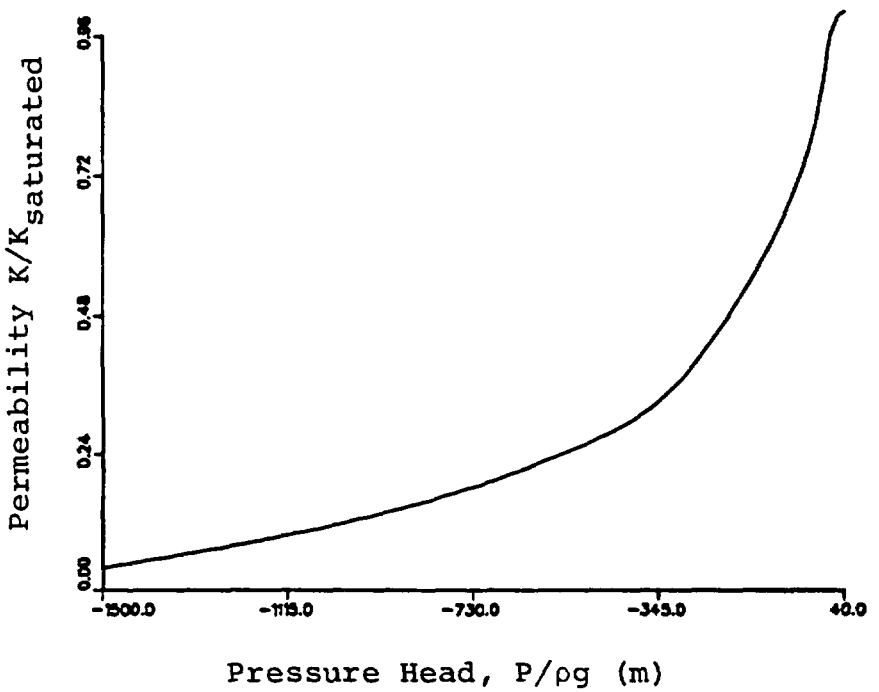

FIGURE 2: Nondimensional Permeability as a Function of Pressure Head.

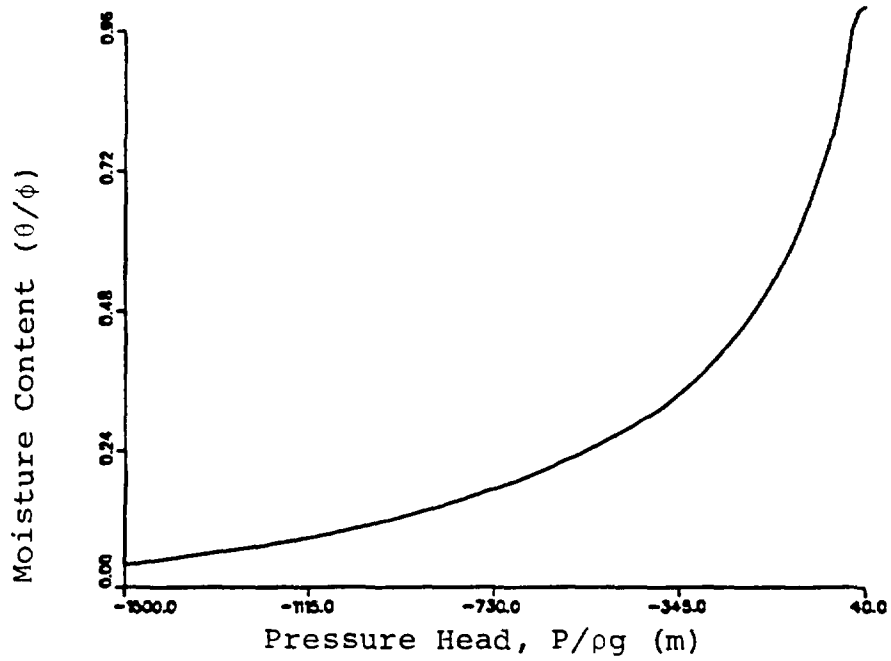

FIGURE 3: Nondimensional Moisture Content as a Function of Pressure Head

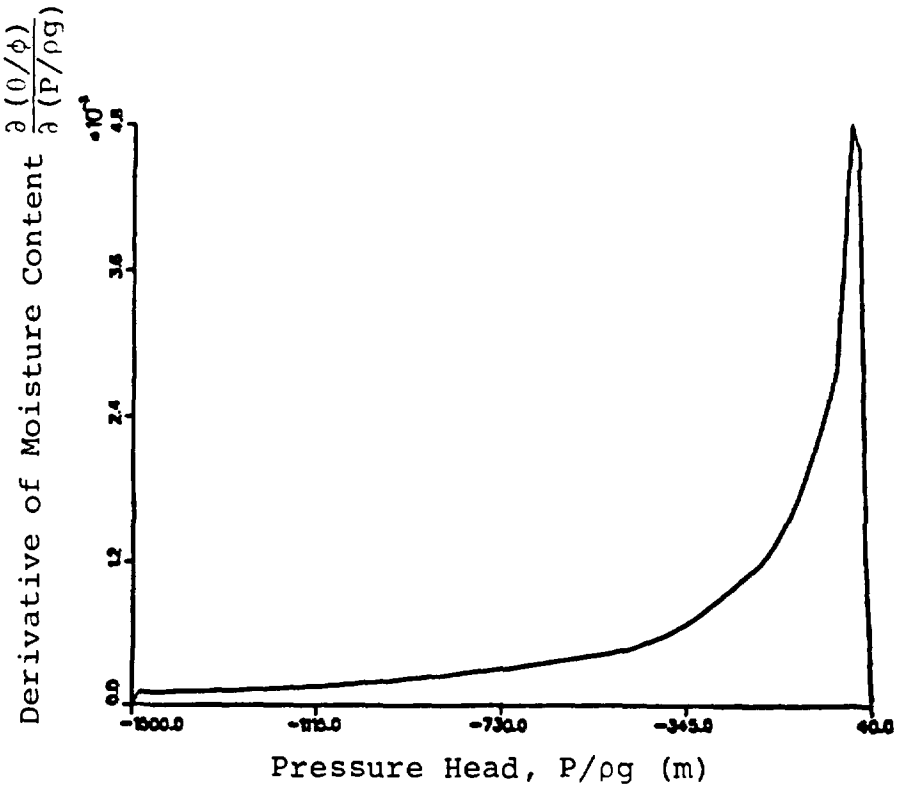

FIGURE 4: Derivative of Moisture Content as a Function of Pressure Head

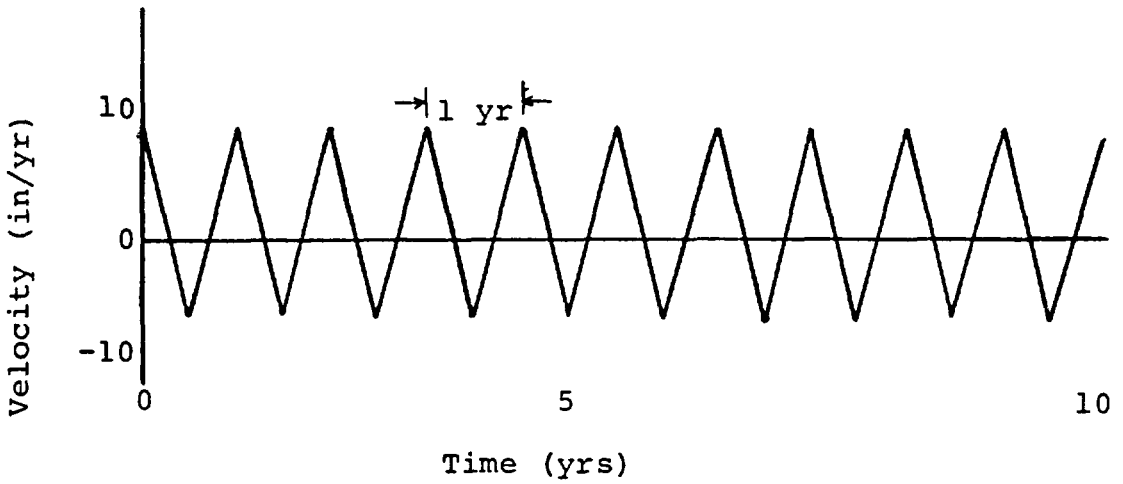

FIGURE 5: Oscillating Influx of Rain at Top Boundary, average flux = 0.7 in/yr.

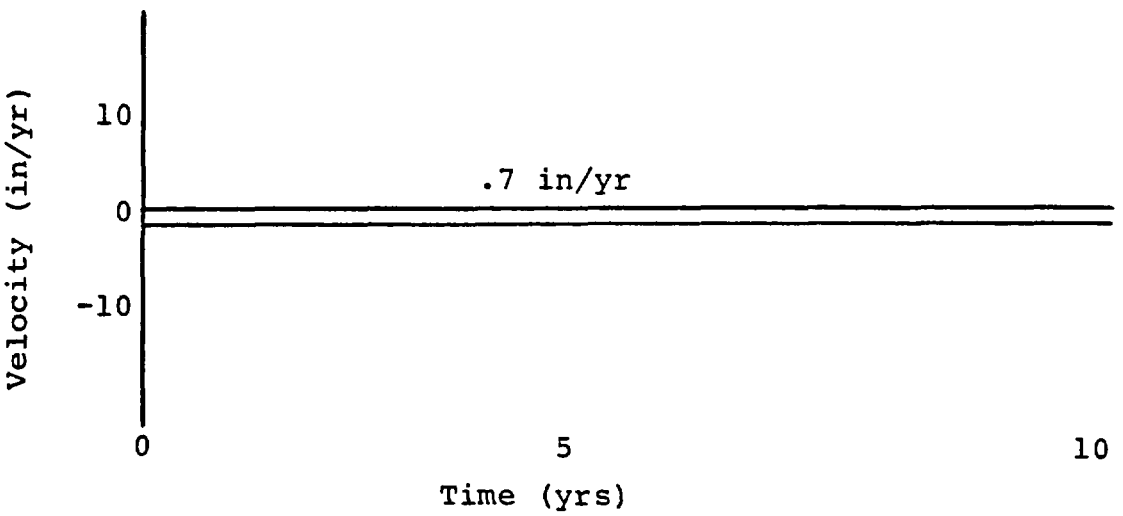

FIGURE 6: Steady Influx of Rain at Top Boundary (flux = 0.7 in/yr.).

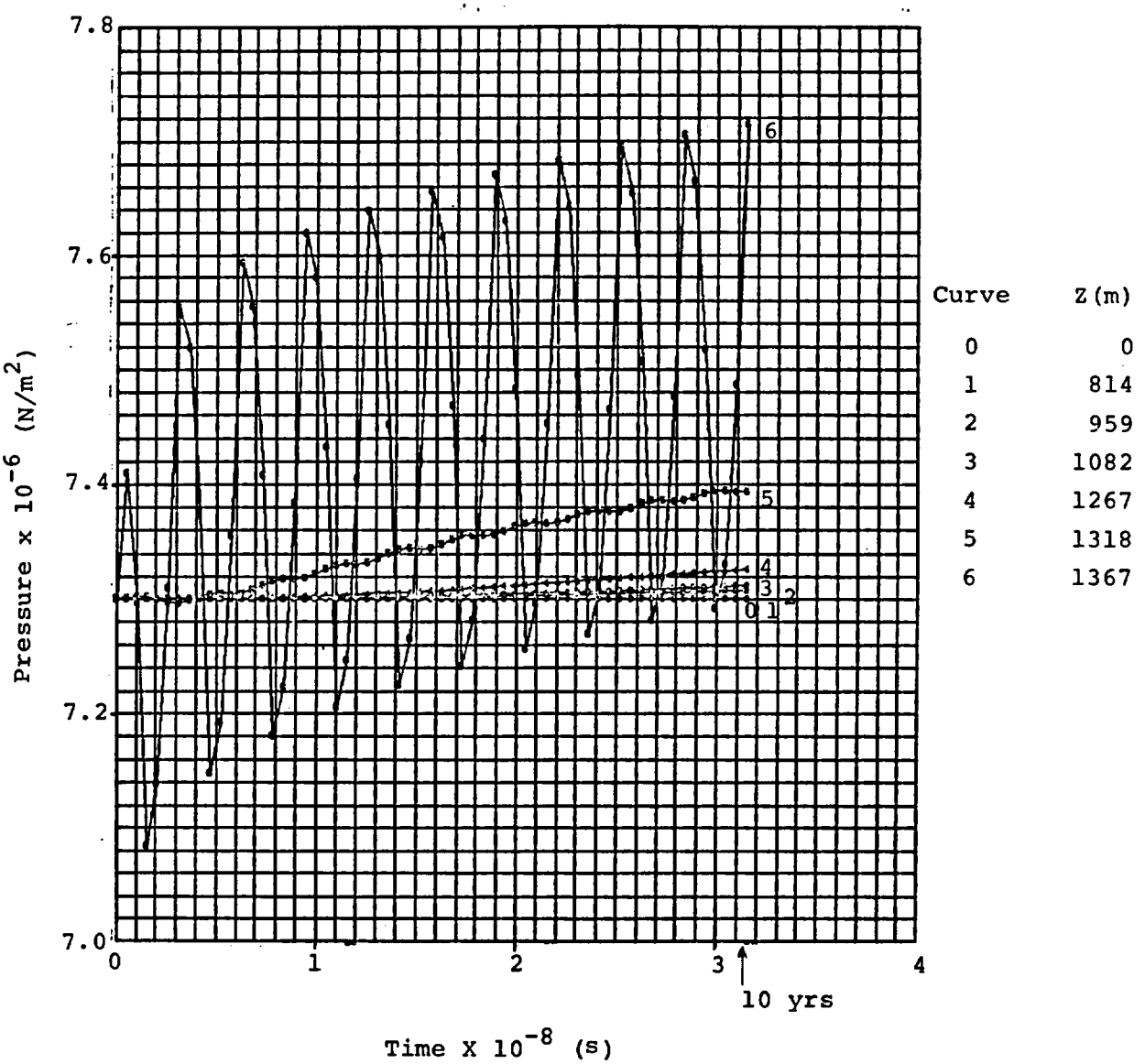

FIGURE 7. Pressure ($p + \rho gz$) as a Function of Time.

a) Oscillating Mass Flux Boundary Condition at Ground Surface, Average Flux = 0.7 in/yr., t_{max} = 10 yr.

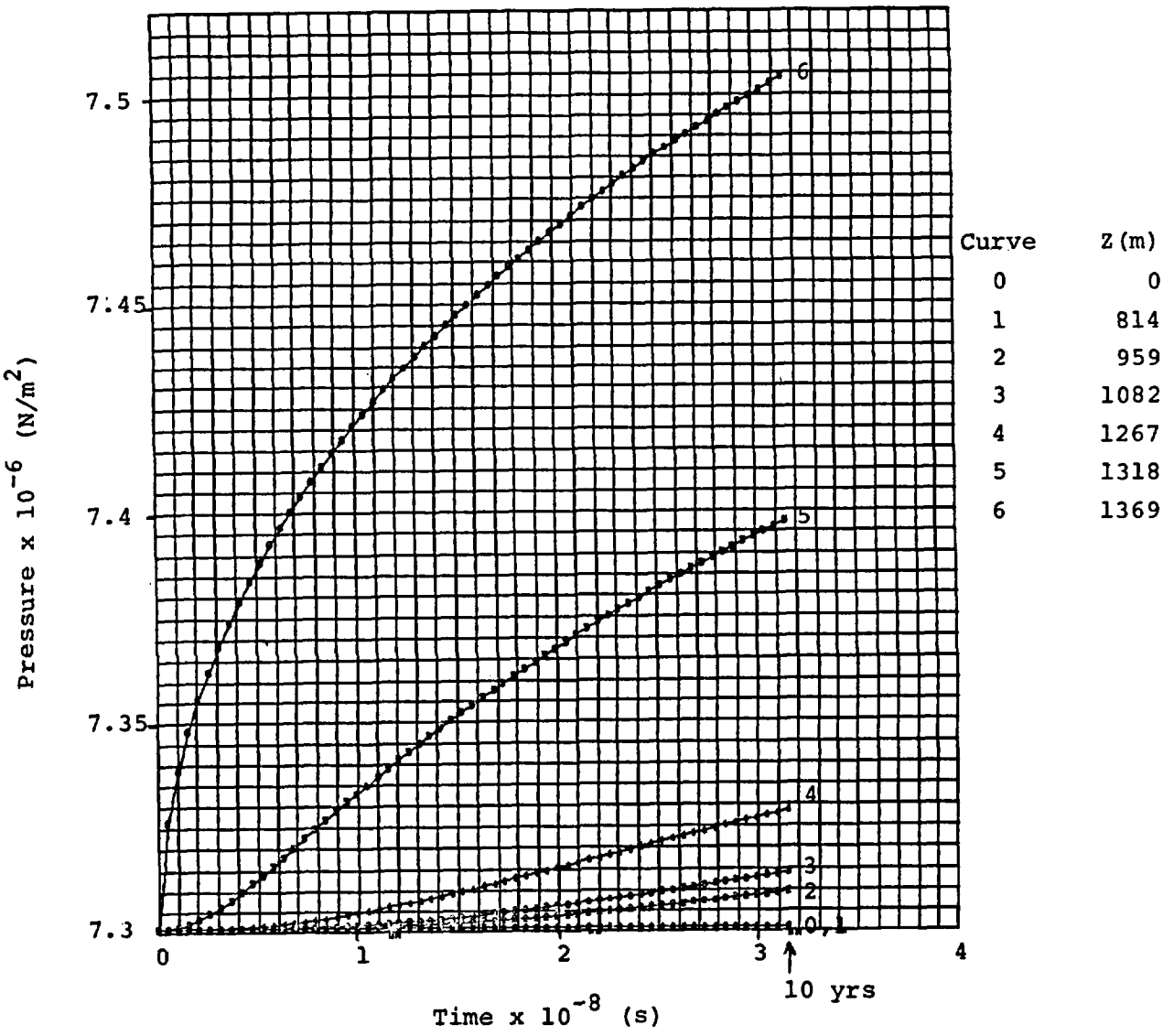

FIGURE 7b: Ground Surface Mass Flux Boundary Condition = 0.7 in/yr., t_{max} = 10 yrs.

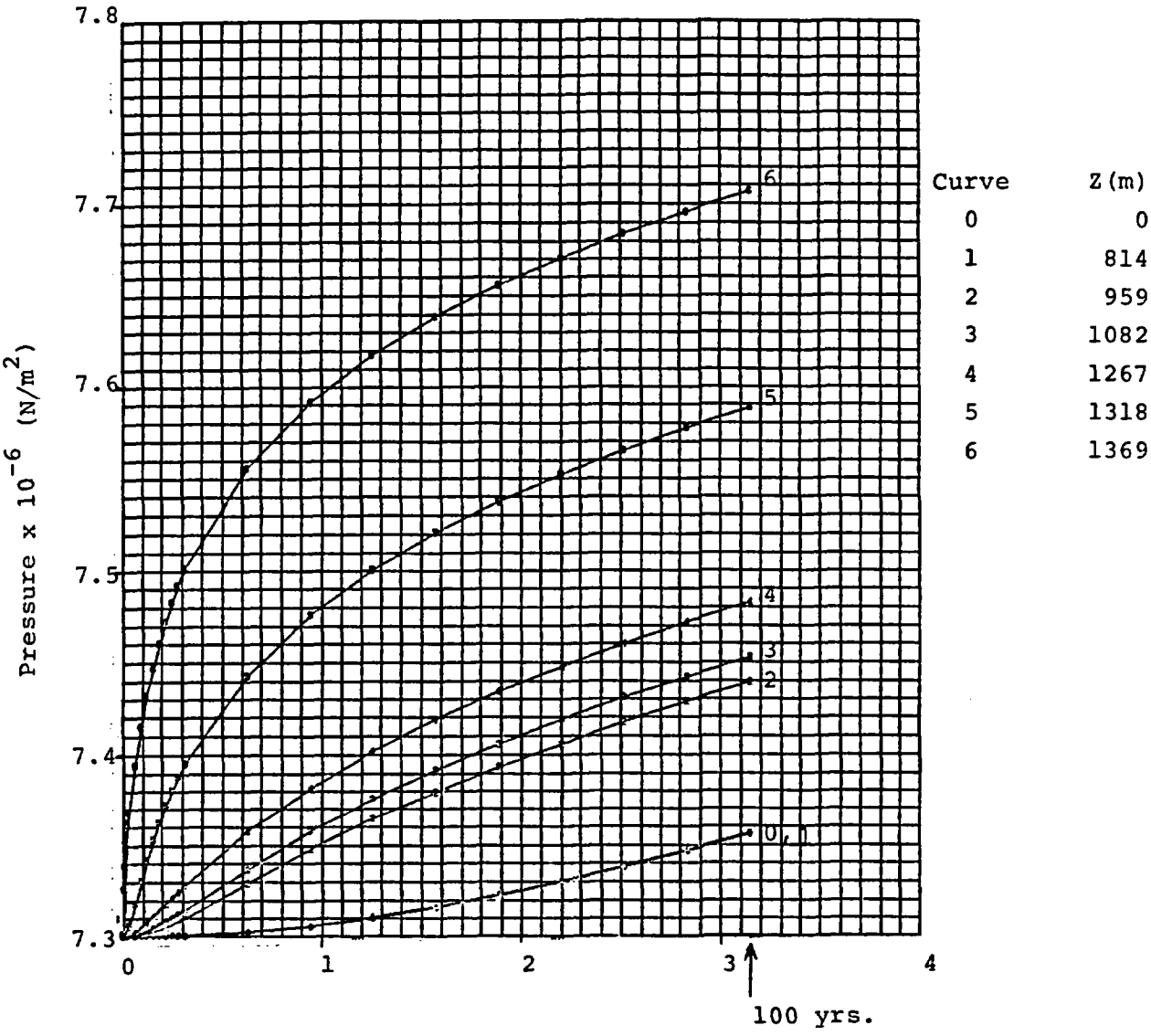

FIGURE 7c: Ground Surface Mass Flux Boundary Condition = 0.7 in/yr, t_{max} = 100 yrs.

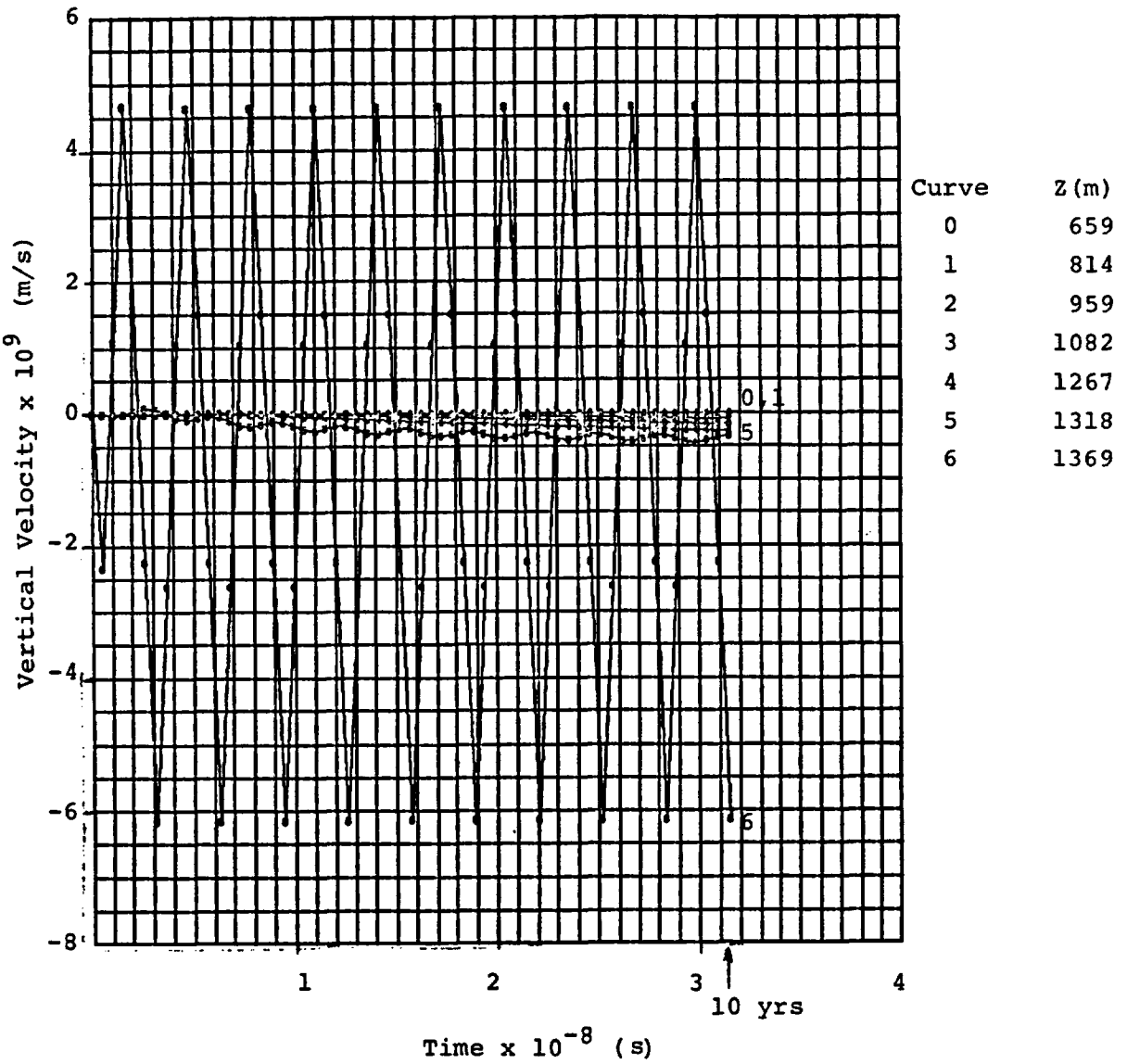

FIGURE 8: Pore Water Velocity as a Function of Time.

a) Oscillating Mass Flux Boundary Condition at Ground Surface, Average Surface Flux = 0.7 in/yr., t_{max} = 10 yrs.

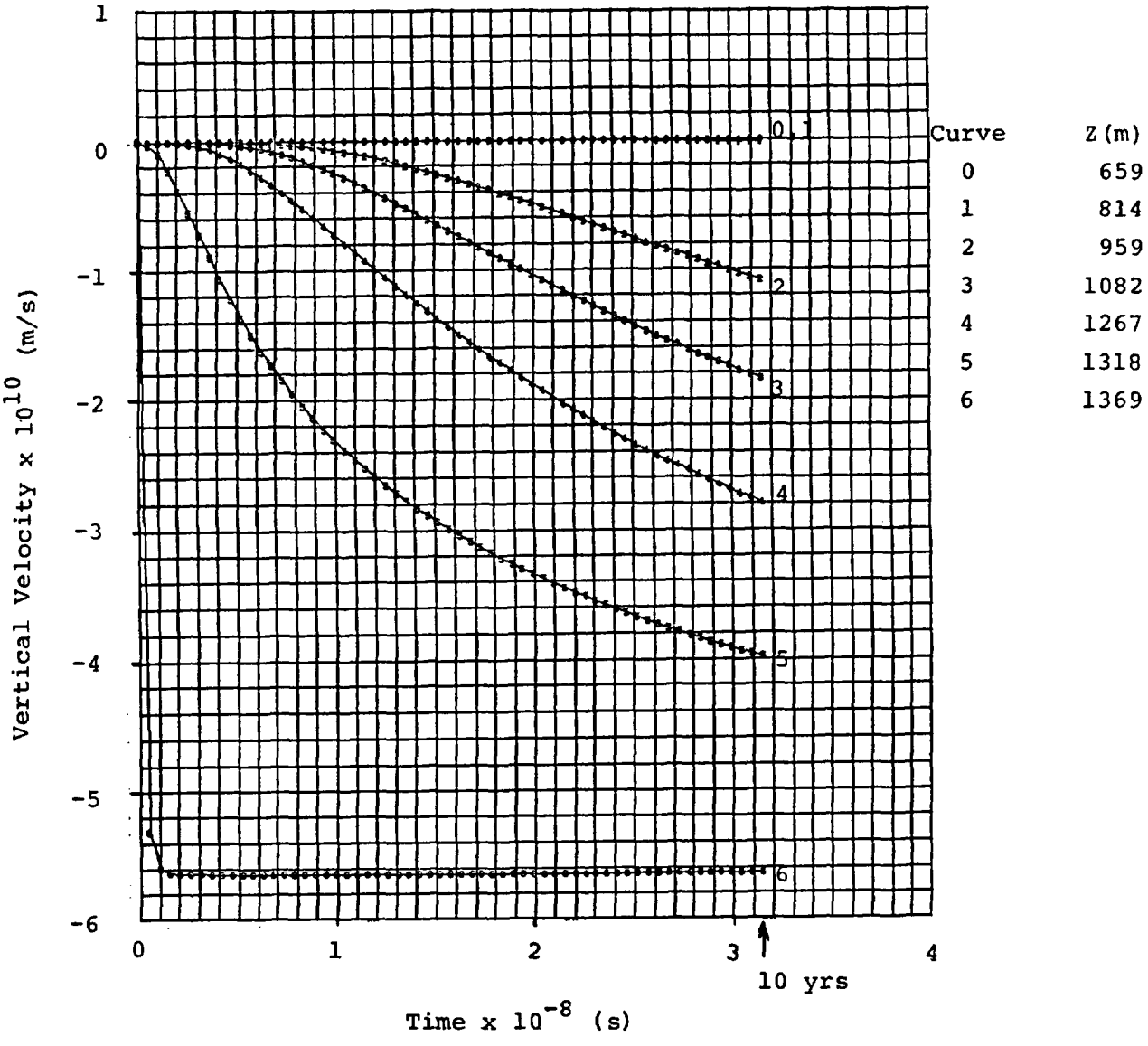

FIGURE 8b) Ground Surface Mass Flux Boundary Condition = 0.7 in/yr, t_{max} = 10 yrs.

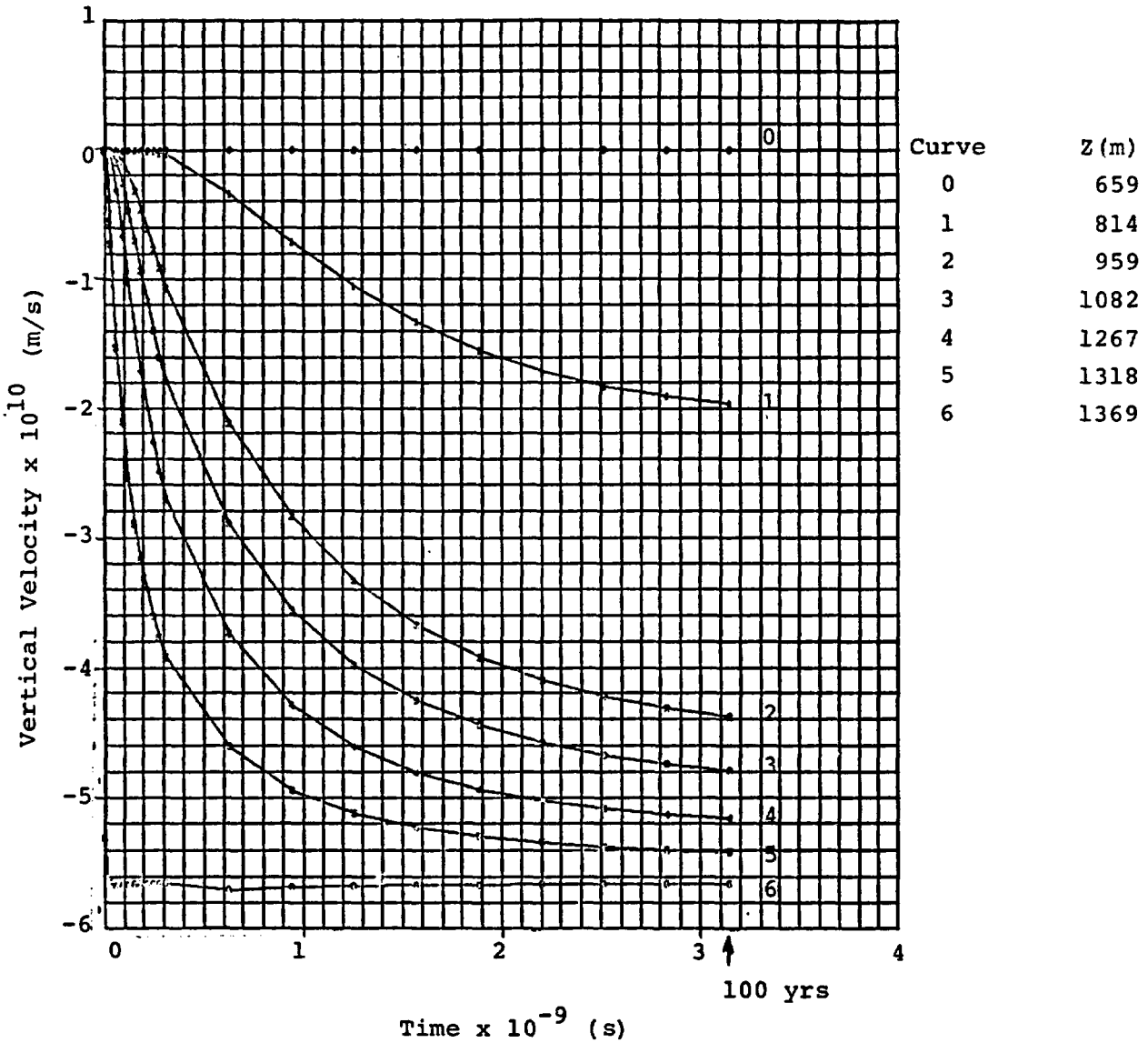

FIGURE 8c: Ground Surface Mass Flux Boundary Condition = 0.7 in/yr, t_{max} = 100 yrs.

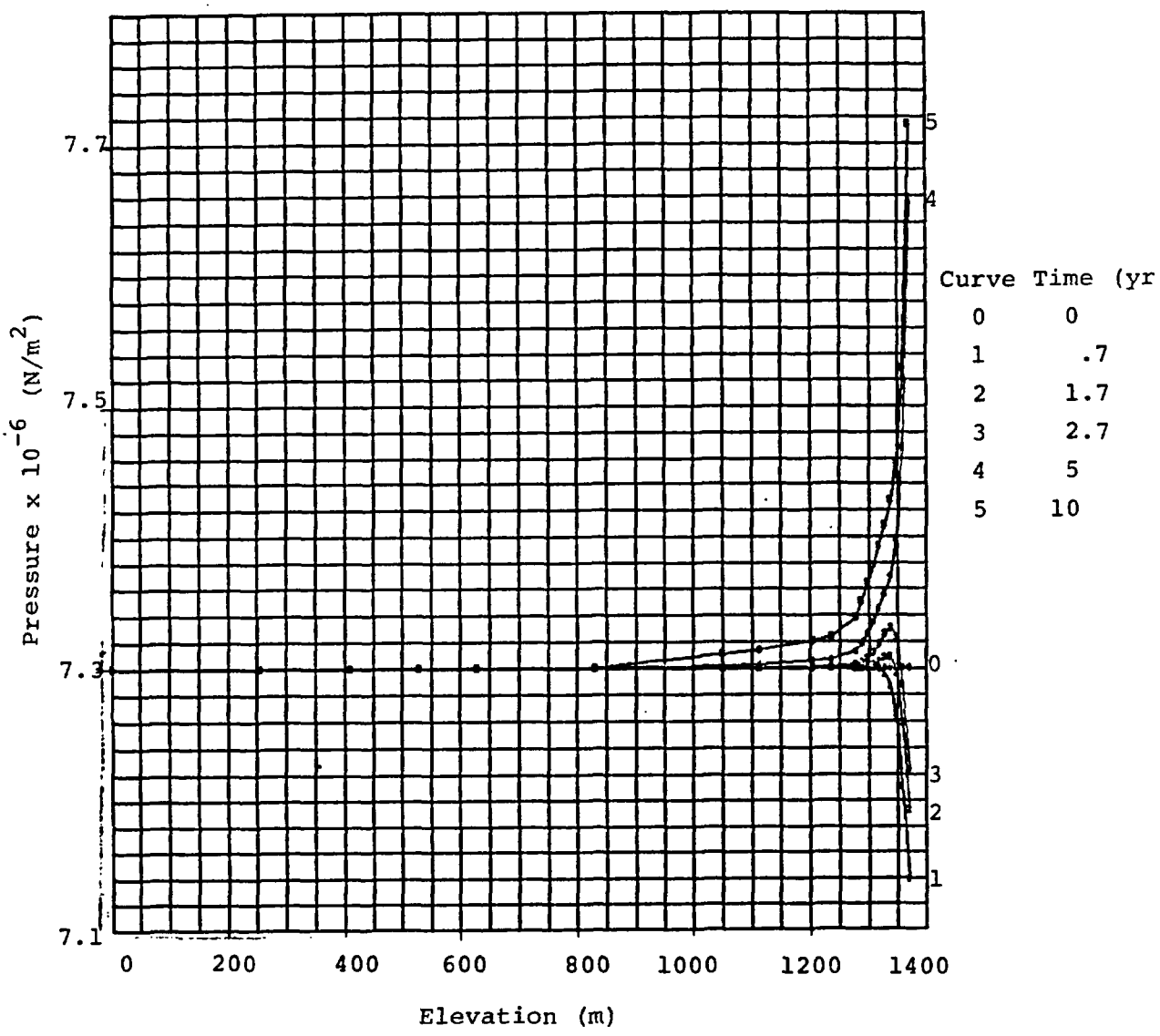

Figure 9: Pressure (P + ρgz) as a Function of Distance.

a) Oscillating Mass Flux Boundary Condition at Ground Surface, Average Flux = 0.7 in/yr., t_{max} = 10 yrs.

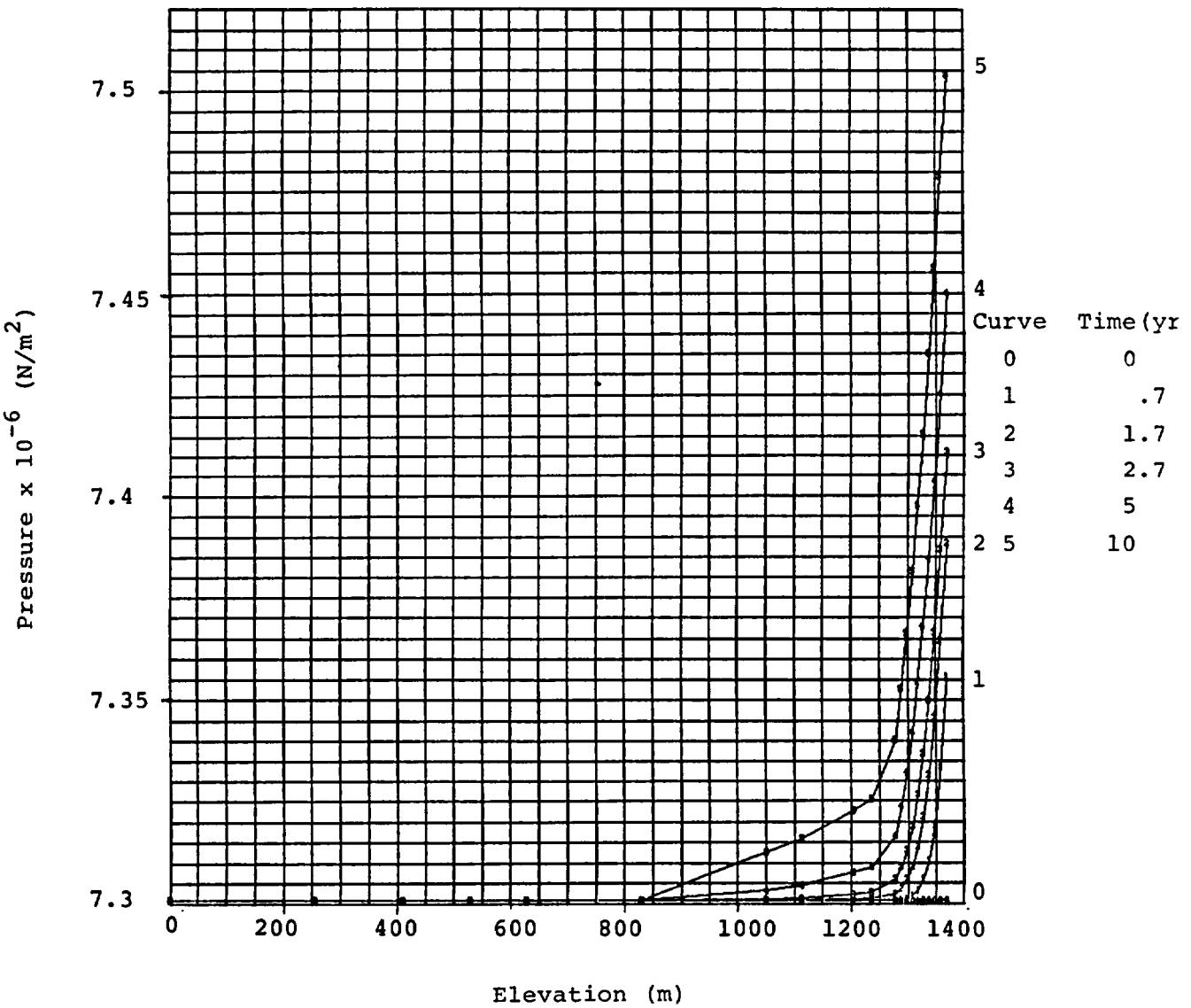

FIGURE 9b: Ground Surface Mass Flux Boundary Condition = 0.7 in/yr., t_{max} = 10 yrs.

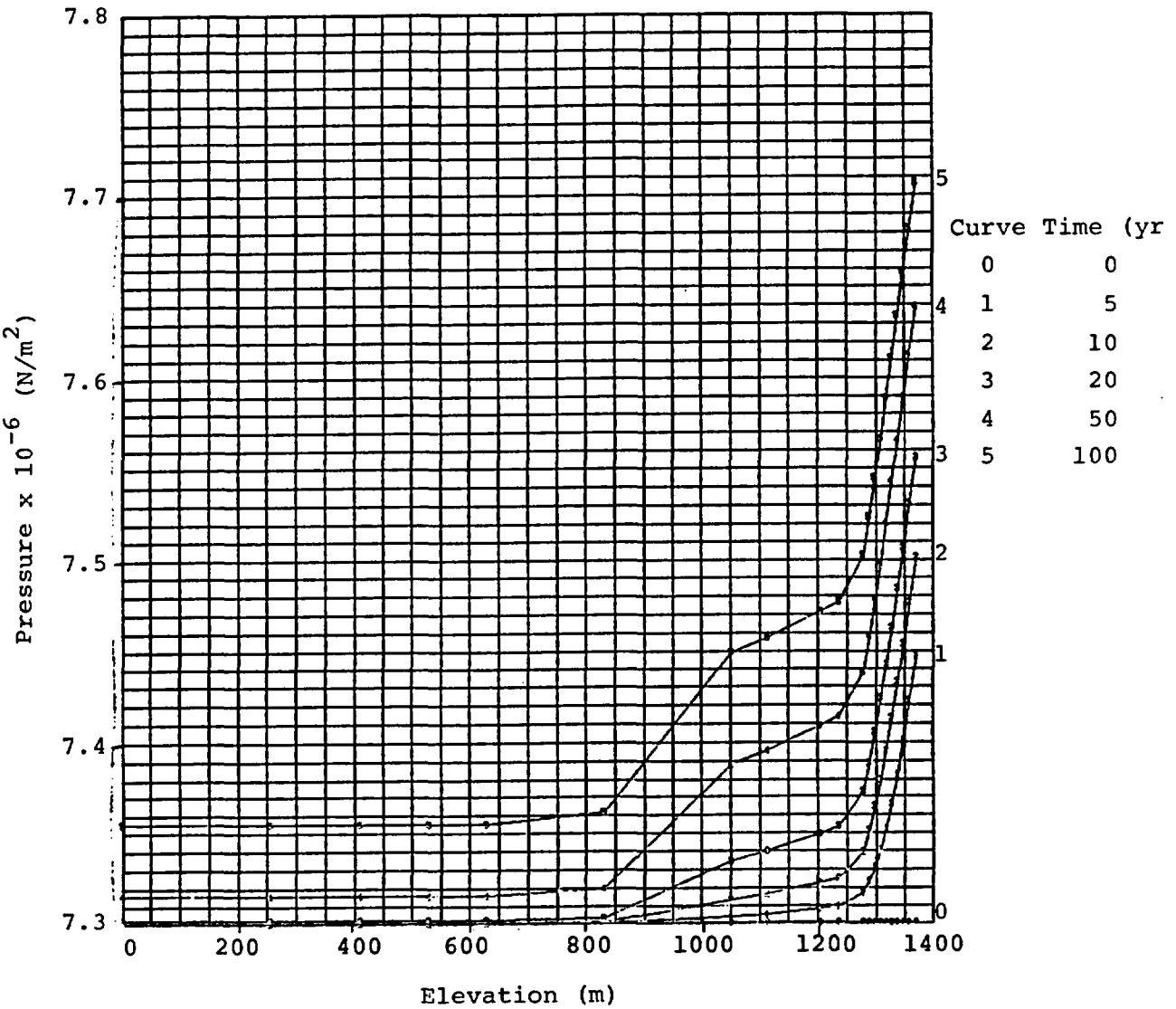

FIGURE 9c: Ground Surface Mass Flux Boundary Condition = 0.7 in/yr, t_{max} = 100 yrs.

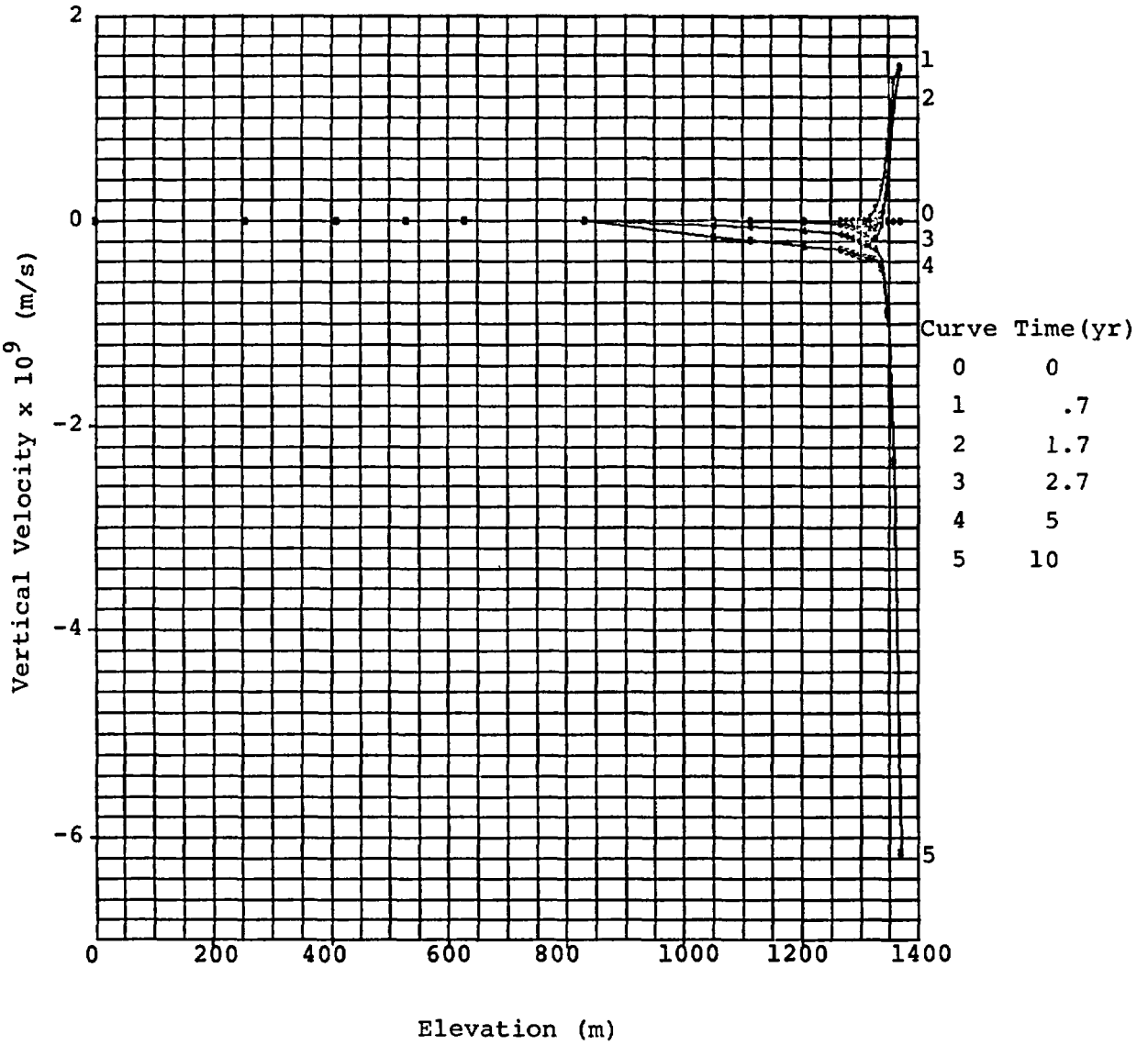

FIGURE 10: Pore Water Velocity as a Function of Distance.

a) Oscillating Boundary Condition at Ground Surface, Average Surface Flux = 0.7 in/yr, t_{max} = 10 yrs.

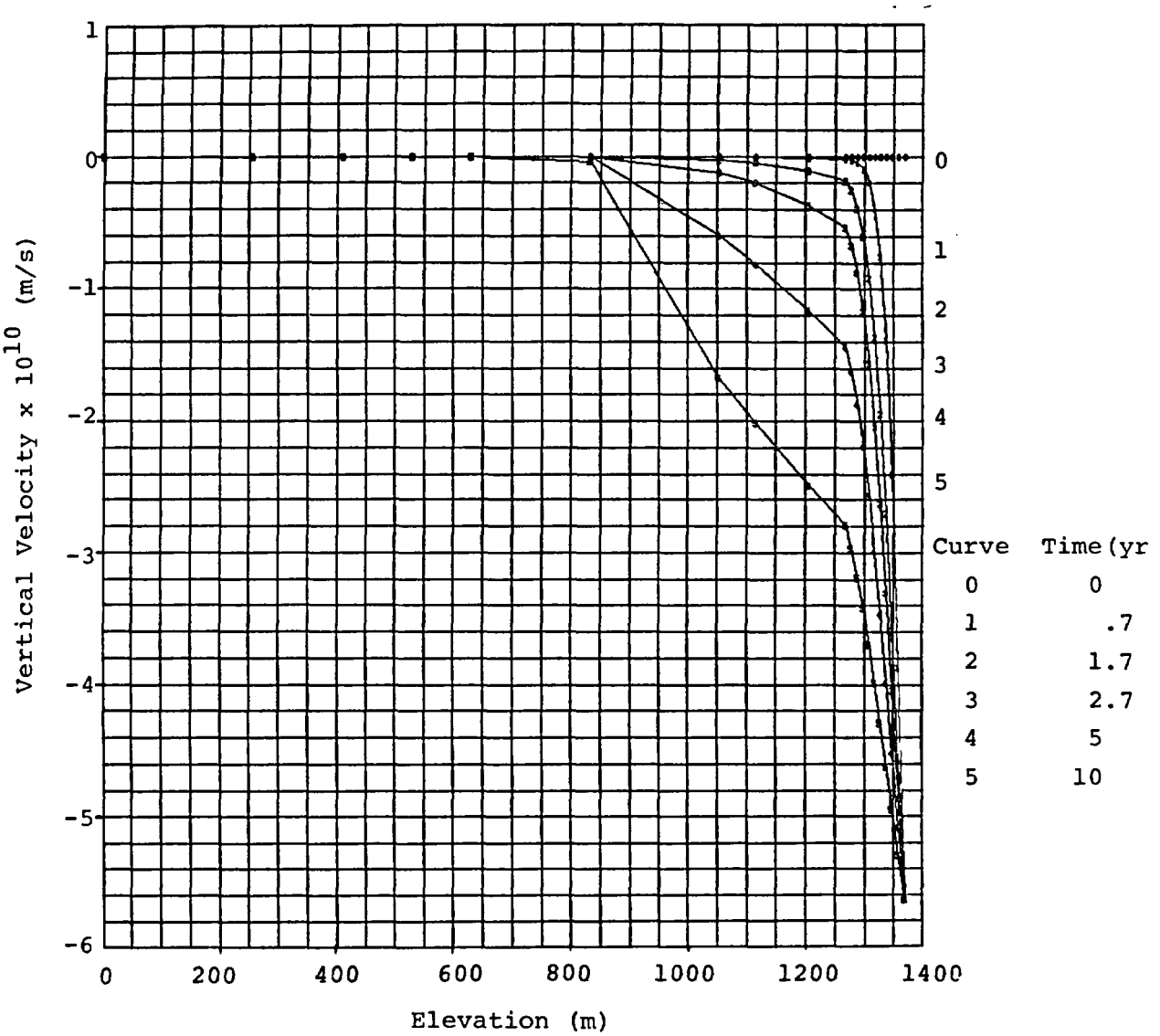

FIGURE 10b: Ground Surface Mass Flux Boundary Condition = 0.7 in/yr, t_{max} = 10 yrs.

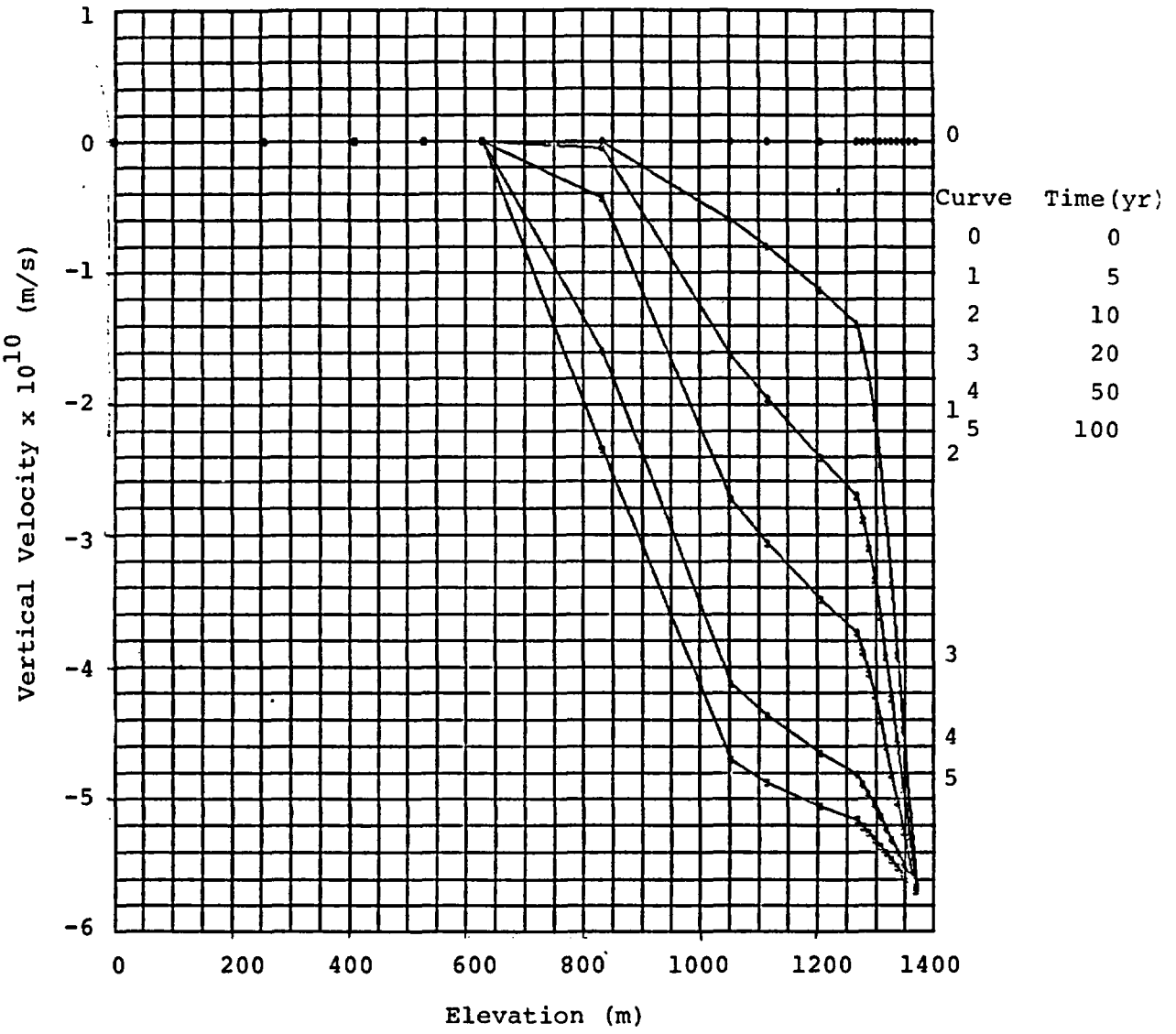

FIGURE 10c: Ground Surface Mass Flux Boundary Condition = 0.7 in/yr, t_{max} = 100 yrs.

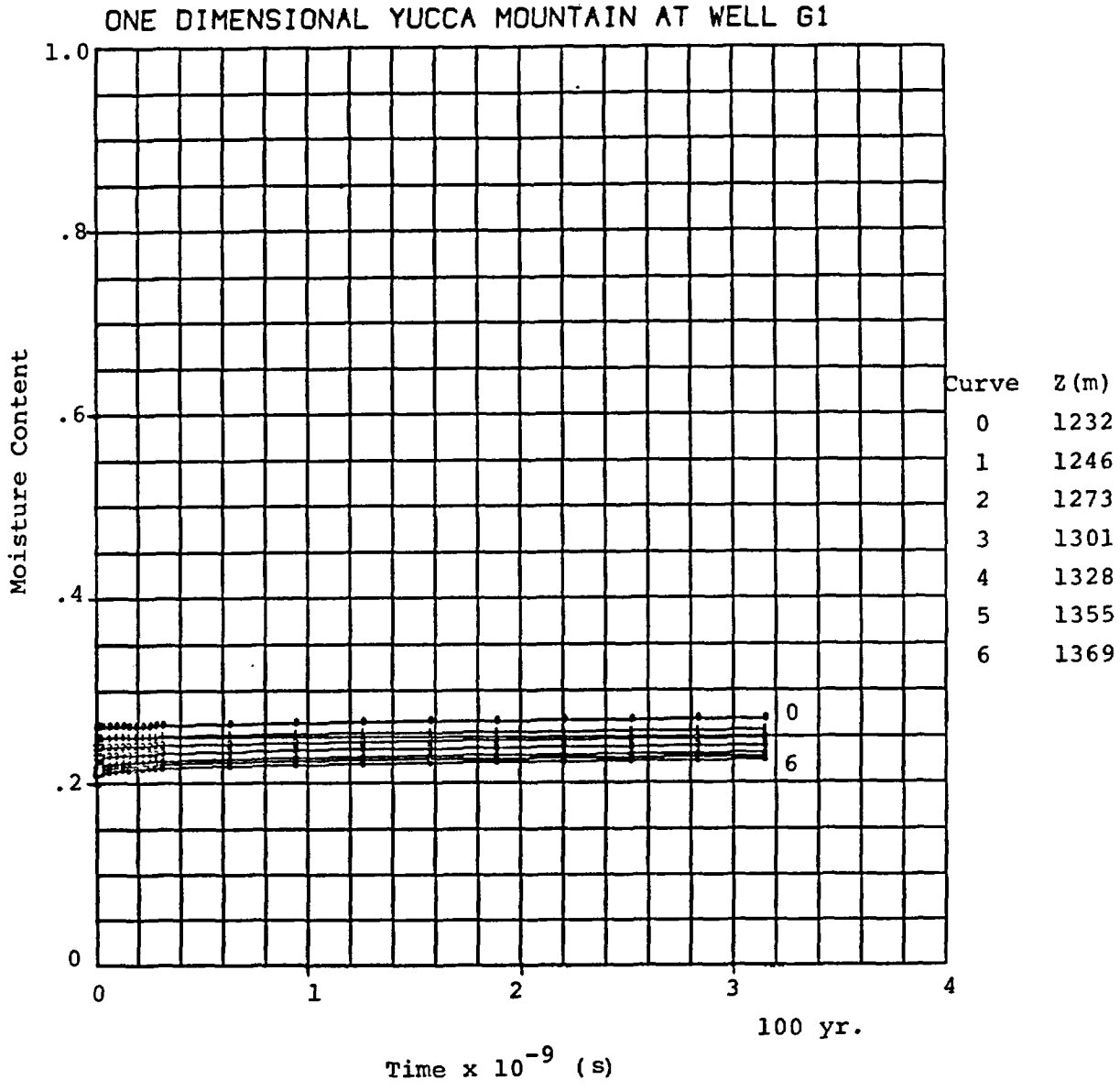

FIGURE 11: Moisture Content as a Function of Time for Constant Ground Surface Flux = 0.7 in/yr., t_{max} = 100 yrs.

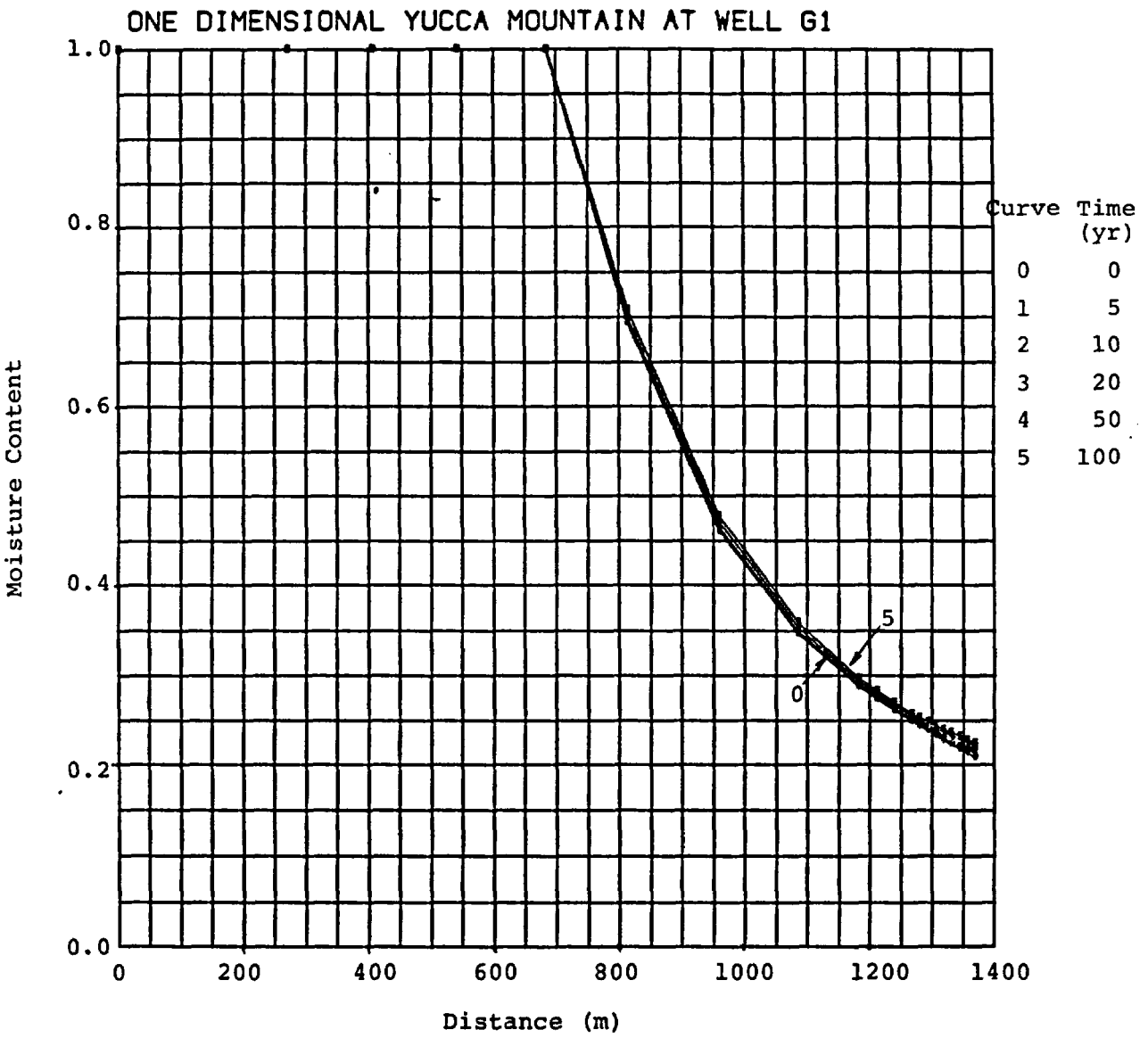

FIGURE 12: Moisture Content as a Function of Distance for Constant Ground Surface Flux = 0.7 in/yr., t_{max} = 100 yrs.

Distribution:
1510 D. B. Hayes
1511 J. W. Nunziato
1511 N. E. Bixler
1511 R. R. Eaton (10)
1511 D. K. Gartling
1511 C. E. Hickox
1511 C. M. Korbin
1511 M. J. Martinez (10)
1511 R. K. Wilson
1512 J. C. Cummings
1512 L. A. Mondy
1512 C. E. Sisson
1513 D. W. Larson
1520 T. B. Lane
1521 R. D. Krieg
1521 C. M. Stone
1530 L. W. Davison
1531 M. L. Blanford
1540 W. C. Luth
1541 H. C. Hardee
1541 J. C. Dunn
8120 L. D. Bertholf
8124 R. J. Gallagher
8125 M. J. Fish
9730 W. D. Weart
9731 A. Lappin
9732 T. O. Hunter
9734 D. R. Anderson
9734 R. D. Klett
9760 R. W. Lynch
9761 L. W. Scully
9762 L. D. Tyler
9762 J. K. Johnstone
9762 R. R. Peters
9762 N. K. Hayden
9762 Y. T. Lin
9763 J. R. Tillerson
9763 R. M. Zimmerman

8214 M. A. Pound
3141 L. J. Erickson (5)
3151 W. L. Garner (3)
for DOE/TIC

DOE/TIC (25)
(C. H. Dalin, 3154-3)

Distribution:
Second Printing
UC-70

J. W. Bennett, Director
Geologic Repository Division
U.S. Department of Energy
NE-22
Washington, DC 20545

M. W. Frei
Geologic Repository Division
U.S. Department of Energy
NE-22
Washington, DC 20545

C. R. Cooley
Geologic Repository Division
U.S. Department of Energy
NE-22
Washington, DC 20545

C. H. George
Geologic Repository Division
U.S. Department of Energy
NE-22
Washington, DC 20545

J. J. Fiore
Geologic Repository Division
U.S. Department of Energy
NE-22
Washington, DC 20545

J. G. Vlahakis
Geologic Repository Division
U.S. Department of Energy
NE-22
Washington, DC 20545

T. P. Longo
Geologic Repository Division
U.S. Department of Energy
NE-22
Washington, DC 20545

C. Klingsberg
Geologic Repository Division
N.S. Department of Energy
NE-22
Washington, DC 20545

NTS Project Manager
High-Level Waste Technical
Development Branch
Division of Waste Management
U.S. Nuclear Regulatory Commission
Washington, DC 20555

Chief, High-Level Waste Technical
Development Branch
Division of Waste Management
U.S Regulatory Commission
Washington, DC 20555

J. O. Neff, Program Manager
National Waste Terminal
Storage Program Office
U.S. Department of Energy
505 King Avenue
Columbus, OH 43201

N. E. Carter
Battelle
Office of Nuclear Waste Isolation
505 King Avenue
Columbus, OH 43201

ONWI Library (5)
Battelle
Office of Nuclear Waste Isolation
505 King Avenue
Columbus, OH 43201

O. L. Olson, Project Manager
Basalt Waste Isolation Project Office
U.S. Department of Energy
Richland Operations Office
Post Office Box 550
Richland, WA 99352

R. Deju
Rockwell International Atomics
International Division
Rockwell Hanford Operations
Richland, WA 99352

Distribution (cont.):

Governor's Office Planning
Coordinator
Nevada State Planning Coordination
State Capitol Complex, Second Floor
Carson City, NV 89710

J. I. Barnes, Director
Department of Energy
State of Nevada
400 W. King St., Suite 106
Carson City, NV 89710

K. Street, Jr.
Lawrence Livermore National
Laboratory
Mail Stop L-209
P.O. Box 808
Livermore, CA 94550

L. D. Ramspott
Technical Project Office
Lawrence Livermore National
Laboratory
P.O. Box 808
Mail Stop L-204
Livermore, CA 94550

D. C. Hoffman
Los Alamos National Laboratory
P.O. Box 1663
Mail Stop E-515
Los Alamos, NM 87545

D. T. Oakley
Technical Project Officer
Los Alamos National Laboratory
P.O. Box 1663
Mail Stop F-671
Los Alamos, NM 87545

W. W. Dudley, Jr.
Technical Project Officer
U.S. Geological Survey
P.O. Box 25046
Mail Stop 418
Federal Center
Denver, CO 80225

W. S. Twenhofel
820 Estes Street
Lakewood, CO 80215

R. W. Lynch
Technical Project Officer
Sandia National Laboratories
P.O. Box 5800
Organization 9760
Albuquerque, NM 87185

G. F. Rudolfo
Technical Project Officer
Sandia National Laboratories
P.O. Box 5800
Organization 7254
Albuquerque, NM 87185

A. E. Stephenson
Sandia National Laboratories
P.O. Box 14100
Organization 9764
Las Vegas, NV 89114

D. L. Vieth, Director (5)
Waste Management Project Office
U.S. Department of Energy
P.O. Box 14100
Las Vegas, NV 89114

D. F. Miller, Director
Office of Public Affairs
U.S. Department of Energy
P.O. Box 14100
Las Vegas, NV 89114

D. A. Nowack (8)
U.S. Department of Energy
P.O. Box 14100
Las Vegas, NV 89114

B. W. Church, Director
Health Physics Division
U.S. Department of Energy
P.O. Box 14100
Las Vegas, NV 89114

A. E. Gurrola
Holmes & Narver, Inc.
P.O. Box 14340
Las Vegas, NV 89114

Distribution (cont.):

H. D. Cunningham
Reynolds Electrical &
Engineering Company, Inc.
P.O. Box 14400
Mail Stop 555
Las Vegas, NV 89114

J. A. Cross
Fenix & Scisson, Inc.
P.O. Box 15408
Las Vegas, NV 89114

R. H. Marks
U.S. Department of Energy
CP-1, M/S 210
P.O. Box 14100
Las Vegas, NV 89114

A. R. Hakl, Site Manager
Westinghouse - AESD
P.O. Box 708
Mail Stop 703
Mercury, NV 89023

M. Spaeth
Science Applications, Inc.
2769 South Highland Drive
Las Vegas, NV 89109

G. Tomsic
Utah Dept. of Community
Economic Development
Room 6290, State Office Bldg.
Salt Lake City, UT 89114

U.S. Department of Energy (2)
Technical Information Center
P.O. Box 62
Oak Ridge, TN 37830

667 -4681

Org.	Bldg.	Name	Rec'd by	Org.	Bldg.	Name	Rec'd by

Sandia National Laboratories